

TIME SERIES ANALYSIS OF GPS PERMANENT STATIONS AROUND EAST
ANATOLIA

by

Wumiti Julaiti

B.S, Geology, China University of Geosciences (Beijing), 2011

Submitted to Kandilli Observatory and Earthquake Research Institute
in partial fulfilment of the requirements for the degree of
Master of Science

Graduate Program in Geodesy

Boğaziçi University

2016

ACKNOWLEDGEMENTS

It is great pride that I hereby present my master thesis. During this nearly six month long process, I have gained a lot of experience from this subject and it has been beneficial to my development in the future career and studies. I would like first to express absolute gratitude to my thesis supervisor, Prof. Dr. Semih Ergintav for his meaningful assistance, tireless guidance, patience and persistent support in my undertaking of this study.

I would also like to extend my appreciation to Prof. Dr. Haluk Özener and Prof. Dr. Uğur Doğan, who are the member of the jury, for their time, encouragement, and valuable advices.

I would also like to thank Assoc. Prof. Dr. Aslı Doğru, Res. Assist. Aslı Sabuncu and Dr. Yin Chen for their help and kindness words.

I would also like to acknowledge Dr. Mike Floyd, Dr. Kerem Halıcıoğlu, Dr. Onur Yılmaz, Mr. Bülent Turgut and Ms. Belgin Gümüş for sharing their experience in the related realm of studies.

In the end, I want to thank my family for their moral and material support. Especially my mother, God bless her in the haven.

ABSTRACT

TIME SERIES ANALYSIS OF GPS PERMANENT STATIONS AROUND EAST ANATOLIA

The eastern part of Anatolia is a significant location in the world due to its tectonically active background. It includes one of the major fault zone of Anatolia: left-lateral East Anatolian Fault (EAF), forming a boundary between the Anatolian and the Arabian plates. Its long-term slip rate as well as localizations of creeping zones, locking depth and the surface offsets can be obtained by using inter-seismic Global Positioning system (GPS) velocities and proper models. However, the quality of position time series generated from each GPS station directly determines the accuracy of the velocity estimation.

The Continuous Operating Reference Stations (CORS) of Turkish National Permanent GNSS Network-Active (TNPGN-Active), mainly using the GPS measurements, covers the most area of Turkey, including the whole segments of the EAF. In the thesis duration, a limited part of the TNPGN-Active data could be archived. Then, as a thesis objective, we decided to control the quality of GPS velocities, estimated from limited data of stations around the EAF, in order to improve the GPS velocity field in this region.

In this study, 2-year span GPS data from 37 sites of TNPGN-Active were processed by using GAMIT/GLOBK to generate daily position time series of each station as well as the related velocity estimates. For the GPS time series, mainly noise analysis was applied to distinguish which station is sufficient enough for using its velocity estimates. Finally, it has been found that the velocity estimates of at least three specific stations with spectral indices > 0.7 and linear trend uncertainties > 2.5 mm on horizontal components, which are MUUS, HINI and GEME, are not quite reliable with the limited 2-year data. This result will be highly likely an important reference for the campaign type GPS study along Hazar-Palu segment of the EAF in the future. To estimate a high quality velocity field, new campaign sites could be added around the problematic TNPGN-Active stations.

ÖZET

DOĞU ANADOLU CİVARINDAKİ SABİT GPS İSTASYONLARININ ZAMAN SERİSİ ANALİZİ

Doğu Anadolu bölgesi, aktif tektoniği açısından, dünyanın önemli bölgelerinden birisidir. Anadolu'nun, önemli fay zonlarından olan ve Anadolu ile Arap plakaları arasında bir sınırdaki yer alan, sol yanal atımlı Doğu Anadolu Fayı (DAF) bu bölgede yer almaktadır. DAF'ın uzun dönem hızını, krip eden olası yerlerini, kilitlenme derinliğini ve yüzey atımını, Küresel Konumlama Sistemi (GPS) verileri tarafından hesaplanan, intersismik GPS hızları ve uygun modeller yardımı ile belirlemek mümkündür. Fakat, her GPS istasyonundan, elde edilen koordinat zaman serileri hız kestiriminin doğruluğunu etkilemektedir.

Türkiye Ulusal Sabit GNSS Ağı-Aktif (TUSAGA-Aktif), Türkiye genelinde sürekli çalışan bir GPS sistemi (CORS) olup DAF fayı da dahil olmak üzere, Türkiye'nin büyük bir bölümünü kapsamaktadır. Bu tez süresinde, TUSAGA-Aktif istasyonlarının, limitli boyutta verisine ulaşmak mümkün olmuştur. Bundan dolayı, tezin ana konusu olarak, kısıtlı veriden elde edilen GPS hızların kalitesini kontrol etmeye ve bölgeye ait GPS hız alanının kalitesini artırmaya karar verilmiştir.

Çalışma kapsamında, çalışma alanında yer alan 37 adet TUSAGA-Aktif istasyonuna ait 2 yıllık günlük bazdaki veriler, GAMIT/GLOBK programı ile değerlendirilmiş, günlük zaman serileri üretilmiş ve GPS hızları kestirilmiştir. İzleyen adımda, GPS zaman serilerine gürültü analizi uygulanmış ve bu verilerin hız kestirimi için uygun olup olmadığı sorgulanmıştır. Sonuç olarak, spektral indeksi >0.7 ve yatay doğrusal değişim belirsizliği $>2.5\text{mm}$ 'dan büyük olan 3 istasyon (MUSS HIN ve GEME) belirlenmiş ve bu istasyonlar için iki yıllık veri ile hız kestiriminin mümkün olmadığına karar verilmiştir. Elde edilen sonuçlar Doğu Anadolu Fayının Hazar Palu segmentinde gerçekleştirilecek GPS kampanyaları için önemlidir. Kaliteli bir hız alanı için, sorunlu noktaların bulunduğu yerlerde, kampanya noktaları oluşturulmalı ve hız alanının kalitesi iyileştirilmelidir.

TABLE OF CONTENTS

ACKNOWLEDGEMENTS.....	iii
ABSTRACT.....	iv
ÖZET	v
LIST OF FIGURES	viii
LIST OF TABLES	xii
LIST OF SYMBOLS	xiii
LIST OF ACRONYMS / ABBREVIATIONS	xiv
1. INTRODUCTION	1
2. SEISMOTECTONIC FEATURES OF STUDY AREA.....	3
3. DESCRIPTION OF GPS TIME SERIES	8
3.1. Noise Analysis.....	10
3.2. Noise in GPS Time Series.....	11
4. GPS TIME SERIES ANALYSIS	12
4.1. GPS Data.....	12
4.2. GPS Data Processing	16
4.2.1. GAMIT Processing.....	16
4.2.2. GLOBK Processing.....	18
4.3. Time Series Analysis Strategy.....	21
4.3.1. Remove outliers and offset.....	21
4.3.2. First Order Gauss-Markov Extrapolation.....	25
4.3.2.1. Analysis Software: Tsview.....	25
4.3.3. Maximum Likelihood Estimate	26
4.3.3.1. Analysis Software: Hector.....	28
5. EXPERIMENTS AND RESULTS	29
5.1. Noise Analysis.....	29
5.1.1. Random Walk Noise Model	29
5.1.2. White + Power law Noise Model	32

5.2. Velocity Analysis	39
5.3. Compare With The Latest Velocity Study	47
6. DISCUSSION AND CONCLUSION	56
REFERENCES	58
APPENDIX A: SESSION TABLE.....	64
APPENDIX B: PROCESS.DEFAULTS	70
APPENDIX C: SLURM	72
APPENDIX D: HECTOR CONTROL FILE	75
APPENDIX E: GPS POSTION TIME SERIES OF ALL STATIONS.....	76

LIST OF FIGURES

Figure 2.1. Tectonic plates connection and motions in the east Anatolia..	4
Figure 2.2. Main earthquakes (circles and stars) happened since last century and faults' location (brown lines) in East Anatolia.	5
Figure 2.3. Seismic region along East Anatolian Fault and major earthquake developed surface fault between 1822 and 1971 (Bayrak et al, 2015).	7
Figure 2.4. The probability of earthquake occurring for region 2 in EAFZ (Bayrak et al, 2015).	7
Figure 3.1. An example of additive model decomposition in time series [Kong et al, 2015].	9
Figure 3.2. Power spectrum of white noise, flicker noise and random walk noise.	11
Figure 4.1. Distributions of the GPS stations belong to CORS-TR of TNPGN-Active.....	12
Figure 4.2. IGIR (Igdir) and DIYB (Diyarbakir) stations of TNPGN.....	13
Figure 4.3. Selected TNPGN-Active stations in East Anatolia to test our methodology. ..	14
Figure 4.4. Sky plots of BTMN station on July 8th, 2015, which shows phase residuals of GAMIT daily solution.	17
Figure 4.5. Sky plots of BTMN station on October 4th, 2015, which has an acceptable daily solution. Compare it with Figure 4.4.	18
Figure 4.6. Position time series of station BTMN.	20
Figure 4.7. The histogram of scatter nrms and wrms for each site after the first step of removing outliers.	22
Figure 4.8. The histogram of scatter nrms and wrms for each site after the second step of removing outliers.	23

Figure 4.9. Examples of raw time series and cleaned time series.	24
Figure 4.10. Interface of Tsview for GPS time series analysis.....	26
Figure 5.1. χ^2 as function of averaging interval for horizontal components at stations ELAZ, ERGN, TNCE and BING..	31
Figure 5.2. Histogram of the 22 stations with at least one larger value (>0.6) of spectral index in one of the horizontal components.	38
Figure 5.3. Histogram of trend rate (mm/yr) for each site on horizontal components.	44
Figure 5.4. Histogram of trend rate uncertainties (mm/yr) for each site on horizontal components.	44
Figure 5.5. Velocity differences between Ozdemir (2016) and this study..	49
Figure 5.6. Comparison of our velocity solution with Ozdemir (2016)'s. The velocity error ellipses are at 95% confidence level.	50
Figure 5.7. Velocity differences between Aktug et al. (2016) and this study..	53
Figure 5.8. Comparison of our velocity field with Aktug et al (2016)'s. The velocity error ellipses are at 95% confidence level.	54
Figure 5.9. GPS position time series of station MUUS.	55
Figure C.1. Slurm components	73
Figure E. 1. GPS time series of station ADIY.	77
Figure E. 2. GPS time series of station ARPK.	78
Figure E. 3. GPS time series of station ARTV.	79
Figure E. 4. GPS time series of station BAYB.	80
Figure E. 5. GPS time series of station BING.	81

Figure E. 6. GPS time series of station BTMN.	82
Figure E. 7. GPS time series of station DIVR.	83
Figure E. 8. GPS time series of station DIYB.	84
Figure E. 9. GPS time series of station EKIZ.	85
Figure E. 10. GPS time series of station ELAZ.	86
Figure E. 11. GPS time series of station ERGN.	87
Figure E. 12. GPS time series of station ERZ1.	88
Figure E. 13. GPS time series of station ERZR.	89
Figure E. 14. GPS time series of station FASA.	90
Figure E. 15. GPS time series of station GEME.	91
Figure E. 16. GPS time series of station GIRS.	92
Figure E. 17. GPS time series of station GUMU.	93
Figure E. 18. GPS time series of station GURU.	94
Figure E. 19. GPS time series of station HINI.	95
Figure E. 20. GPS time series of station HORS.	96
Figure E. 21. GPS time series of station MALY.	97
Figure E. 22. GPS time series of station MARA.	98
Figure E. 23. GPS time series of station MUUS.	99
Figure E. 24. GPS time series of station RDIY.	100
Figure E. 25. GPS time series of station RHIY.	101

Figure E. 26. GPS time series of station RZE1.	102
Figure E. 27. GPS time series of station SAM1.	103
Figure E. 28. GPS time series of station SIRT.	104
Figure E. 29. GPS time series of station SIVE.	105
Figure E. 30. GPS time series of station SIVS.	106
Figure E. 31. GPS time series of station SSEH.	107
Figure E. 32. GPS time series of station TNCE.	108
Figure E. 33. GPS time series of station TOK1.	109
Figure E. 34. GPS time series of station TRBN.	110
Figure E. 35. GPS time series of station TUF1.	111
Figure E. 36. GPS time series of station TVA1.	112
Figure E. 37. GPS time series of station UDER.	113

LIST OF TABLES

Table 4.1. TNPGN sites used in this study.	15
Table 4.2. Selected IGS stations for stabilization in GLOBK process.	19
Table 5.1. Maximum likelihood results of the white plus power law noise models for time series.	34
Table 5.2. Stations with spectral indices larger than 0.6 on horizontal components.	39
Table 5.3. Linear trend of time series for each site due to different noise models processed.	41
Table 5.4. Station with spectral indices > 0.7 and linear trend uncertainties > 2.5 mm on horizontal components.	46
Table 5.5. Comparing the velocity solution from the same station between previous study and this one.	48
Table 5.6. Velocity field in Eurasia fixed frame from the 37 stations.	51
Table 5.7. Comparing the velocity solution from the same station between previous study and this one.	52

LIST OF SYMBOLS

M	Earthquake Magnitude
X_t	Time Series
S_t	Seasonal Component
T_t	Trend-Cyclic Component
E_t	Irregular or Remainder Component
f	Frequency
κ	Spectral Index (Common)
lik	Likelihood Function
$\hat{\mathbf{v}}$	Observation Residuals
C	Covariance Matrix
det	Determination of Matrix
I	Unit Matrix
E	Power Law Noise's Covariance Matrix
d	Spectral Index (Hector)
ϕ	Control Parameter
σ^2	Variance
ΔT	Sampling Period
σ_{PL}	Power Law Noise Amplitude
σ_W	White Noise Amplitude

LIST OF ACRONYMS / ABBREVIATIONS

GNSS	Global Navigation Satellite System
GPS	Global Positioning System
GLONASS	Global'naya Navigatsionnaya Sputnikovaya Sistema
CORS	Continuously Operating Reference Stations
IGS	International GNSS Service
NAF	North Anatolian Fault
EAF	East Anatolian Fault
DSF	Dead Sea Fault
GPE	Gravitational Potential Energy
RTK	Real Time Kinematic
RINEX	Receiver Independent Exchange
TEQC	Translation, Editing and Quality Check Software
TNPGN	Turkish National Permanent GNSS Network
TUSAGA	Türkiye Ulusal Sabit GNNS Ağı
RMS	Root Mean Square
NRMS	Normalized RMS
WRMS	Weighted RMS
EOP	Earth Rotation Parameter
GMT	Generic Mapping Tools
FOGM	First Order Gauss-Markov
MLE	Maximum Likelihood Estimation
PSD	Power Spectral Density

SOPAC	Scripps Orbit and Permanent Array Center
NNR	No-Net-Rotation
ITRF	International Terrestrial Reference Frame
VMF	Vienna Mapping Function
NWM	Numerical Weather Model

1. INTRODUCTION

Global Navigation Satellite System (GNSS) refers to a constellation of satellites providing signals from space transmitting positioning and timing data with global coverage. GNSS receivers determine location to high precision by using the timing and positioning data encoded in the signal transferred along a line of sight by radio from satellites. As of date, only the USA NAVSTAR Global Positioning System (GPS) and Russian Global'naya Navigatsionnaya Sputnikovaya Sistema (GLONASS) are global operational GNSSs. China is in the process of expanding its regional BeiDou Navigation Satellite System into global Compass navigation system by 2020 [Xu, 2016], and the European Union's Galileo GNSS is still in initial deployment phase, there has been 12 satellites on the orbits now, it will consist of 24 satellites scheduled to be fully operational also by 2020 at the earliest [European Space Agency, 2016]. Continuously Operating Reference Stations (CORS) are a common network that provides the GPS data consisting of carrier phase and code range measurements in support of the three dimensional positioning, meteorology, space weather, and geophysical applications throughout a country's territories. One of the main goal of CORS network is to provide mm-level accuracy for monitoring plate tectonics, measuring deformation and contributing to earthquake prediction and prior warning systems. In Turkey, CORS-TR of Turkish National Permanent GNSS Network-Active (TNPNGN-Active) is such a network being operated since 2009, which makes it more efficient for geodesist to investigate the motion of the principle plate in this region, the Anatolian plate.

It is a well-known fact that the Anatolian plate has been keeping westward excursion by the influence of the Arabian plate moving towards the Eurasian plate. The eastern portion of Anatolia is a significant location in the world due to its tectonically active background. It constitutes the mainland of eastern Turkey and borders on Eurasia at northeast and Arabia at southeast. Correspondingly, those boundaries comprise two main fault zones in this area, the eastern portion of the North Anatolian Fault (NAF) zone and the whole body of the East Anatolian Fault (EAF) zone. These two fault zones meet at the Karliova triple junction which

is the intersection point of the east end of the NAF and the north end of the EAF. Due to the active tectonics, earthquakes have been great natural hazard in Turkey that threaten the specific area socially and economically. Therefore, it is crucial to have the knowledge in the characteristic, kinematics and dynamics of the tectonic fault line to mitigate the earthquake hazard, which is an important mission in Turkey that has been confirmed to be partly accomplished by the outcomes of TNPGN-Active. All data recorded from the stations in Receiver Independent Exchange (RINEX) format files can be processed by the academic and/or commercial software (e.g. GAMIT/GLOBK) to generate stations' position time series and estimate their displacement velocities. At this point, stable and reliable stations will be much more useful by providing their mostly uninterrupted data in a high level temporal resolution. There are several factors causing the instability and unreliability of the stations, but by figuring out the noise in position time series of each station, people can give the interpretations of the reasons and avoid to use the stations with bad qualities in the future research.

In this study, because of the limitation of available data, about 730 days (2014 ~ 2015) of GPS observation data using 37 TNPGN stations in the eastern Turkey, as study objects, were processed with GAMIT/GLOBK software package in the computer clusters of Ankara and the generated position time series were analyzed. Two different combinations of noise models in the position time series were estimated, which are random walk noise model and white plus power law noise model. And the results indicates which station has large amount of noise in its position time series and whether all the stations are reliable for velocity field estimates with 2-year data. The estimated velocity from these stations in different reference frame are compared with the previous studies, which are derived after assuming random walk noise in time series of these stations'.

2. SEISMOTECTONIC FEATURES OF STUDY AREA

The catalases of the African craton in time of Oligocene led up to the opening of the Red Sea and the Gulf of Suez, and later the Gulf of Aqaba, separating Arabia from Africa. The northward motion of Arabia with respect to Africa, in essence, turned into the DSF, which essentially accomplished the individualization of Arabia. During the time from the Late Oligocene to the Middle Miocene, the northern margin of Arabia formed submerged southern boundary of the (second) Tethys Sea which kept shrinking. In the late Miocene the intercontinental collision along the Bitlis-Zagros suture occurred between the Arabian and Eurasian Plate, which cut off the deep marine connection between the Mediterranean Sea and the Indian Ocean. This epoch coincides in time with the onset of eastern Anatolian volcanic activity, uplifting of the East Anatolian Accretionary Complex, and the beginning of the North and East Anatolian Fault accompanying the westward escape of Anatolian plate [Lyberis N. et al, 1992; S. K. Husing et al, 2009]. Nowadays, the eastern portion of the Anatolian plate has been proved by GPS data that it moves at a rate of over 20 mm/yr with respect to Eurasian plate (Figure 2.1). And the velocity increases gradually to almost 30 mm/yr in west of Anatolia where it is from about 32°E near the Hellenic Trench [Nocquet, 2012]. The mechanism that forces Anatolian plate's motion has been argued, mainly focusing on several different hypothesis, such as: Whether the tectonic plates are rigid in behavior [Heidbach, 2005]? Does the difference in gravitational potential energy (GPE) in crust play a key role [Ozeren and Holt, 2010]? Or, does there exist a toroidal flow in the asthenosphere that might drag the lithosphere above [Faccenna and Becker, 2010; Le Pichon and Kremer, 2010]? Therefore, bounding the deformation in the area of EAF and around the triple junction among Anatolian, Eurasian and Arabian plates may provide critical information for comprehending the dynamics and kinematics of westward motion of Anatolia [Cavalié, O. and S. Jónsson, 2014].

East Anatolian Fault (EAF) is recognized as the major left-lateral strike-slip fault, forming the tectonic boundary between westward-moving Anatolian plate and northward-migrating Arabian plate, in eastern Turkey. However, studies have shown that the fault is one of the large results of the convergence of the African and Arabian plates with respect to the Anatolian plate. It merges with North Anatolian Fault (NAF) at the Karliova Triple Junction in north end and connects to Dead Sea Fault (DSF) at Maras Triple Junction in south, extending over 400 km long.

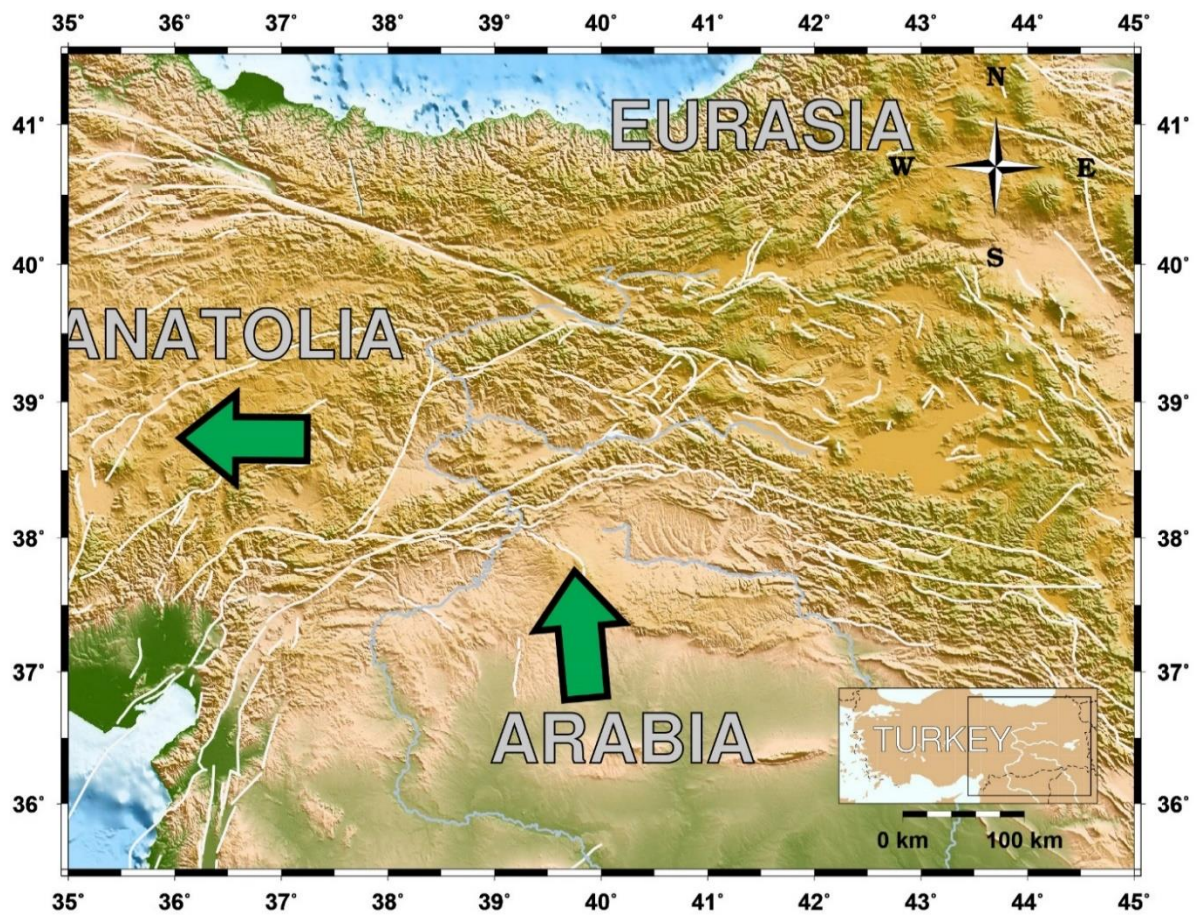


Figure 2.1. Tectonic plates connection and motions in the east Anatolia. Those arrows show the westward excursion of Anatolia with respect to Eurasia and northward migrating of Arabia with respect to Eurasia. White lines show those faults in this area (Emre et al, 2013).

The EAF was first described by Allen (1969) and mapped by Arpat and Saroglu (1971). It has been placed generally on the basis of seismic observations. Earthquakes related to ENS-WSW oriented faults are presenting sinistral strike-slip motion [Arpat and Saroglu, 1971; McKenzie, 1972, 1976, 1978; Hempton, 1987; Jackson and Mckenzie, 1984]. As a long narrow strip of active seismicity and tectonism that joins the eastern end of the NAF, which has generated a notable series of westward migrating $M > 7$ earthquakes that activated almost the whole fault zone since last century [e.g., Toksoz et al., 1979], the EAF has been comparatively quiescent with quite a few large seismic event on record since the last century [Ambraseys and Jackson, 1998].

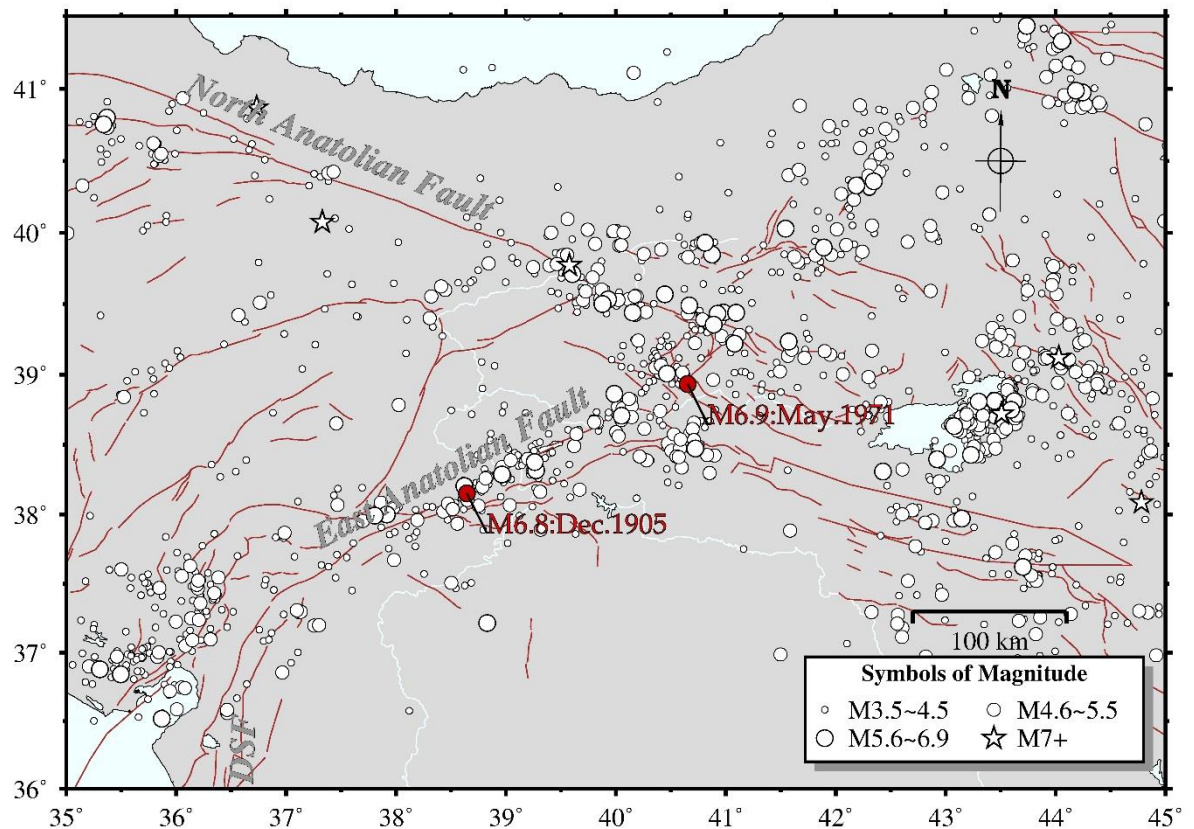


Figure 2.2. Main earthquakes (circles and stars) happened since last century and faults' location (brown lines) in East Anatolia. Annotations in red show the two large earthquakes happened in last century along EAF. (Earthquake catalog is from USGS which is short for United States Geological Survey.)

The present slip rate through the entire EAF varies from 6 to 10 mm/y as the result of variant measurement techniques (seismic moments of earthquakes [Taymaz et al., 1991]; GPS measurements [McClusky et al., 2000]). Additionally, Bulut et al. (2012) latterly had ascertained low seismicity rates along the eastern part of the EAF (from 38°E to 41°E) for the time period 2007 ~ 2011. In the past 500 years, there are also some periods of low seismic activity identified in this area, for example, during the years from 1544 to 1789 [Ambraseys, 1989]. In the next 116 years followed, a series of large earthquakes occurred, then this area underwent another period of quiescence [Cavalié, O. and S. Jónsson, 2014]. Those known strongest earthquakes along the EAF happened on November 29, 1114 ($M > 7.8$), March 28, 1513 ($M > 7.4$) and March 2, 1893 ($M > 7.1$) [Ambraseys and Jackson, 1998], and there were only two huge earthquakes ($M > 6.5$) throughout the last century – recorded on December 4, 1905 with M 6.8 and on May 22, 1971 with M 6.9 [Nalbant et al., 2002] (Figure 2.2). Ambraseys [1970] introduced that the EAF was seismically active while the NAF was relatively silent, and Cetin et al. [2003] explained the apparent seismic silence along the EAF with the indication that the fault is currently locked. However, according to the recent study of Bayrak et al. (2015), the EAF was divided into five seismic regions (Figure 2.3), and the Region 2, in which the Hazar-Palu segment is, was indicated to be the second most dangerous region with the mean return period ranging between 16 and 122 years for magnitude 5.0 and 6.0. The expected maximum magnitude (M_t) for the following 100-year time interval was estimated as 6.0. And it also indicated that Hazar- Palu segment's seismic activity is especially higher than other places of the EAF. The probability for earthquake occurring with respect to the maximum expected magnitude during the time span of 25-50-100 years was plotted as the Earthquake hazard curve of this region (Fig. 2.4). Hence, studying of this area still remains great significance.

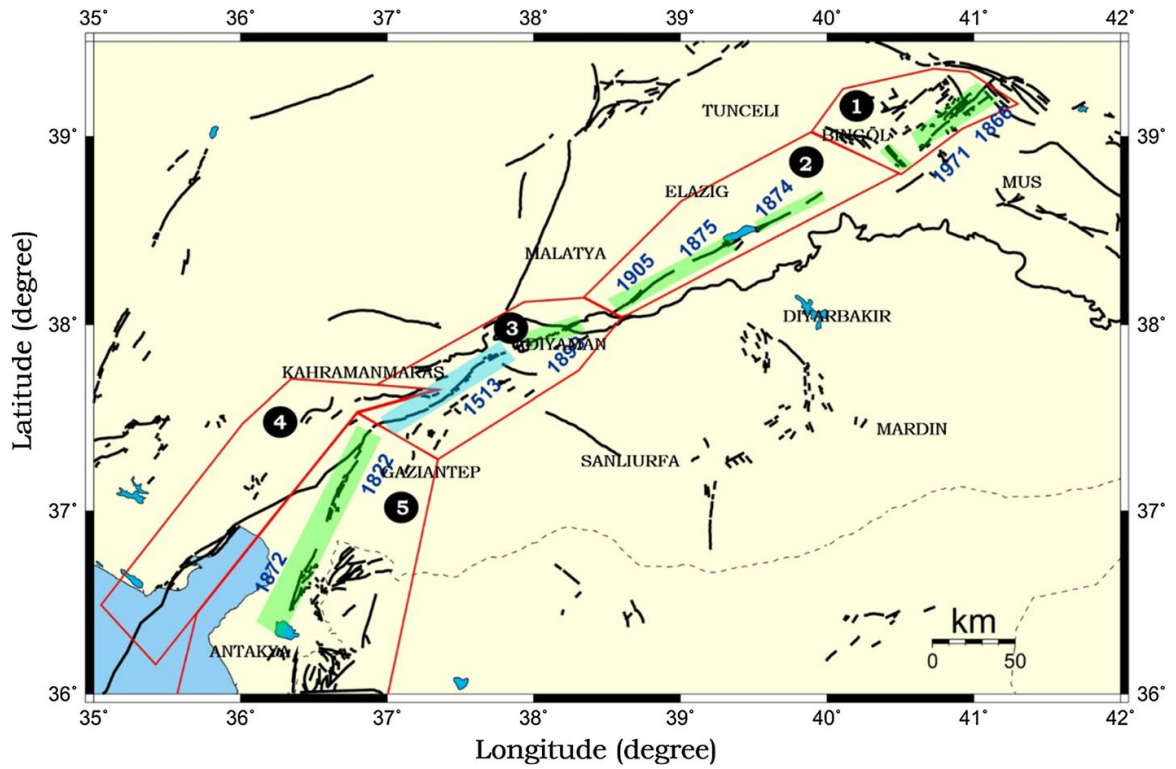


Figure 2.3. Seismic region along East Anatolian Fault and major earthquake developed surface fault between 1822 and 1971 (Bayrak et al, 2015).

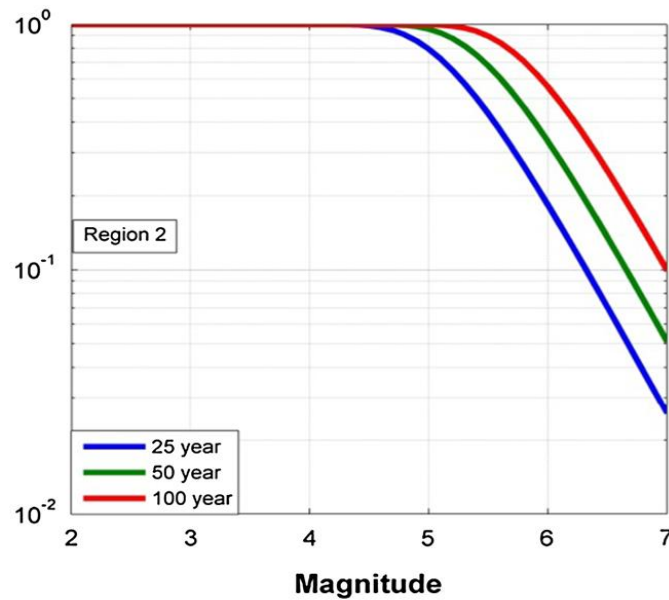


Figure 2.4. The probability of earthquake occurring for region 2 in EAFZ (Bayrak et al, 2015).

3. DESCRIPTION OF GPS TIME SERIES

Generally, the time series refers to a series of position data points which consists of consecutive measurements made over a successive time interval with at most one data point in each unit. Time series analysis is consist of multiple methods to break down time series data for purpose of extracting significant statistics and other meaningful characteristics of the data. Those methods can be usually divided into two sections, which are time-domain methods and frequency-domain methods, involving the concepts of Fourier transform, power spectral density and, sometimes, Wavelet analysis in signal processing.

GPS time series are related with changing position of target place. Clearly, GPS time series usually consist of four main components (i) Trend, which exists as there is a long term increase or decrease in the data; (ii) Seasonal, which is a long-term regular pattern existing in data due to seasonal factors; (iii) Cyclic, any pattern showing up rises and falls without regular period; (iv) Irregular, other unpredictable random variable existing in data [Mann 1995].

However, in practice, GPS time series X_t are usually regarded as comprising three components: a seasonal component S_t , a trend-cyclic component T_t which is contacting both trend and cyclic, and an irregular or remainder component E_t . Then, a proper model will be established for decomposing those three components from time series to achieve a purpose that all of them except irregular one can be given appropriate explanation. There is a common model for GPS time series, the additive model [Friedman and Stuetzle, 1981]:

$$X_t = S_t + T_t + E_t \quad (3.1)$$

The additive model (Figure 2.1) is the most appropriate model because of the magnitude of the variation around the trend-cyclic or the seasonal fluctuations do not change with the level of the GPS time series.

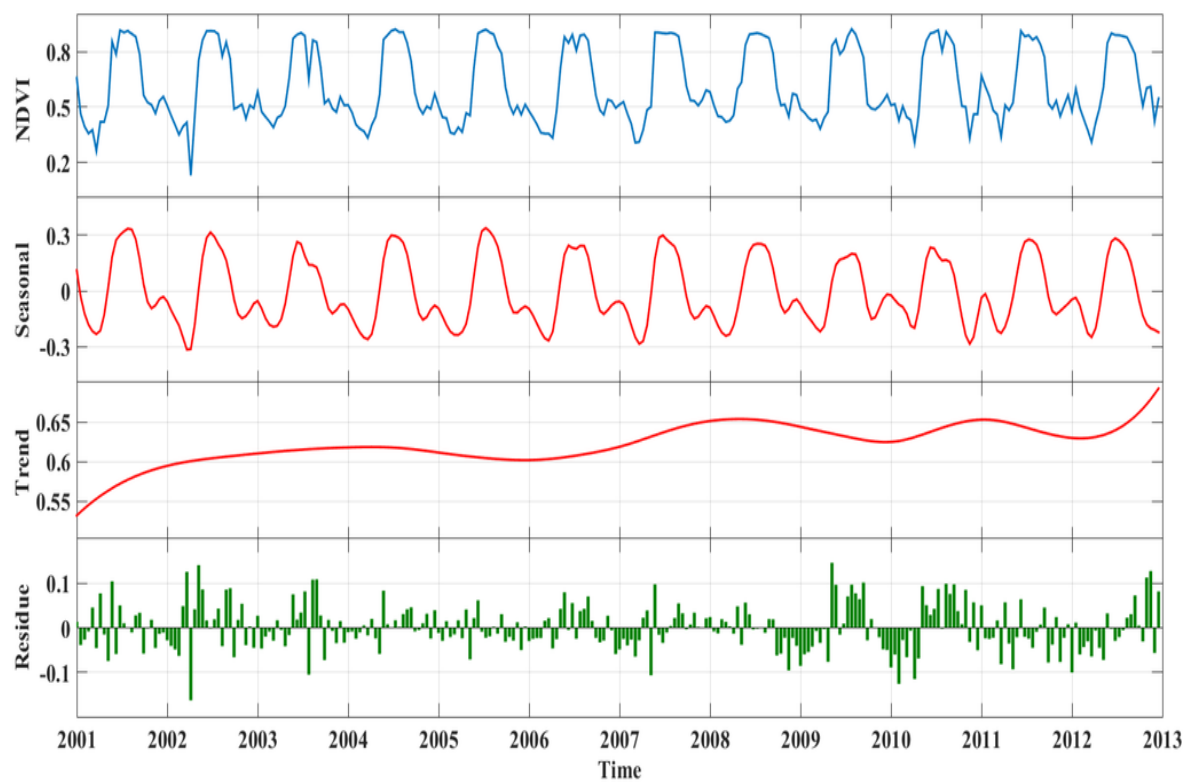


Figure 3.1. An example of additive model decomposition in time series [Kong et al, 2015].

3.1. Noise Analysis

GPS time series are recognized as a series of sample signal defined at discrete position in time. This kind of physical signal can be transferred to frequency domain signal and then decomposed into several discrete frequencies components, or a spectrum of frequencies over a continuous range, according to Fourier analysis, which is a concept of signal processing. The power spectrum (or power spectral density, i.e. PSD) of a time series describes the distribution of power into frequency components composing that signal. The estimation of power spectrum is to estimate the spectral density of an irregular component from a time series samples [Wibur B. et al, 1987].

Noise in the GPS position time series can be depicted as a power law process of which the power spectrum has the form as follow:

$$P_x(f) = P_0 \cdot \left(\frac{f}{f_0}\right)^\kappa \quad (3.2)$$

where f is the temporal or spatial frequency, P_0 and f_0 are normalizing constants, and κ is the spectral index [Mandelbrot and Van Ness, 1968]. With respect to the different spectral index, the character of power law for noise in time series can be presented by several sorts of models. For the white noise, the spectral index κ equals to 0 with constant power spectral density. For the colored noise, the index κ has value of -1 for flicker noise and of -2 for random walk noise (Figure 2.2). According to the previous studies of Zhang et al. (1997) and Mao et al. (1999), the noise in continuous GPS time series was most properly described by a combination of white noise and flicker noise models. Williams et al. (2004) agree with this but also suggest that the amplitude and spectral index of the power law noise should be estimated simultaneously with white noise.

3.2. Noise in GPS Time Series

As a main part of irregular component, noise in GPS time series is big concern, which principally consists of white noise and colored noise. White noise means a random signal with data point uncorrelated in time as well as with a flat power spectrum, which is equally sampled in the logarithm of frequency with almost flat slope, the other existing noises in the signal with totally different features are generally called Colored noise, mainly comprised of flicker noise and random walk noise. Power spectral density of the flicker noise spectrum is proportional to $1/f$ and power spectral density of the random walk noise is proportional to $1/f^2$. (Figure 3.2).

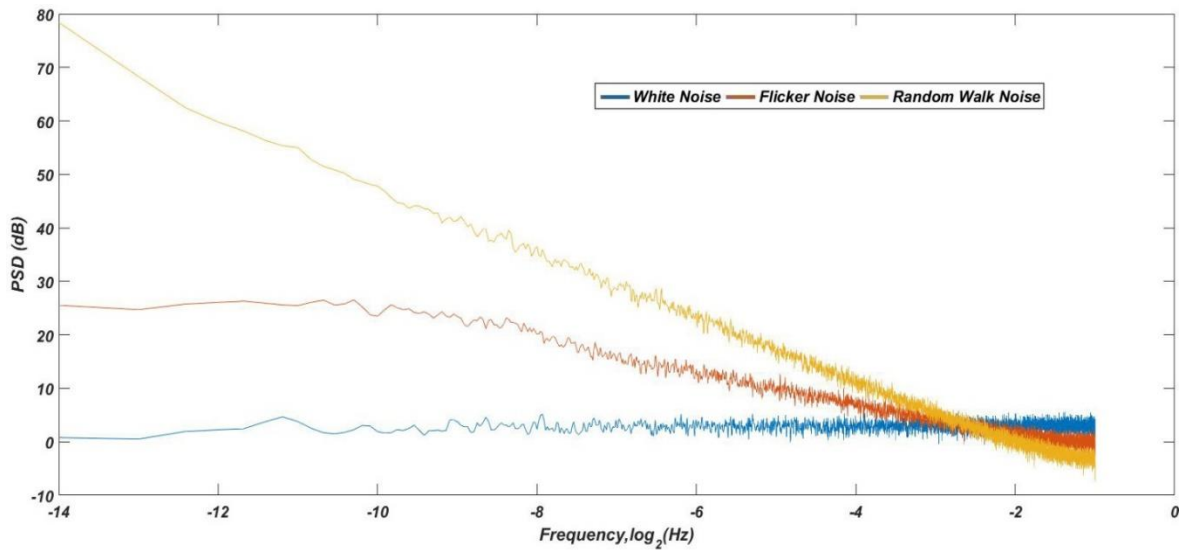


Figure 3.2. Power spectrum of white noise, flicker noise and random walk noise.

4. GPS TIME SERIES ANALYSIS

4.1. GPS Data

Since it was established two decades ago, GPS has found tremendously wide range of utilization in geodynamics and geodesy, and become major tool for studying crustal deformation and earthquake [Hager et al., 1991; Feigl et al., 1993; Segall and Davis, 1997; Niu et al., 2005;]. High-precision geodetic measurements with GPS play vital roles for estimating station coordinate and velocities, stochastic or fundamental interpretation of inter-seismic deformation, satellite orbits, atmospheric delays and Earth orientation parameters. As a critical scientific infrastructure of Turkey, the Continuously Operating Reference Station Project (CORS-TR) was carried out to monitor Earth deformation, plate tectonics and ionosphere around the whole area of Turkey using Real Time Kinematic (RTK) satellite navigation technique, which mainly provides high-precision position data derived from GPS. It contains 146 continuously operating stations covering Turkish mainland and northern Cyprus Island at an 80-100 km distance density (Fig. 4.1) [Mekik et al., 2011].



Figure 4.1. Distributions of the GPS stations belong to CORS-TR of TNPNGN-Active

CORS-TR, which was then affiliated to Turkish National Permanent GNSS Network-Active (TNPGN-Active), has become fully operational since 2009. Each station is located at low risk, stable place and equipped with Trimble NetR5 reference station receiver and Trimble Zephyr Geodetic antenna. GPS data generated at those continuous stations, which has sampling interval for collection of either 30 sec per day (24h) or 1 sec per hour, are transferred via TTVPN and 3G technique to 3 control centers owned by the General Directory of Land Registry and Cadaster (TKGM) and General Command of Mapping (HGK). Most of the stations can keep functioning 24/7 with enough power and be sustained for more than decades, and have good sky visibility on wide flat (Fig.4.2) [Mekik et al., 2011].



Figure 4.2. IGIR (Iğdir) and DIYB (Diyarbakir) stations of TNPGN

Data from each station are stored as Receiver Independent Exchange (RINEX) format [Mekik et al., 2011]. It is a standard format, designed to develop over time according to new sorts of satellites navigation systems and measurements, allowing researchers to do the post-process of raw data in order to come out with more accurate results [Gutner et al., 1989]. However, RINEX files sometimes may provide incorrect header format due to mistakes of initial setup for receivers. Often encountered problems are improper receiver or antenna types and garbled or illogical data format. Therefore, the Translation, Editing and Quality Check (TEQC) software package were developed by UNAVCO, a non-profit university-governed consortium which facilitates geoscience research and education using geodesy, to solve such pre-processing problems with GPS data, in raw (company format) or RINEX

format. Briefly, TEQC can be used to translate certain native binary formats (e.g., Trimble *.dat) to RINEX observation and/or navigation files, edit all existing RINEX files' header and output the result in new files, check the quality of a valid RINEX observation files and create a new RINEX file with different sample interval [Estey and Meertens, 2014].

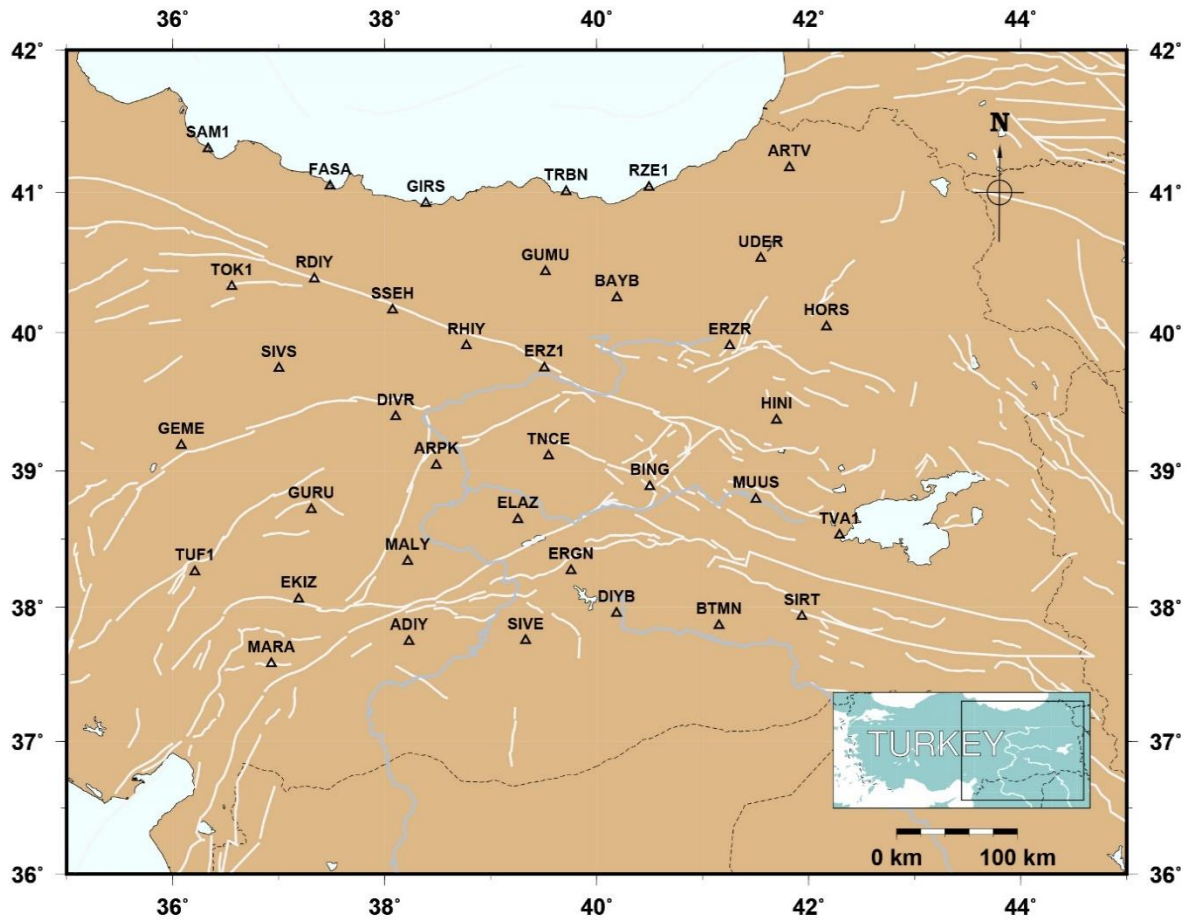


Figure 4.3. Selected TNPGN-Active stations in East Anatolia to test our methodology.

Table 4.1. TNPGN-Active stations used in this study.

St. Name	Province	County	St. Name	Province	County
ADIY	Adiyaman	Merkez	HORS	Erzurum	Horasan
ARPK	Malatya	Arapkir	MALY	Malatya	Merkez
ARTV	Artvin	Merkez	MARA	K.Maras	Merkez
BAYB	Bayburt	Merkez	MUUS	Mus	Merkez
BING	Bingöl	Merkez	RDIY	Tokat	Resadiye
BTMN	Batman	Merkez	RHIY	Erzincan	Refahiye
DIVR	Sivas	Divirgi	RZE1	Rize	Merkez
DIYB	Diyabakir	Merkez	SAM1	Samsun	Merkez
EKIZ	K.Maras	Ekinözü	SIRT	Siirt	Merkez
ELAZ	Elazig	Merkez	SIVE	Sanliurfa	Siverek
ERGN	Diyabakir	Ergani	SIVS	Sivas	Merkez
ERZ1	Erzincan	Merkez	SSEH	Sivas	Susehri
ERZR	Erzurum	Merkez	TNCE	Tunceli	Merkez
FASA	Ordu	Fatsa	TOK1	Tokat	Merkez
GEME	Sivas	Gemerek	TRBN	Trabzon	Merkez
GIRS	Giresun	Merkez	TUF1	Adana	Tufanbeyli
GUMU	Gümüşhane	Merkez	TVA1	Bitlis	Tatvan
GURU	Sivas	Gürün	UDER	Erzurum	Uzundere
HINI	Erzurum	Hinis			

RINEX data from 37 TNPGN-Active stations (Figure 4.3, Table 4.1) are selected in eastern Turkey for our test studies. TNPGN-Active uses the Hatanaka file compression strategy for all those RINEX data files. Conversion program CRX2RNX from Geospatial Information Authority of Japan (GSI) can be operated in the UNIX system to convert the Hatanaka files into RINEX observation files. Then these files were processed by GAMIT/GLOBK (version 10.6 in this study) to obtain high-precision coordinates of stations and relevant solutions [Herring et al, 2015].

4.2. GPS Data Processing

GAMIT/GLOBK is a comprehensive software toolkit applied to implement GPS analysis models, which is developed by the Massachusetts Institute of Technology (MIT), the Harvard-Smithsonian Center for Astrophysics (CfA), Scripps Institution of Oceanography (SIO), and Australian National University (ANU). GAMIT is short for GPS Analysis at MIT with purpose that is organizing the data, both station log sheets and receiver output, in a way which it can be processed efficiently by the program modules, such as makex, fixdrv, arc and model. GLOBK stands for Global Kalman filter VLBI and GPS analysis program, which is designed to combine solutions from quasi-observations by using Kalman filter [Herring et al, 2015] (Appendix A) .

4.2.1. GAMIT Processing

For GAMIT processing, the directory named tables is crucial to define the correct information about data set. It contains several types of files, such as: (1) station.info, the file provides receiver and antenna information for each site; (2) sestbl., session control table, it is specifying the a prior measurements errors and satellite constraints and the main method of analysis (Appendix B); (3) process.defaults, files to give the directory names of processing sources and solution, and other control environment parameters (Appendix C). (4) sites.defaults, files to control the use of stations in the processing, especially the global stations whose data can be downloaded remotely (Appendix 5); (5) apr file and L-file, both of them include the coordinates of all the stations to be used in the GAMIT and GLOBK, they help you get proper a prior coordinates for the processing.

In this study, we ran the whole GAMIT daily solutions on the computer clusters of Turkish National Science e-Infrastructure (i.e. TRUBA), by using SLURM (Appendix D), from 2014 to 2015 of 37 CORS-TR sites and 12 IGS sites (i.e. NOT1, GLSV, NICO, ZECK, BUCU, CRAO, RAMO, YEBE, TUBI, WTZR, ISTA, and GRAZ). Completing for once

this whole GAMIT process cost only a week, which will take more than two month if it is operated in single computer. In the processing, we used International Terrestrial Reference Frame 2008 (ITRF08) as the reference frame and fixed the orbits by setting the mode of experiment as BASELINE. And the Vienna Mapping Function 1 (VMF1) was also invoked, which is derived at 6-hour intervals from numerical weather model (NWM) and updates daily [Boehm et al., 2006b]. Inspecting the final result from the processing recorded in GAMIT summary files, in “sh_gamit_ddd.summay” file in each day directory (ddd refers to Julian day), we found that most of the expected data were included except one station with too much noisy phase among some of those days, the station BTMN. Despite of this station, a large amount of sites have about 2500 “good” marked for daily data set shown in the editing report of module autcln’s action, which is acceptable. And every one of these sites has values of 5-12 mm of one-way post-fit root mean squares (RMS) residuals by satellite and station. The percentage of wide-lane (WL) and narrow-lane (NL) ambiguities resolved is at least above 88% for each day’s solution. It is shown in Figure 4.4 of a bad day and a good day solution of station BTMN as an example for this result.

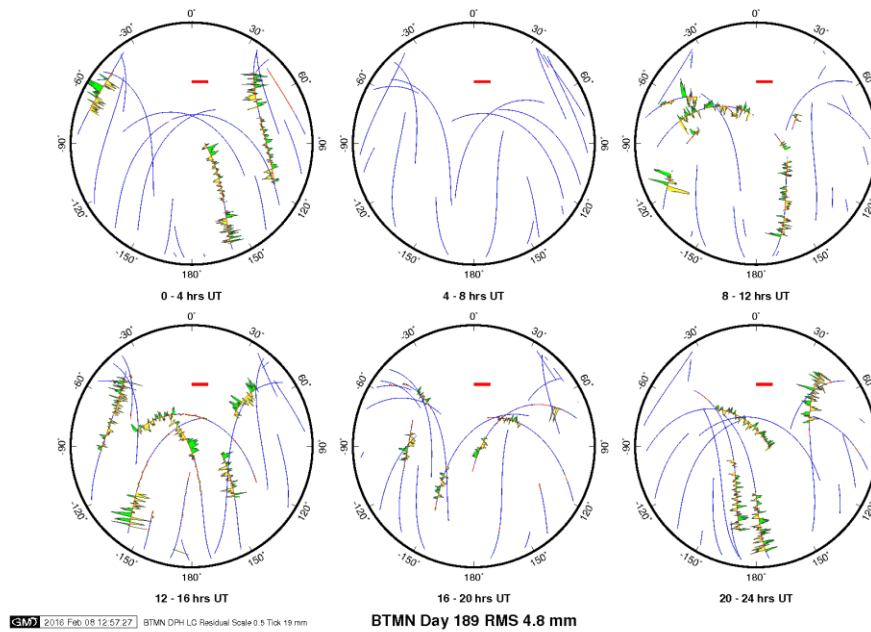


Figure 4.4. Sky plots of BTMN station on July 8th, 2015, which shows phase residuals of GAMIT daily solution. The ticks outside of circle indicate the station’s azimuth from 0 ~ 360°, 0° is in the north direction. Blue dots describe the received satellites path at that day from elevation 0 ~ 90°.

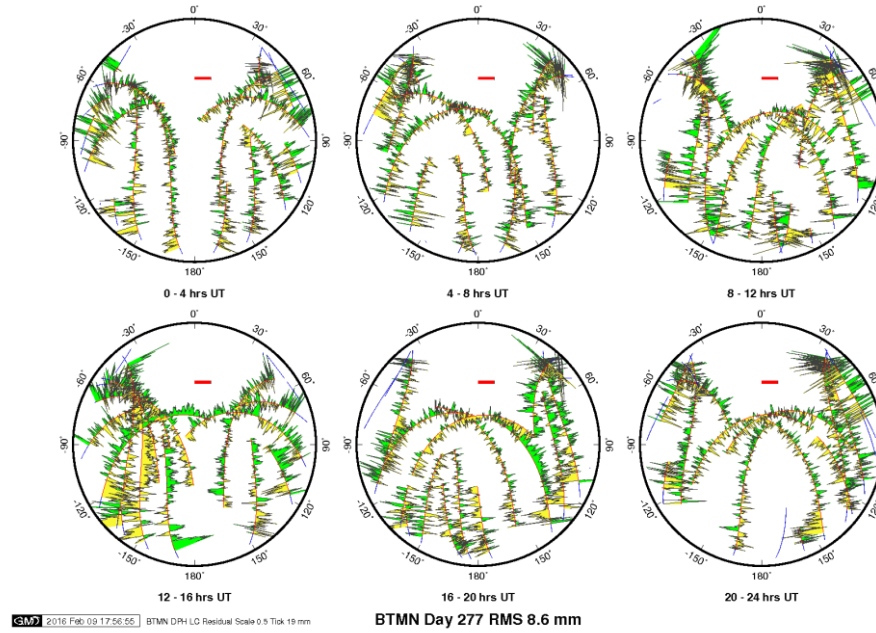


Figure 4.5. Sky plots of BTMN station on October 4th, 2015, which has an acceptable daily solution. Compare it with Figure 4.4.

4.2.2. GLOBK Processing

After obtaining the primary solution loosely constrained, we apply those in the final combine solution with GLOBK to estimate station positions' time series and velocities [Dong et al, 1998]. It involves four different program modules: (1) htoglb, it converts the ASCII solution files from GAMIT to globk binary h-files; (2) globk and glred, these two modules are almost alike except the way they treat h-files, they both use those binary h-files as input to a Kalman filter together with the an a-prior station files, an Earth orientation parameter table and the command files to generate a combine solution, but glred provides a method of producing coordinate repeatabilities rather than a strict Kalman back solution as globk does; (3) glorg, it performs generalized constraints to those combine solutions, which has the reference frame of the solutions to be fixed after the combination. It can be invoked from within globk/glred.

The ‘loose’ GAMIT daily solutions from 37+12 sites provide a group of ASCII h-files for input to GLOBK to produce day-to-day repeatability time series (as an example, Figure 4.7) and the combined binary h-files for further estimation of station velocities. Here we used 11 of those IGS station (exclude GLSV due to not very good stability, refer to Table 4.2) applied in GAMIT for the sites stabilization.

Table 4.2. Selected IGS stations for stabilization in GLOBK process.

Station	Location
NOT1	Noto, Italy
NICO	Nicosia, Cyprus
ZECK	Zelenchukskaya, Russia
BUCU	Bucharest, Romania
CRAO	Crimean Peninsula
GRAZ	Graz, Austria
RAMO	Mitzpe Ramon, Israel
WTZR	Wettzell, Germany
YEBE	Yebes, Spain
ISTA	Istanbul, Turkey
TUBI	TUBITAK, Turkey

For the GLOBK command files, the maximum chi-square, pre-fit coordinate difference and rotation for an h-file to be used are 100, 5.0 m and 20000 mas, respectively. And the maximum sigma for each component of time series to be limited are North 5 mm, East 5 mm and Up 20 mm. A priori constraints on each site for three component are all 20 (m). As for satellite orbit parameter, it is suppressed in the output because the constraints which were present in the input h-files are used. The Earth rotation parameters (EOP) are treated loosely with the UT1 and pole position are 10 mas and the rates of change are zero.

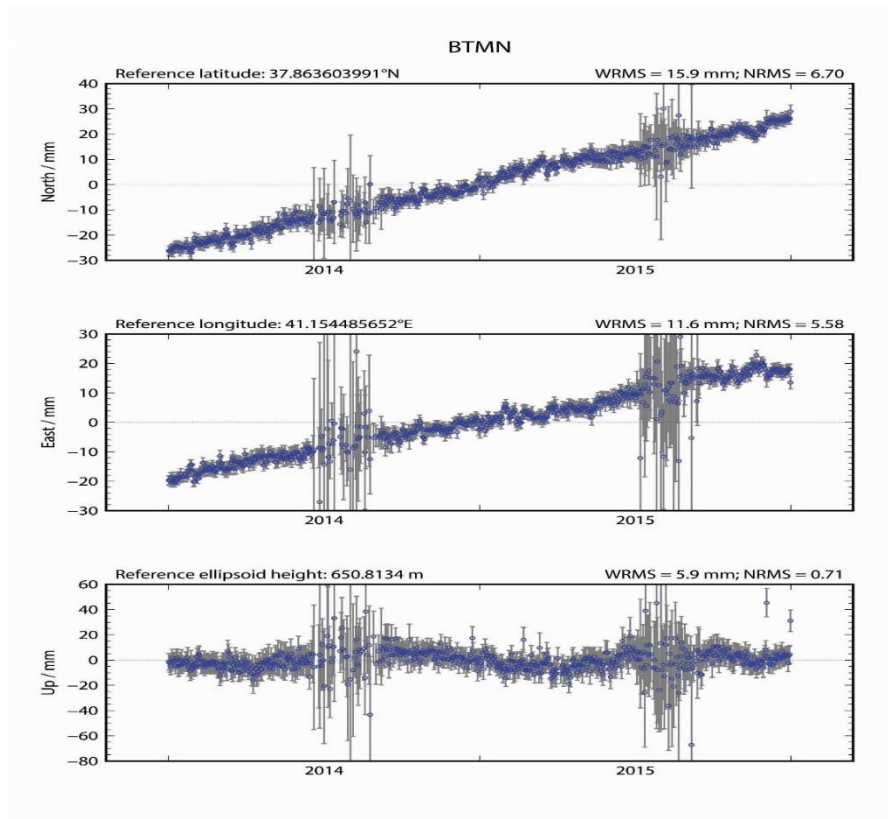


Figure 4.6. Position time series of station BTMN.

From the GAMIT process, it has been known that the station BTMN receives signal with noisy phase on several specific days. Correspondingly, the position time series of this station shows points with large error bars and fluctuation on those specific days. However, the trend of the whole time series is still seemed smooth and linear, so the estimation of velocity in later process will not be affected.

4.3. Time Series Analysis Strategy

4.3.1. Remove outliers and offset

When carried in to GLOBK as quasi-observations, the h-files were considered individually first by using glred to generate time series. However, this solution may be corrupted if the included data are statistical outliers. An error existing in one component of a site's time series will have no effect on any other site and may barely affect the other components, but once the h-files are combined with common parameters, whether results from multiple days or combined subnetworks on a single day, the uncommon estimates from the same parameter will conflict, which will raise the value of chi-square and twist the solution [Herring et al., 2015]. For the purpose of a clean time series, the outliers should be removed first. Some outliers may be caused by the stability issues. To exclude outliers, we present a linear trend fitting to the original raw time series by using least-squares estimation and afterwards calculate the differences between the linear trend and observation data to produce residuals, which are ordered by size. And then the computation of the interquartile range is carried out, that is the value at 75% of the ordered array of the residual minus the value at 25% of it. Residual with a value < 3 times this interquartile range, below or above the median, is regarded as an outlier [Langbein and Bock, 2004]. Here we use the rename command of the eq_file in the globk command file to remove those outlier, here the extent of each renames are specified as XCI which will exclude all the data from both solutions of position and velocity. We accomplished the removal by iterated steps while trying to generate clean time series plot: Firstly, we ran the script sh_plot_pos on those glred solution files (*.org) with the specific tsfit command file which includes the maximum sigma constraints mentioned previously to produce PBO-style pos files as well as GMT plot of time series for each of the stations and create a rename file containing those unfit data; Secondly, we ran glred again having this rename file in the globk command file to generate new solution files without those data of defined outliers and then ran the sh_plot_pos for the second time to gain new pos files; Thirdly, we remove manually some outliers skipped from second step via the program Tsview, a Matlab based interface program will be described later in this chapter, which also can create a rename file contain those manually removed outliers'

information; Finally, we introduce the newly generated rename files in another glred run to derive the final solution files as well as the final time series GMT plot and pos files produced by sh_plot_pos. When we ran the script sh_plot_pos, a pair of histograms showing the distribution of weighted and normalized root mean squares (rms) day-to-day repeatabilities can also be generated. Here are the outcomes of those distribution from the first automatically removing outliers step and the second manually removing outliers step (Figure 4.8 – 4.11): The time series weighted rms (WRMS) and the normalized rms (NRMS) just have varied slightly through these two steps. After ultimately removing the outliers, for all 49 stations, the mean and standard deviation of WRMS for north component are 1.6 mm and 0.7 mm, for east component are 1.8 mm and 0.8 mm and for vertical component are 4.9 mm and 1.4 mm, respectively, and the mean and standard deviation of NRMS for north component are 0.7 mm and 0.3 mm, for east component are 0.9 mm and 0.4 mm and for vertical component are 0.6 mm and 0.1 mm, respectively. From the result we can see that the distribution of scatters among our sites is approximately Gaussian with the median nrms ~ 1.0 and the most sites' horizontal components have value of wrms 1-2 mm. It indicate that the number of outliers has be reduced to a reasonable level without losing too much data.

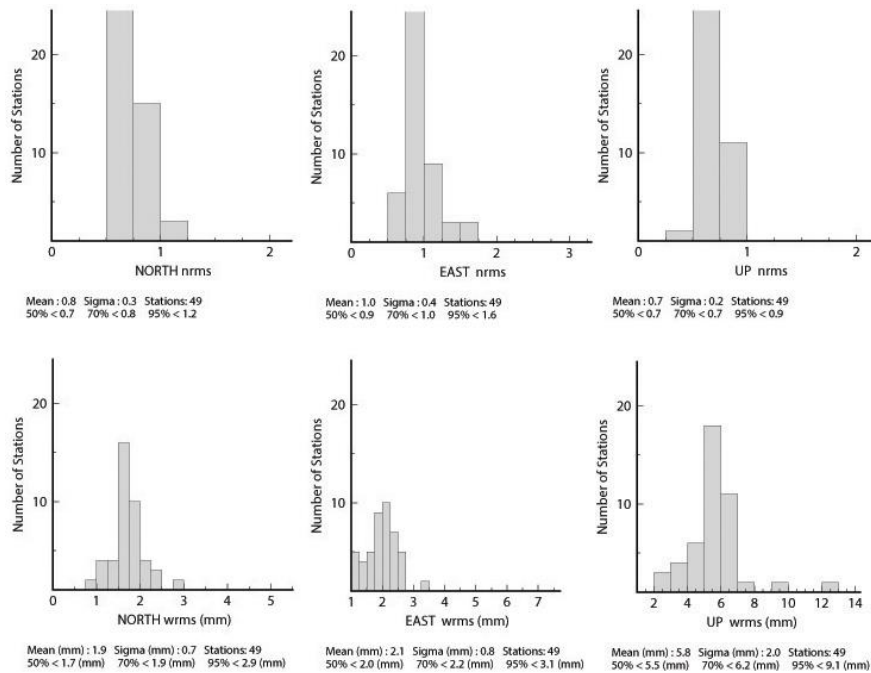


Figure 4.7. The histogram of scatter nrms and wrms for each site after the first step of removing outliers.

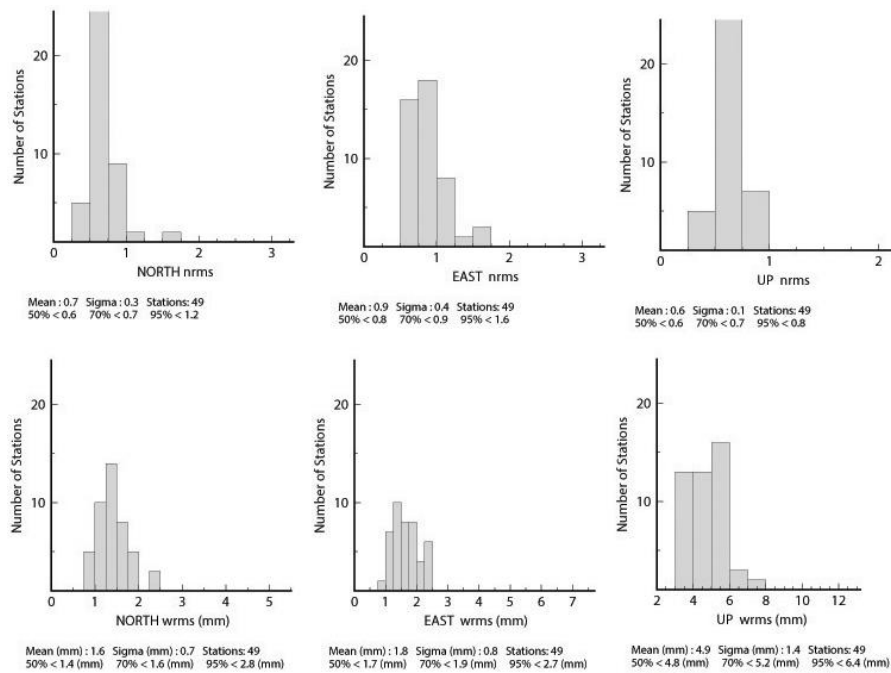


Figure 4.8. The histogram of scatter nrms and wrms for each site after the second step of removing outliers.

During the timing we chose, there were several moderate seismic events ($M_w > 4.8$) that have occurred in the area those sites are distributed (Table 4.3).

Table 4.3. Earthquakes recorded along the area where the stations are selected.

Earthquake Names	Date	Mw.	Depth
Kigi-Bingol Earthquake	Dec. 2 nd , 2015	5.3	10.66 km
Hekimhan-Malatya Earthquake	Nov. 29 th , 2015	5.0	17.45 km
Erbaa-Tokat Earthquake	Oct. 9 th , 2015	4.9	20.17 km

* Earthquake information from BOUN KOERI Regional Earthquake-Tsunami Monitoring Center.

Here we can use again the syntax “rename” in eq_file to eliminate the offset caused in time series by those earthquakes or a different one that define those events by details in the same file.

After getting the cleaned time series (Figure 4.9), one can perform the noise analysis, trend rate estimate, periodicity analysis, and the velocity solution in specific reference frame for each component of the stations' time series.

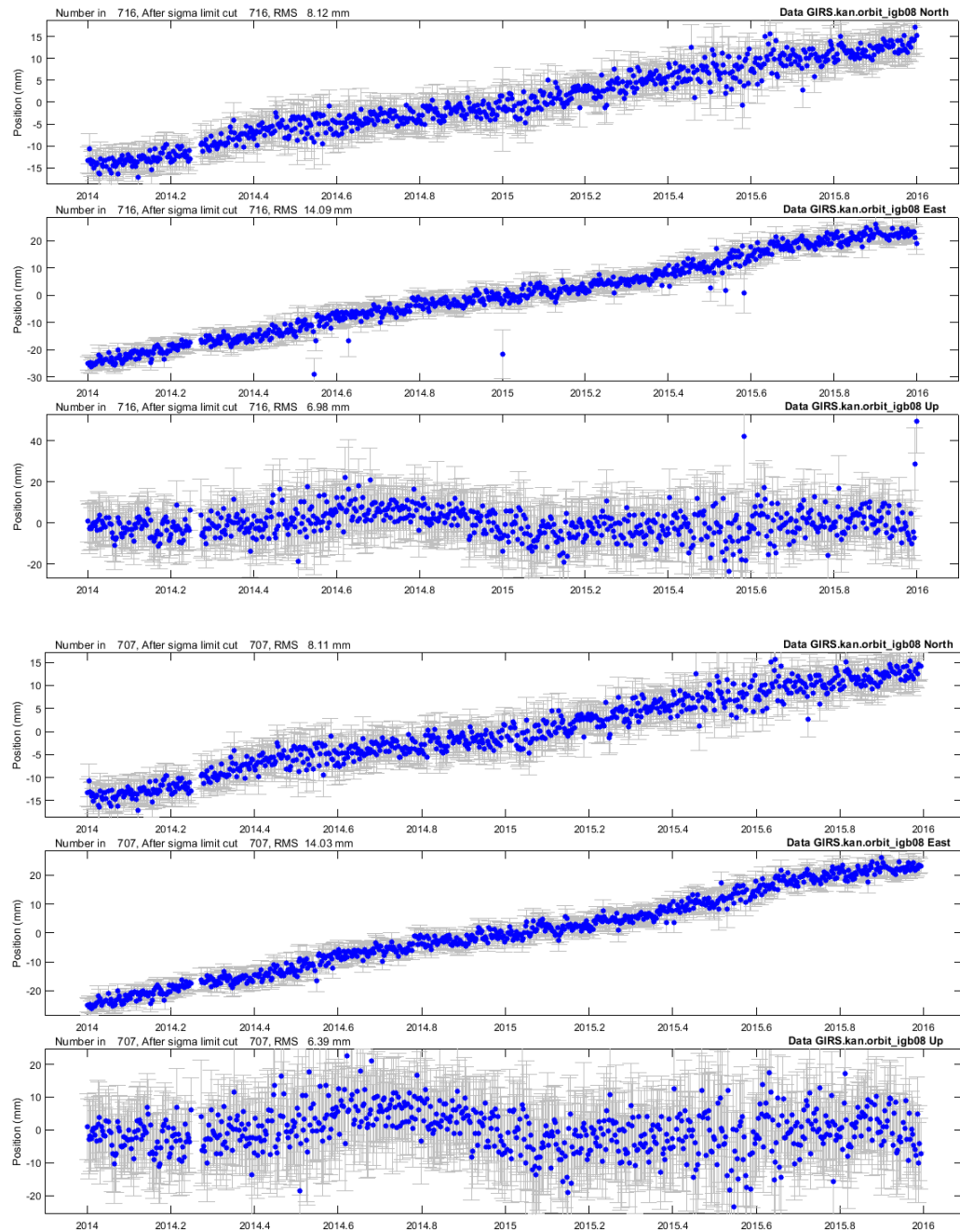


Figure 4.9. Examples of raw time series and cleaned time series.

4.3.2. First Order Gauss-Markov Extrapolation

The primary way which accounts for the long term noise that mostly influences the linear trend rate estimates is by introducing a random walk to the noise model used by globk. The appropriate value of the random walk noise for each component of estimated time series can be extrapolated using the First Order Gauss-Markov (FOGM) process [Herring, 2003]. This process uses the scatters in the time series for all available averaging time, for example, 1 day to 365 days for a 730-day time series, to determine how the time series statistics depart from white noise, that is the χ^2 -per-degree of freedom of the average value are computed. For almost all time series, the χ^2 -per-degree of freedom increases as the averaging time goes up. Whereas the value would remain constant if it was a white noise process. The rate of increase is fit to a correlation function of time for the noise process, and the function is aimed to compute realist sigma for the fits by scaling the white noise estimates of the sigma. Later section (4.3.1.) will give details and examples about this process.

4.3.2.1. Analysis Software: Tsview Tsview is a tool based on Matlab to access the quality of GPS time series and to generate control files for GLOBK which will exclude bad site position estimates and account for jumps in time series (Figure 4.10). We can use the feature of “edit” to delete individual points from the time series and that of “break” to select times graphically for break offset. Also, Tsview can read a globk eq_file to automatically add breaks and earthquake on loaded GPS time series that would be used by globk. These feature helped us a lot in removing outliers and offset in GPS time series. Another feature named Real Sigma of Tsview is used here to perform the Realist Sigma algorithm that assumes the noise model process is a FOGM process.

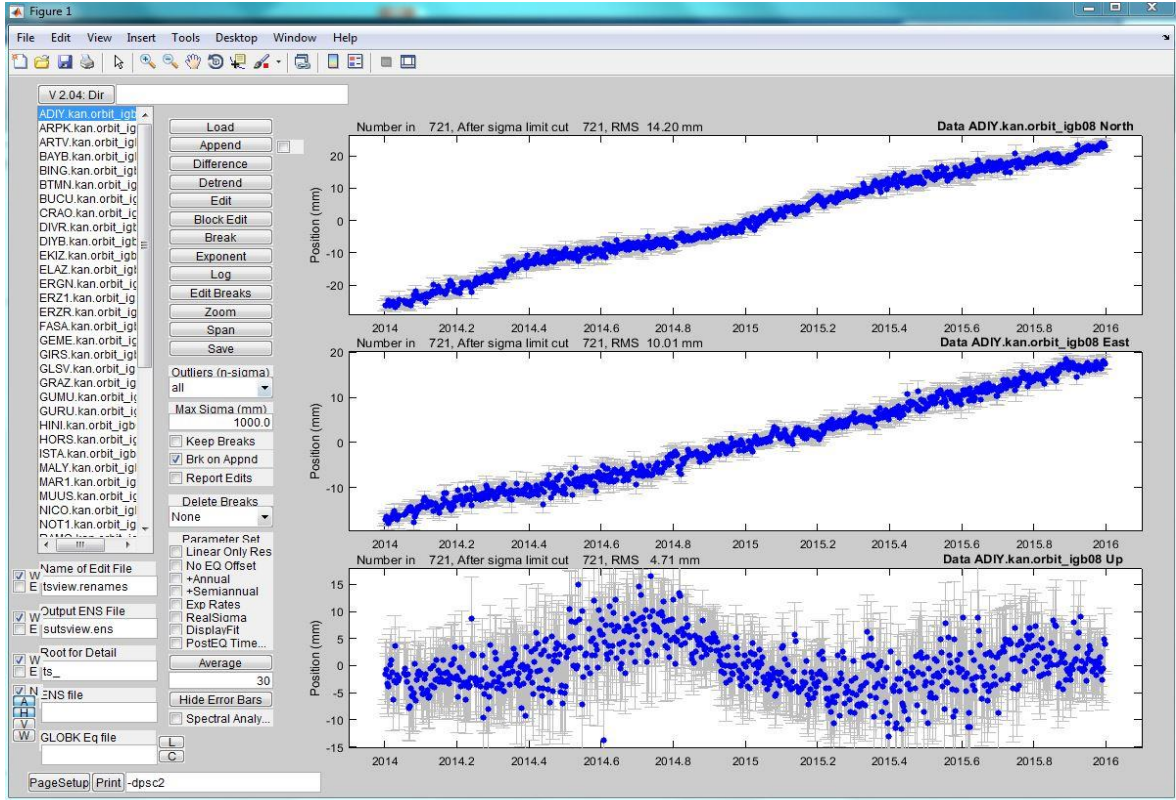


Figure 4.10. Interface of Tsview for GPS time series analysis

4.3.3. Maximum Likelihood Estimate

Another way to measure the noise in time series mainly discussed in this study is to use power law plus white noise models in the estimation, which is based on the theory of the Maximum Likelihood Estimation (MLE) method. The MLE is the mostly applied technique for noises analysis in the GPS time series [e.g. Langbein and Jonson, 1997; Zhang et al., 1997; Mao et al., 1999; Williams et al., 2004], which is defined by that the likelihood linear function is maximized while estimating the noise components and parameters whose values have occurred for the given observations. If a Gaussian distribution is assumed, the likelihood is as:

$$\text{lik}(\hat{\mathbf{v}}, \mathbf{C}) = \frac{1}{(2\pi)^{N/2} \cdot (\det \mathbf{C})^{1/2}} \cdot \exp(-0.5 \cdot \hat{\mathbf{v}}^T \mathbf{C}^{-1} \hat{\mathbf{v}}) \quad (4.1)$$

where **lik** means likelihood function; $\hat{\mathbf{v}}$ is the residuals to the linear trend of observations using least square; \mathbf{C} is the observation data covariance matrix, which directly influences the uncertainties of the liner parameters derived from the time series and may cause sorts of noises occurring; N is the number of the epochs.

Then the logarithm of the likelihood is maximized for better numerical quality:

$$\ln[\mathbf{lik}(\hat{\mathbf{v}}, \mathbf{C})] = -\frac{1}{2} [\ln(\det \mathbf{C}) + \hat{\mathbf{v}}^T \mathbf{C}^{-1} \hat{\mathbf{v}} + N \ln(2\pi)] \quad (4.2)$$

All details accounting for this algorithm is described by Langbein and Johnson (1997) and Langbein (2004). In this study, we referred to the reformulated MLE, which invokes creating a Toeplitz structure for covariance matrix to be inverted, discussed by Bos et al. (2008 and 2012). A Toeplitz structure matrix is a matrix that has constant values in its descending diagonal from left to right.

According to Williams (2008), the covariance matrix \mathbf{C} of the popular combination of power law plus white noise models can be written as follow:

$$\mathbf{C} = \sigma^2 (\cos^2 \phi \mathbf{I} + \sin^2 \phi \mathbf{E}(d)) \quad (4.3)$$

where \mathbf{I} is the unit matrix, which together with coefficients forms the white noise's covariance matrix, and \mathbf{E} consists in the power law noise's covariance matrix, which depends on the spectral index d . The parameter ϕ controls the distribution of the magnitude for both noise models. All variance of the noise is then set by σ^2 , which is so-called the “innovation noise” in the result. This equation can be generalized to:

$$\mathbf{C} = \sigma^2 (\phi_1 \mathbf{E}_1 + (1 - \phi_1) \phi_2 \mathbf{E}_2 + \cdots + (1 - \phi_1)(1 - \phi_2) \cdots (1 - \phi_N) \phi_{N+1} \mathbf{E}_{N+1}) \quad (4.4)$$

for those $N+1$ noise models, all parameters (ϕ) vary within $0 \sim 1$. Noise is assumed to be stationary so that makes it possible to introduce combinations of different noises, which results in creating a Toeplitz covariance matrix.

4.3.3.1. Analysis Software: Hector Hector is a software package operated in Linux system that can be used to estimate the linear trend of time series in which the temporal correlated noise exists and the parameters of the chosen noise model using the MLE method. It can make several combinations of noise model in the process, but according to previous studies [Williams et al., 2004; Bos et al., 2008, 2013; Wang et al., 2011; Klos et al., 2014, 2015] the white plus power law noise model is often used and always preferred, so we also chose this only combination for our study using the software. After the processing applied by this software, we got fractions of white and power law noise, estimated amplitude of each noise and spectral index of the power law noise in the final output files. Details about other features of this software are given in Hector user manual (version 1.5.1) [Bos and Fernandes, 2015].

5. EXPERIMENTS AND RESULTS

5.1. Noise Analysis

In the noise model analysis process, both the white noise and colored noise in the GPS observation ought to be considered of their effects. As known, the main noise in GPS time series usually have correlation times which may vary from minutes to months, such as multipath, water vapor, station distortion because of unstable monument, and etc. It will be huge mistake if we ignore that. According to the different methodology introduced in previous sections, here are two types of noise model combinations discussed.

5.1.1. Random Walk Noise Model

Once outliers and offset in time series have been removed, as well as the common-mode errors by realizing those 11 reference stations (Table 4.2), but there are still irregular factors in the time series should be considered. Long period time series show that dominant noise in a short period of time (i.e. a few days) is white noise but increases periodically for longer time [Zhang et al., 1997; Mao et al., 1999; Williams et al., 2004]. Since we analyze the time series of continuous data, we can decide the noise character in the long period of time which is related to the long-term decay after an earthquake or estimating the velocity error for each site. A single Kalman filter performed by globk is not able to implement all possible noise models, especially the flicker noise model, but good enough to realize the white noise and the random walk noise models that are used together to obtain significant short-term statistics for qualifying data and uncertainties of estimated velocities. Random walk noise caused by monument motion is mostly recognized as being present in geodetic time series. For all sites in this study with over 700 days' position estimates, the First Order

Gauss-Markov (FOGM) Extrapolation or realistic sigma algorithm [Herring, 2003] can be used to determine the reasonable value of the random walk for each component. By fitting chi-square against averaging time to an exponential function (Figure 5.7), which is obvious in FOGM Extrapolation process, and extend this function to an infinite averaging time, this algorithm not only determines the scale factor involved in the white noise velocity sigma to achieve a realistic sigma but also provides the random walk noise value (with magnitude $5.30\text{e-}7 \text{ mm}^2/\text{yr}$ and $7.46\text{e-}7 \text{ mm}^2/\text{yr}$ on the horizontal coordinates) which will derive this sigma in the combine solution.

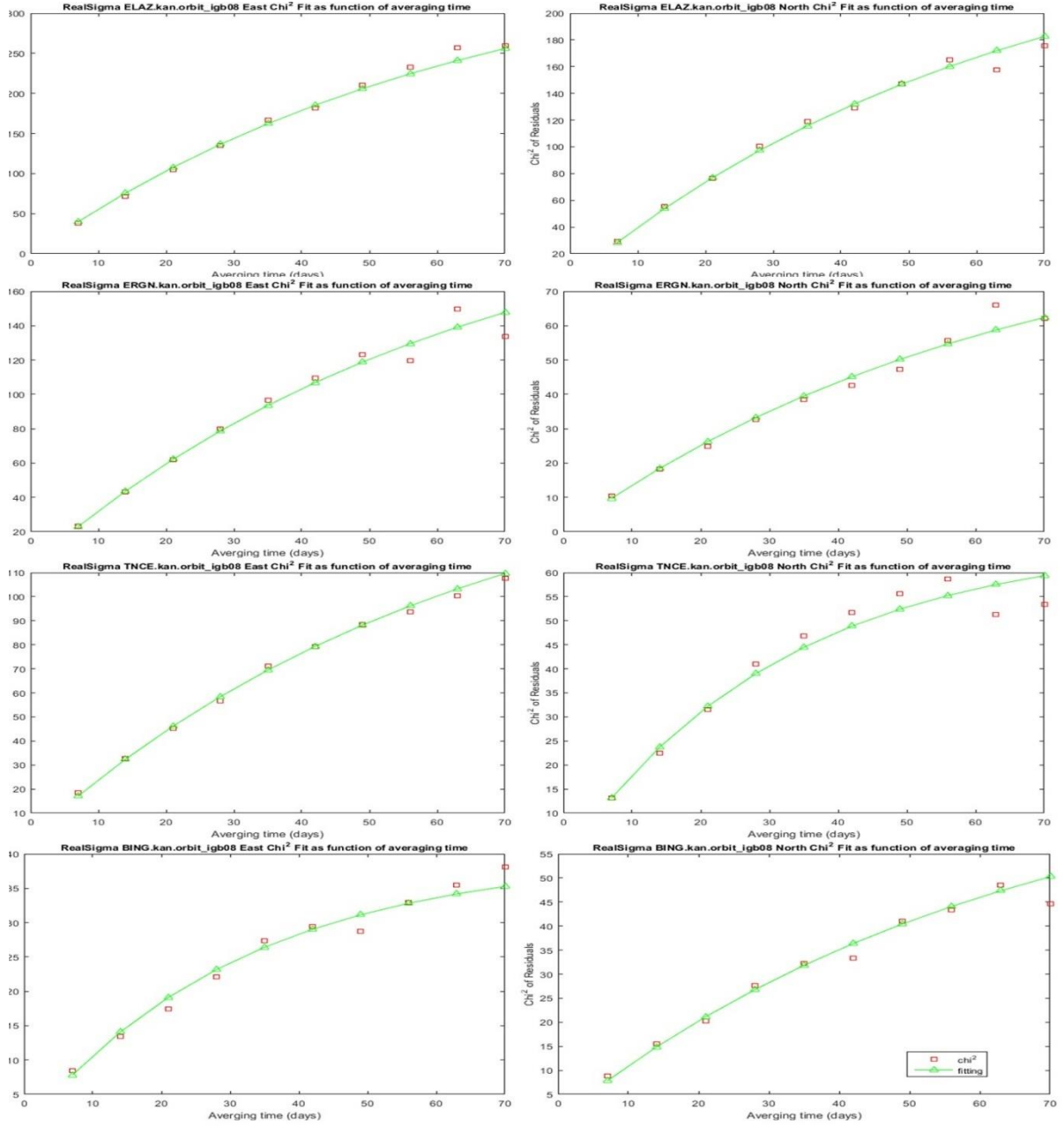


Figure 5.1. χ^2 as function of averaging interval for horizontal components at stations ELAZ, ERGN, TNCE and BING. The white noise estimated sigma are multiplied by the value of the green curve at infinite averaging time corrected for the error bar scaling.

5.1.2. White + Power law Noise Model

Noise sources are not single. It is useful to give a specific type of noise mode for all those time series. By doing so, it gets much easier to assume the sites are may affected by the same noise sources and therefore have almost alike power spectrum, and to figure out the differences among the noise characteristics. To allow the involvement of a larger amount of noise mode processes, MLE is widely applied to demonstrate an overall power law noise model which describes the data most properly. Here we use software package Hector [Bos, M.S. et al., 2013] involving MLE to estimate both linear trend in time series with temporal correlated noise and the parameters of the selected noise model. It is a sufficient tool to exhibit the power spectral density (PSD) of chosen noised model in observations which is easily to be found. The chosen noised models are a combination of power law noise plus white noise and the chosen Likelihood method is the algorithm of Ammar and Gragg (1988). Due to the noise models we chose, the noise amplitudes of them need to be estimated. As mentioned prior, the parameter ϕ decides the distribution of power law and white noise indicated as fractions. For example (Table 5.1), for noise model in the time series of station ADIY, the fraction of white noise in the east component is $1-0.693 = 0.307$ by taking note that parameter ϕ determine the distribution of variance in eq.(4) . The innovation noise σ^2 for this case has a standard deviation of 0.9415 mm, then the standard deviation of white noise is:

$$\sigma_w = \sqrt{0.307} \times 0.9415 = 0.5220 \text{ mm}$$

For the covariance matrix in Hector, it has omitted the scaling factor $\Delta T^{d/2}$ used by Williams (2003), where ΔT means the sampling period in years, since here only GPS daily solution discussed [Bos et al., 2012]. However, in order to get comparable amplitude values for power law noise using standard MLE, the estimated amplitude value is still divided by $\Delta T^{d/2}$ for this noise model:

$$\sigma_{PL} = \frac{\sqrt{0.693} \times 0.9415}{\left(\frac{1}{365.25}\right)^{0.3975/2}} = 2.654 \text{ mm/yr}^{d/2}$$

Here the number 0.3975 in exponent is the spectral index d of the power law noise showed in final result of Hector, which is $-1/2$ times the more often used spectral index κ in other papers of noise analysis on GPS time series [Williams 2003, Williams et al., 2004].

Table 5.1. Maximum likelihood results of the white plus power law noise models for time series.

Station	Power law noise ($\sigma_{PL} : mm/yr^{d/2}$)									White noise ($\sigma_W : mm$)					
	East			North			Up			East		North		Up	
	Fraction	d	σ_{PL}	Fraction	d	σ_{PL}	Fraction	d	σ_{PL}	Fraction	σ_W	Fraction	σ_W	Fraction	σ_W
ADIY	0.693	0.4134±0.0687	2.654	0.260	0.6873±0.0712	3.455	0.127	0.6636±0.0985	8.539	0.3073	0.5220	0.7399	0.7671	0.8732	3.1631
ARPK	0.637	0.4581±0.0754	3.639	0.189	0.6114±0.1016	3.237	0.224	0.6516±0.0845	12.292	0.3634	0.7117	0.8113	1.1054	0.7762	3.3479
ARTV	1.000	0.3872±0.0000	4.800	0.593	0.4325±0.0796	5.594	0.708	0.4081±0.0773	17.363	0.0000	0.0029	0.4073	1.2946	0.2923	3.3465
BAYB	0.773	0.4748±0.0681	3.691	0.615	0.5244±0.0776	3.597	0.232	0.6004±0.0880	8.726	0.2270	0.4929	0.3854	0.6063	0.7676	2.6971
BING	0.705	0.4594±0.0709	3.916	0.506	0.4726±0.0777	3.470	0.468	0.5463±0.0728	13.954	0.2955	0.6539	0.4938	0.8498	0.5319	2.9682
BTMN	1.000	0.4557±0.0000	3.736	0.678	0.4553±0.0788	3.314	0.166	0.7158±0.0987	11.946	0.0000	0.0022	0.3216	0.5956	0.8335	3.2345
BUCU*	0.886	0.3849±0.0800	2.487	0.332	0.6583±0.0747	2.663	0.718	0.4766±0.0716	9.153	0.1138	0.2863	0.6676	0.5413	0.2817	1.4050
CRAO*	0.149	0.8487±0.0840	5.237	0.274	0.5146±0.1218	3.020	0.941	0.1751±0.1336	6.428	0.8507	1.0219	0.7263	1.0777	0.0589	0.9594
DIVR	0.438	0.6409±0.0663	5.572	0.494	0.3917±0.0929	2.529	0.306	0.5410±0.0806	9.789	0.5620	0.9528	0.5055	0.8052	0.6937	2.9851
DIYB	0.292	0.7174±0.0695	4.798	0.468	0.6000±0.0656	4.118	0.379	0.4031±0.1009	7.495	0.7083	0.9006	0.5317	0.7472	0.6211	2.9216
EKIZ	0.137	0.7560±0.0931	4.734	0.436	0.4579±0.0908	3.041	0.399	0.5146±0.0864	11.638	0.8631	1.2774	0.5636	0.8949	0.6011	3.1307
ELAZ	0.484	0.6975±0.0578	6.004	0.393	0.7414±0.0638	5.610	0.064	0.8500±0.0000	11.056	0.5163	0.7924	0.6070	0.7824	0.9356	3.4327
ERGN	0.418	0.6868±0.0652	5.028	0.697	0.4430±0.0662	3.252	0.545	0.4621±0.0781	10.532	0.5818	0.7819	0.3029	0.5802	0.4550	2.4617
ERZ1	0.380	0.7160±0.0628	6.549	0.737	0.4809±0.0732	4.879	0.167	0.6835±0.0962	13.177	0.6200	1.0118	0.2629	0.7053	0.8333	3.9212
ERZR	0.590	0.5469±0.0662	4.585	0.594	0.4131±0.0950	3.124	0.352	0.5805±0.0771	12.188	0.4104	0.7619	0.4057	0.7628	0.6485	2.9859
FASA	0.979	0.3763±0.0734	2.905	0.199	0.6250±0.0972	2.451	0.323	0.4975±0.1004	7.839	0.0210	0.1402	0.8006	0.7767	0.6767	2.6131
GEME	0.428	0.7579±0.0580	7.065	0.811	0.7198±0.0504	8.975	0.403	0.4992±0.0831	8.778	0.5718	0.8725	0.1892	0.5185	0.5969	2.4493

Table 5.1. Maximum likelihood results of the white plus power law noise models for time series. (continue)

GIRS	0.406	0.5012±0.0804	4.021	0.247	0.4681±0.1065	3.108	0.132	0.5919±0.1100	10.953	0.5941	1.1087	0.7533	1.3647	0.8683	4.9050
GLSV*	0.249	0.6794±0.0757	3.679	0.668	0.6831±0.0553	6.480	1.000	0.4131±0.0000	14.138	0.7506	0.8598	0.3324	0.6094	0.0000	0.0040
GRAZ*	0.420	0.4922±0.0899	2.714	0.125	0.6894±0.1063	2.092	0.798	0.3602±0.0834	8.380	0.5797	0.7461	0.8749	0.7238	0.2025	1.4590
GUMU	0.502	0.5701±0.0662	4.346	0.741	0.3459±0.0854	2.569	0.140	0.6723±0.0926	10.330	0.4979	0.8050	0.2595	0.5482	0.8603	3.5270
GURU	0.392	0.6881±0.0634	5.102	0.327	0.4616±0.1045	2.816	0.064	0.7438±0.1223	8.739	0.6077	0.8338	0.6732	1.0352	0.9363	3.7335
HINI	0.492	0.7348±0.0603	8.184	0.276	0.8500±0.0000	7.947	0.689	0.3343±0.0989	9.863	0.5078	0.9510	0.7237	1.0477	0.3109	2.4709
HORS	0.743	0.4912±0.0732	4.940	0.487	0.5050±0.0832	3.551	0.381	0.5384±0.0813	12.047	0.2572	0.6824	0.5135	0.8222	0.6187	3.1342
ISTA*	0.655	0.2995±0.1014	1.883	0.973	0.3603±0.0743	2.595	0.617	0.4298±0.0722	10.472	0.3453	0.5651	0.0270	0.1492	0.3825	2.3191
MALY	0.203	0.7613±0.0709	4.233	0.340	0.6152±0.0762	3.221	0.181	0.6445±0.0864	9.333	0.7969	0.8874	0.6599	0.7305	0.8193	2.9678
MARA	0.932	0.2707±0.0931	2.939	0.354	0.4689±0.1001	3.742	0.021	0.8500±0.0000	8.856	0.0682	0.3578	0.6459	1.2673	0.9789	4.9132
MUUS	0.365	0.8500±0.0000	10.070	0.268	0.8500±0.0000	9.268	0.221	0.8500±0.0000	26.941	0.6353	1.0825	0.7317	1.2466	0.7791	4.1213
NICO*	0.144	0.6893±0.1033	2.885	0.719	0.4576±0.0636	2.863	0.479	0.3770±0.0972	7.035	0.8560	0.9203	0.2806	0.4636	0.5209	2.4119
NOT1*	0.135	0.6180±0.1233	3.354	0.386	0.4940±0.1008	2.647	1.000	0.2377±0.0000	7.526	0.8652	1.3725	0.6140	0.7776	0.0000	0.0179
RAMO*	0.259	0.6405±0.0867	2.768	0.594	0.6058±0.0604	3.808	0.314	0.5060±0.0955	5.781	0.7406	0.7070	0.4056	0.5267	0.6864	1.9221
RDIY	0.609	0.3962±0.0897	2.778	1.000	0.3465±0.0000	3.859	0.835	0.2587±0.1066	8.952	0.3910	0.6917	0.0000	0.0059	0.1654	1.8576
RHIY	0.978	0.4334±0.0670	4.301	0.992	0.3187±0.0867	2.976	0.358	0.5764±0.0729	11.369	0.0222	0.1806	0.0080	0.1046	0.6415	2.7773
RZE1	1.000	0.4033±0.0000	6.110	0.393	0.6701±0.0676	7.039	0.218	0.6285±0.1008	12.329	0.0001	0.0139	0.6070	1.2114	0.7821	3.6572
SAM1	0.228	0.4854±0.1059	2.763	0.033	0.7328±0.1551	2.287	0.114	0.7597±0.1057	15.481	0.7722	1.2147	0.9667	1.4169	0.8860	4.5882
SIRT	0.669	0.6412±0.0637	5.996	0.283	0.7730±0.0721	5.830	0.625	0.4776±0.0826	16.370	0.3305	0.6353	0.7173	0.9493	0.3753	3.1008

Table 5.1. Maximum likelihood results of the white plus power law noise models for time series. (continue)

SIVE	0.581	0.5391±0.0685	3.717	0.339	0.7261±0.0653	4.679	0.047	0.8500±0.0000	9.680	0.4191	0.6436	0.6610	0.7670	0.9534	3.5654
SIVS	0.452	0.6185±0.0650	3.927	0.529	0.4370±0.0837	2.495	0.092	0.7022±0.1413	7.524	0.5483	0.6976	0.4713	0.6488	0.9083	2.9824
SSEH	0.429	0.5380±0.0801	3.930	0.643	0.3017±0.0994	2.197	0.245	0.5664±0.0866	10.134	0.5707	0.9266	0.3567	0.6718	0.7545	3.3416
TNCE	0.474	0.6297±0.0661	4.682	0.493	0.5885±0.0727	4.082	0.186	0.7028±0.0821	13.026	0.5265	0.7704	0.5069	0.7293	0.8142	3.4288
TOK1	0.405	0.5539±0.0877	3.201	0.184	0.6211±0.1025	2.588	0.269	0.5331±0.1059	8.404	0.5949	0.7568	0.8160	0.8722	0.7306	2.8717
TRBN	0.597	0.3503±0.0878	3.822	0.352	0.4617±0.1052	3.570	0.568	0.4492±0.0781	13.023	0.4034	1.1181	0.6477	1.2400	0.4324	3.0201
TUBI*	0.353	0.4814±0.0966	2.135	0.209	0.3746±0.1432	1.103	0.131	0.6088±0.1191	7.094	0.6470	0.6983	0.7909	0.7104	0.8693	3.0356
TUF1	0.200	0.7012±0.0808	4.637	0.277	0.6562±0.0809	4.317	0.405	0.3678±0.1182	8.542	0.7996	1.1704	0.7226	1.0055	0.5954	3.5010
TVA1	0.371	0.7428±0.0665	7.329	0.070	0.5831±0.1714	2.009	0.161	0.6737±0.1100	11.644	0.6293	1.0672	0.5207	1.3142	0.8389	3.6401
UDER	0.495	0.5699±0.0668	4.465	0.414	0.3115±0.1296	2.012	0.326	0.5631±0.0885	11.565	0.5047	0.8390	0.5754	0.9554	0.6738	3.1554
WTZR*	0.711	0.5282±0.0695	4.211	1.000	0.3316±0.0000	2.152	1.000	0.4080±0.0000	9.810	0.2892	0.5653	0.0000	0.0040	0.0000	0.0023
YEBE*	1.000	0.4768±0.0000	4.861	0.781	0.4256±0.0726	2.197	0.405	0.5355±0.0868	7.779	0.0000	0.0068	0.2190	0.3316	0.5948	1.9413
ZECK*	1.000	0.5277±0.0000	5.239	0.508	0.4592±0.0890	2.328	0.254	0.5709±0.0979	7.322	0.0000	0.0075	0.4922	0.5914	0.8732	2.3301

*IGS stations.

As shown in Table 5.1, the spectral indices for all three components of these 49 time series are estimated, and they range from 0.1751 (vertical component of CRAO) to 0.85 (all three components of MUUS). In Hector, as the two principle types of power-law noise, the Flicker noise and Random walk noise are given fixed spectral index d with values of 0.5 and 1.0 respectively according to the previous error analysis studies of GPS time series [Zhang et al., 1997; Mao et al, 1999; Caliais 1999; Williams et al, 2004] . In those studies, white noise plus flicker noise model is preferred for the simulated time series since it is the model having the largest likelihood value. Williams et al (2004) obtained the mean values of the spectral indices from SOPAC solution for the individual components: -0.9 (east), -1.1 (north), -0.8 (vertical), which is consistent with the values observed for the simulated time series, containing white noise plus flicker noise. Due to the different scale factor of covariance matrix used by Hector [Bos et al., 2013], the corresponding values should change into 0.45 (east), 0.55 (north), 0.4 (vertical). Therefore, in this case, there are at most two noise sources if the spectral index of each components for one site close to 0.5. The significantly larger value of the spectral indices for some sites mostly suggests a combination of more than just white plus flicker noise sources. Those stations (Figure 5.2) are ADIY, ARPK, DIVR, DIYB, EKIZ, ELAZ, ERZ1, FASA, GEME, GURU, HINI, MALY, MUUS, RZE1, SAM1, SIRT, SIVE, SIVS, TNCE, TOK1, TUF1 and TVA1, 22 stations of the selected CORS-TR network, which at least in one of the horizontal components have the larger value (>0.6) of spectral index. That means about 59.5% of the selected stations in this study have more complicated noise sources in time series than the others. Furthermore, the stations DIYB, ELAZ, GEME, HINI, MALY, MUUS, SIRT and TUF1 (Table 5.2) even have larger value (>0.6) of spectral indices in both of the horizontal components. The remarkable variation of the spectral indices and amplitudes implies that observations are interrupted various types of noise and it is impossible to explicitly to tell their main source. However, noise sources for those stations may be due to a combination of varied causes that are probably the differences in atmospheric effects from one region to another and local station problems such as type and variety of geodetic monuments and etc. Take an example, the station MUUS has spectral indices of 0.85 for each component. This huge value of spectral indices are quite probably because of the non-tectonic deformation without being modeled at this station. For some particular components of the time series, the fraction of power law noise has value of 1.000,

and correspondingly the fraction of white noise is 0.000, it does not mean there is no source of white noise but only because the dominant noise mainly obey the power law. If in this circumstance the estimated spectral index is still smaller than 0.5, the noise model should also consist with the white plus flicker noise.

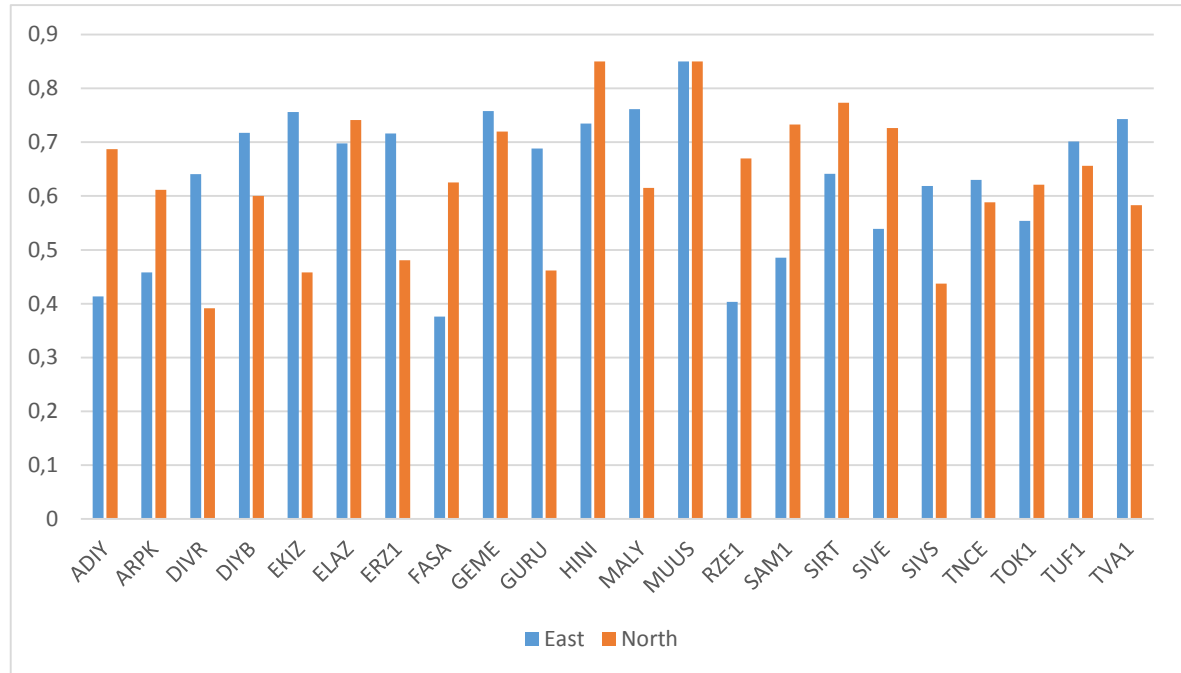


Figure 5.2. Histogram of the 22 stations with at least one larger value (>0.6) of spectral index in one of the horizontal components.

So far, according strictly to spectral index as the criteria concluded by the study result of Williams et al (2004) and the analysis in this section, it has shown that at least 8 stations (Table 5.2) are probably not reliable for velocity estimation with 2-year data.

Table 5.2. Stations with spectral indices larger than 0.6 on horizontal components.

Station	Spectral Index d	
	East	North
DIYB	0.7174	0.6000
ELAZ	0.6975	0.7414
GEME	0.7579	0.7198
HINI	0.7348	0.8500
MALY	0.7613	0.6152
MUUS	0.8500	0.8500
SIRT	0.6412	0.7730
TUF1	0.7012	0.6562

5.2. Velocity Analysis

The reliable velocities of continuous GPS stations account for the interpretation and geodynamic analyses of crustal deformation on the Earth. Within a specific reference frame, they particularly provide the kinematic explanation of relative plate motion. When generating velocity solutions for evaluating the quality of the data and our analysis approach, the theoretical definition of the reference frame is not quite important, though. It is usually suggested to carry out this step in the no-net-rotation (NNR) frame of the ITRF, strictly speaking, we should use this frame in our study when we are not estimating orbits since it is consistent with the EOPS. Another way to say we are trying to calculate the linear trend rate and uncertainties of each time series.

During the FOGM or realist sigma process and the MLE being applied, we can extrapolate a couple of sets of linear trend estimates and uncertainties. Here we used two different tools for implementing the realist sigma algorithm. One is a built-in program of GAMIT/GLOBK, tsfit, which is aimed at fitting time series to a variety of parameters, such

as linear rates, steps, seasonal periodicity and etc. Another is the interface program Tsview mentioned before.

Table 5.3. Linear trend of time series for each site due to different noise models processed.

Site	FOGM (Tsview) (mm/yr)			FOGM(GAMIT/GLOBK) (mm/yr)			MLE (Hector) (mm/yr)		
	East	North	Vertical	East	North	Vertical	East	North	Vertical
ADIY	17.21±0.41	24.67±0.69	0.15±2.39	17.22±0.41	24.69±0.91	0.15±2.38	17.245±0.407	24.708±1.118	1.169±2.583
ARPK	11.35±0.54	19.94±0.84	-2.99±3.53	11.53±0.42	19.84±0.86	-3.31±3.64	10.986±0.626	20.713±0.842	-1.354±3.584
ARTV	28.86±0.26	17.17±0.80	-2.33±1.89	28.88±0.26	17.18±0.80	-2.33±1.88	28.781±0.688	16.975±0.899	-2.041±2.627
BAYB	25.00±0.54	12.88±0.50	-0.35±1.51	25.02±0.43	12.89±0.50	-0.35±1.50	24.995±0.655	13.001±0.727	-0.031±2.184
BING	14.47±0.41	22.26±0.56	1.50±3.51	14.63±0.44	22.36±0.59	0.86±3.68	14.642±0.670	22.376±0.616	1.882±2.993
BTMN	18.72±0.33	25.74±0.43	1.95±2.00	18.73±0.33	25.76±0.34	1.95±1.98	18.893±0.633	25.769±0.564	2.700±4.247
BUCU*	23.31±0.21	11.78±0.66	0.65±1.30	23.32±0.21	11.79±0.65	0.65±1.30	23.271±0.355	11.812±0.787	0.086±1.633
CRAO*	23.44±1.19	13.32±0.33	-0.19±0.50	23.45±1.19	13.33±0.33	-0.19±0.50	23.366±3.019	13.385±0.628	-0.312±0.625
DIVR	9.32±0.91	20.88±0.21	-3.11±1.69	9.78±0.93	20.74±0.22	-3.81±1.73	9.302±1.561	20.997±0.371	-2.068±2.079
DIYB	18.59±0.89	24.83±0.72	-1.59±0.77	18.61±0.88	24.85±0.72	-1.59±0.66	18.622±1.708	24.916±1.024	-1.310±1.137
EKIZ	8.77±1.44	21.04±0.49	-2.36±1.88	8.77±1.43	21.05±0.49	-2.36±1.88	10.133±1.919	21.063±0.521	-1.424±2.300
ELAZ	10.89±1.11	22.39±0.90	-9.59±3.70	10.89±1.10	22.41±0.89	-9.60±3.68	10.449±2.001	22.175±2.158	-6.362±6.245
ERGN	18.44±0.81	24.88±0.54	0.01±2.42	18.46±0.81	24.90±0.54	0.01±2.42	18.468±1.621	24.865±0.534	0.569±1.819
ERZ1	14.82±1.48	16.01±0.46	-3.51±2.32	15.27±1.54	16.13±0.49	-4.33±2.36	14.403±2.318	15.869±0.880	-2.211±4.226
ERZR	25.17±0.78	15.64±0.26	0.73±2.09	25.19±0.78	15.65±0.26	0.73±2.07	25.247±0.983	15.629±0.479	0.540±2.875
FASA	23.31±0.26	13.32±0.29	-0.83±1.23	23.65±0.25	13.41±0.36	-1.49±1.47	23.337±0.406	13.393±0.659	-0.780±1.488

Table 5.3. Linear trend of time series for each site due to different noise models processed (continue).

GEME	6.20±1.73	19.94±2.09	-0.23±1.87	6.20±1.73	19.95±2.09	-0.23±1.42	4.792±2.871	17.297±3.210	0.557±1.668
GIRS	24.36±0.61	13.85±0.33	-0.09±1.83	24.38±0.62	13.86±0.33	-0.09±1.83	24.421±0.770	13.874±0.554	-0.085±2.703
GLSV*	22.34±0.60	12.39±1.59	2.03±0.87	22.36±0.59	12.40±1.58	2.03±0.82	22.397±1.162	12.297±2.063	1.146±2.153
GRAZ*	21.27±0.39	16.81±0.35	0.36±1.06	21.29±0.31	16.83±0.34	0.36±1.06	21.319±0.507	16.602±0.685	0.225±1.134
GUMU	24.33±0.69	13.61±0.26	-0.64±2.76	24.35±0.68	13.62±0.26	-0.64±2.75	24.517±0.994	13.585±0.337	0.452±3.205
GURU	7.85±1.30	20.03±0.31	-3.02±2.30	7.93±1.41	20.03±0.34	-3.92±1.72	7.806±1.653	19.991±0.490	-1.248±3.420
HINI	30.63±1.55	17.02±1.74	0.90±1.08	30.65±1.54	17.03±1.73	0.90±1.08	29.875±3.079	13.262±4.469	0.991±1.267
HORS	25.88±0.55	17.21±0.39	-0.69±1.68	25.90±0.54	17.23±0.39	-0.69±1.67	25.993±0.914	17.139±0.683	-0.901±2.535
ISTA*	22.77±0.19	12.32±0.32	-1.17±1.53	22.79±0.19	12.33±0.31	-1.17±1.52	22.836±0.225	12.354±0.350	-0.906±1.670
MALY	12.42±1.41	23.31±0.81	-1.32±2.36	12.68±1.53	23.49±0.64	-1.66±2.54	11.640±1.744	23.069±0.838	-0.525±2.658
MARA	14.42±0.26	20.26±0.65	-1.88±3.44	14.43±0.26	20.27±0.65	-1.88±3.42	14.447±0.326	20.328±0.661	-0.053±5.038
MUUS	24.56±4.21	28.92±3.27	-0.49±5.24	24.57±4.19	28.94±3.25	-0.49±5.21	23.460±5.660	27.348±5.213	-6.151±15.16
NICO*	18.32±0.42	16.45±0.59	1.15±0.89	18.33±0.42	16.47±0.59	1.15±0.89	18.231±0.943	16.409±0.487	1.357±1.000
NOT1*	22.04±0.39	19.81±0.26	0.72±0.54	22.05±0.39	19.82±0.25	0.72±0.54	22.002±0.887	19.803±0.497	0.862±0.775
RAMO*	23.08±0.45	19.84±0.98	0.10±0.66	23.10±0.45	19.85±0.97	0.10±0.65	23.190±0.777	19.844±0.962	-0.097±1.122
RDIY	13.57±0.26	16.85±0.38	-2.21±0.76	13.92±0.24	16.64±0.44	-2.27±0.92	13.522±0.410	16.966±0.504	-2.324±0.973
RHIY	12.23±0.61	17.61±0.25	-0.84±2.57	12.24±0.61	17.62±0.21	-0.84±1.94	12.201±0.688	17.686±0.365	-0.099±2.651
RZE1	23.26±0.58	12.94±1.69	-1.49±1.94	23.28±0.58	12.95±1.69	-1.49±1.94	23.330±0.912	12.905±2.161	-1.234±3.354

Table 5.3. Linear trend of time series for each site due to different noise models processed (continue).

SAM1	23.15±0.49	13.50±0.48	-0.76±2.52	23.12±0.55	13.52±0.53	-1.24±2.78	23.398±0.546	13.130±0.911	0.409±6.645
SIRT	20.21±1.04	24.52±1.52	4.73±2.28	20.22±1.04	24.54±1.51	4.73±1.81	19.552±1.679	23.641±2.497	4.583±2.935
SIVE	17.99±0.59	24.65±1.24	-0.46±2.49	18.00±0.58	24.67±1.23	-0.46±3.25	18.154±0.781	25.110±1.712	-0.620±5.477
SIVS	6.74±0.59	19.63±0.35	0.85±2.14	6.75±0.59	19.64±0.28	0.85±2.13	6.690±1.030	19.565±0.406	1.650±2.569
SSEH	12.40±0.58	17.47±0.23	0.06±1.67	12.41±0.58	17.48±0.23	0.06±1.67	12.409±0.825	17.465±0.264	1.212±2.308
TNCE	10.68±0.77	20.11±0.49	-2.66±2.62	10.97±0.79	20.27±0.50	-3.70±2.64	10.765±1.269	20.277±0.982	-0.491±4.435
TOK1	6.45±0.57	18.52±0.51	-3.06±2.32	6.69±0.76	18.75±0.64	-4.73±2.10	6.407±0.764	18.509±0.745	-2.043±1.919
TRBN	24.59±0.38	13.39±0.37	1.44±1.99	24.61±0.38	13.40±0.37	1.44±1.98	24.689±0.510	13.388±0.620	1.638±2.179
TUBI*	18.50±0.24	11.84±0.11	-1.46±1.03	18.51±0.23	11.85±0.11	-1.46±1.02	18.568±0.389	11.862±0.162	-0.885±1.829
TUF1	12.66±1.72	18.04±1.38	-1.91±1.48	12.67±1.72	18.05±1.04	-1.91±1.48	11.899±1.610	18.911±1.305	-1.350±1.286
TVA1	18.92±1.86	25.09±0.37	-2.07±2.64	18.93±1.83	25.11±0.37	-2.07±2.60	19.135±3.013	25.060±0.547	2.242±3.920
UDER	26.12±0.72	14.18±0.16	-1.96±1.92	26.14±0.71	14.19±0.15	-1.97±1.91	26.279±1.020	14.207±0.252	-1.663±2.603
WTZR*	19.02±0.40	16.18±0.22	1.85±0.84	19.03±0.40	16.19±0.22	1.85±0.84	19.188±0.858	16.148±0.272	1.526±1.476
YEBE*	18.84±0.66	17.64±0.24	-0.19±1.23	18.85±0.65	17.65±0.24	-0.19±1.22	18.872±0.865	17.717±0.346	0.094±1.623
ZECK*	25.15±0.76	11.64±0.17	1.15±1.08	25.17±0.76	11.65±0.18	1.15±1.08	25.085±1.064	11.799±0.400	1.451±1.687

*IGS stations.

As it can be seen in Table 5.3, the values of linear trend for the horizontal components of each site are not very different from two noise analysis methods. Here we take the results from the Tsview and Hector to make a compare by establishing a histogram (Figure 11).

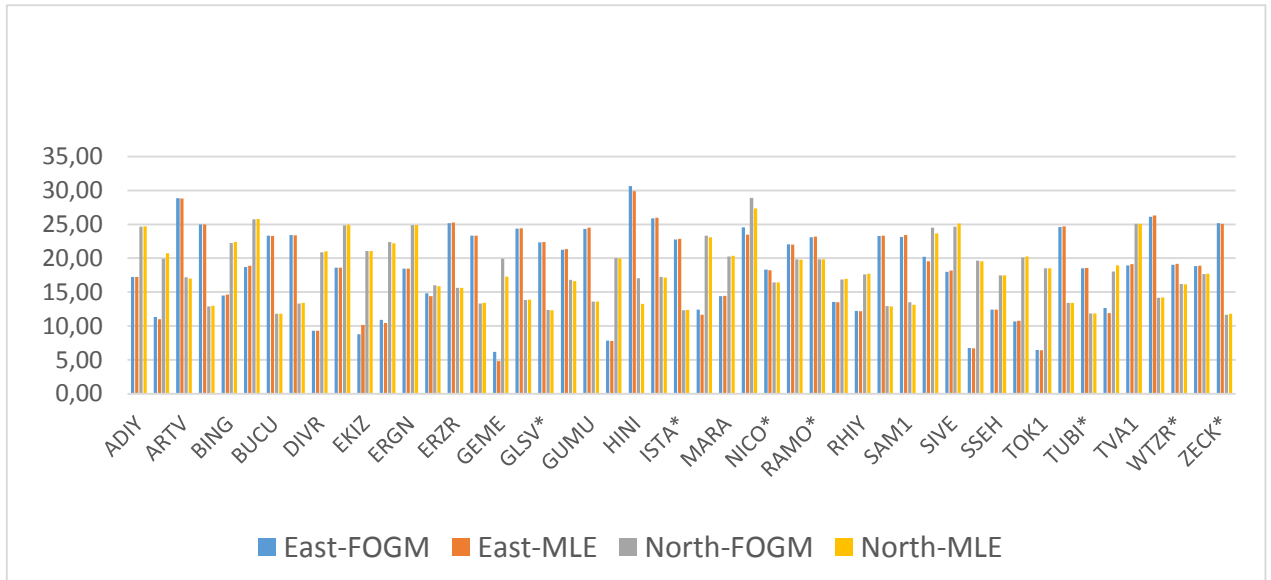


Figure 5.3. Histogram of trend rate (mm/yr) for each site on horizontal components.

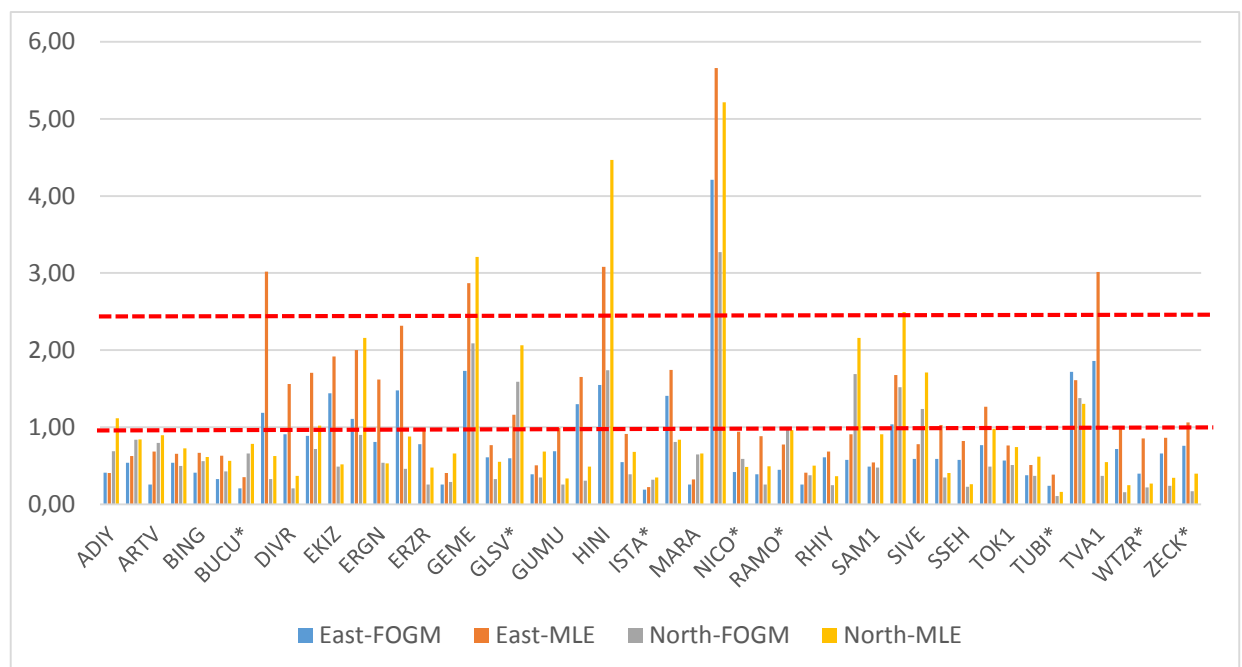


Figure 5.4. Histogram of trend rate uncertainties (mm/yr) for each site on horizontal components.

However, if we compare the uncertainties of the trend rate for those sites' horizontal components, we observed some meaningful differences (Figure 5.4.). Again, the results are from the Tsview and the Hector. When the random walk noise is assumed in the time series, the linear trend uncertainties of time series for horizontal components of station HINI have values of 1.55 mm/yr (East) and 1.74 mm/yr (North), respectively, when the white plus power law noise model is assumed, they are 3.079 mm/yr and 4.469, respectively. Similarly, the linear trend uncertainties of horizontal components for station MUUS have values of 4.21 mm/yr (East) and 3.27 mm/yr (North) respectively when the random walk noise is assumed in time series, and they have values of 5.660 mm/yr and 5.213mm/yr respectively when the white plus power law noise model is assumed. For the stations, if only the random walk noise model is assumed in time series, then velocity estimates of them are bit underestimated than that of white plus power law noise model assumed. But they both show a more realist sigma for the velocity estimates of each station compared to the results if there are no noise models involved.

Up to now, if we are focused on the sites which have spectral indices larger than 0.6 and linear trend uncertainties over 1 mm on horizontal components, which is assuming the white plus power law noise model in time series, we can mark out the stations DIYB, ELAZ, GEME, HINI, MUUS and SIRT from the 37 selected stations. More strictly, if we look at the sites with spectral indices > 0.7 and linear trend uncertainties > 2.5 mm on horizontal components, we have sites GEME, HINI and MUUS excluded (Table 5.4). There are reasons to doubt those stations reflect bad position time series, especially the later three are highly doubtable. The result that predicts station MUUS, HINI and GEME are not quite stable consists with the study outcome of Ozdemir (2016) that evaluated the performance of stations on the whole Turkish National Permanent GNSS Network (TNPNGN). So if both the spectral index and velocity uncertainties, assuming white plus power law noise model in time series, are used as the criteria to decide which station are reliable and stable for velocity estimates with 2-year data, it has shown there are at least 3 stations not very ideal (Table 5.4).

Table 5.4. Station with spectral indices > 0.7 and linear trend uncertainties > 2.5 mm on horizontal components.

Stations	East		North	
	Spectral Index	Velocity Uncertainty	Spectral Index	Velocity Uncertainty
MUUS	0.8500	5.660	0.8500	5.213
HINI	0.7348	3.079	0.8500	4.469
GEME	0.7579	2.871	0.7198	3.210

To see whether the prediction makes sense, the related velocity estimates of the stations are compared with results of the published study.

5.3. Compare With The Latest Velocity Study

In previous section, it has been mentioned that the velocities of selected 37 stations in NNR frame of the ITRF were estimated. By involving the random walk noise model in time series done by FOGM process, this study got a set of velocity and uncertainty solutions with the 2-year length data. These results, especially those on horizontal components, are compared with one of the latest studies, i.e. Ozdemir (2016), which estimated the velocities of whole TNPGN stations with 7-year length data by considering the same noise model and using the similar NNR frame of the ITRF.

Table 5.5. Comparing the velocity solution from the same station between previous study and this one.

SITE	Ozdemir, 2016		This Study	
	East	North	East	North
ADIY	18.41±0.38	22.01±0.14	17.22±0.41	24.69±0.91
ARPK	10.46±0.26	19.05±0.30	11.53±0.42	19.84±0.86
ARTV	31.75±0.42	13.19±0.23	28.88±0.26	17.18±0.80
BAYB	25.70±0.19	11.03±0.14	25.02±0.43	12.89±0.50
BING	16.05±0.22	18.99±0.23	14.63±0.44	22.36±0.59
BTMN	19.70±0.20	23.51±0.14	18.73±0.33	25.76±0.34
DIVR	9.95±0.19	18.6±0.17	9.78±0.93	20.74±0.22
DIYB	18.6±0.31	24.4±0.35	18.61±0.88	24.85±0.72
EKIZ	12.13±0.28	17.98±0.14	8.77±1.43	21.05±0.49
ELAZ	10.11±0.14	19.19±0.14	10.89±1.10	22.41±0.89
ERGN	17.99±0.27	23.54±0.16	18.46±0.81	24.90±0.54
ERZ1	13.37±0.33	14.20±0.70	15.27±1.54	16.13±0.49
ERZR	26.13±0.34	11.81±0.13	25.19±0.78	15.65±0.26
FASA	24.04±0.56	11.44±0.16	23.65±0.25	13.41±0.36
GEME	6.18±0.58	15.72±0.37	6.20±1.73	19.95±2.09
GIRS	24.97±0.18	11.66±0.14	24.38±0.62	13.86±0.33
GUMU	25.30±0.21	10.79±0.16	24.35±0.68	13.62±0.26
GURU	10.56±0.26	17.77±0.15	7.93±1.41	20.03±0.34
HINI	25.93±0.22	14.94±0.32	30.65±1.54	17.03±1.73
HORS	28.03±0.35	13.03±0.63	25.90±0.54	17.23±0.39
MALY	11.84±0.43	19.56±0.14	12.68±1.53	23.49±0.64
MARA	14.99±0.21	18.70±0.18	14.43±0.26	20.27±0.65
MUUS	13.66±0.52	21.53±1.40	24.57±4.19	28.94±3.25
RDIY	14.65±0.15	15.07±0.17	13.92±0.24	16.64±0.44
RHIY	12.61±0.13	15.41±0.15	12.24±0.61	17.62±0.21
RZE1	24.49±0.62	11.05±0.17	23.28±0.58	12.95±1.69
SAM1	23.90±0.31	11.47±0.39	23.12±0.55	13.52±0.53
SIRT	20.70±0.21	23.21±0.21	20.22±1.04	24.54±1.51
SIVE	18.92±0.22	22.25±0.31	18.00±0.58	24.67±1.23
SIVS	7.11±0.14	16.81±0.14	6.75±0.59	19.64±0.28
SSEH	13.28±0.17	15.72±0.20	12.41±0.58	17.48±0.23
TNCE	11.10±0.15	18.13±0.29	10.97±0.79	20.27±0.50
TOK1	7.03±1.11	14.62±1.88	6.69±0.76	18.75±0.64
TRBN	25.81±0.21	11.09±0.19	24.61±0.38	13.40±0.37
TUF1	7.54±1.26	17.51±0.90	12.67±1.72	18.05±1.04
TVA1	20.24±1.23	20.50±1.91	18.93±1.83	25.11±0.37
UDER	26.96±0.20	11.03±0.24	26.14±0.71	14.19±0.15

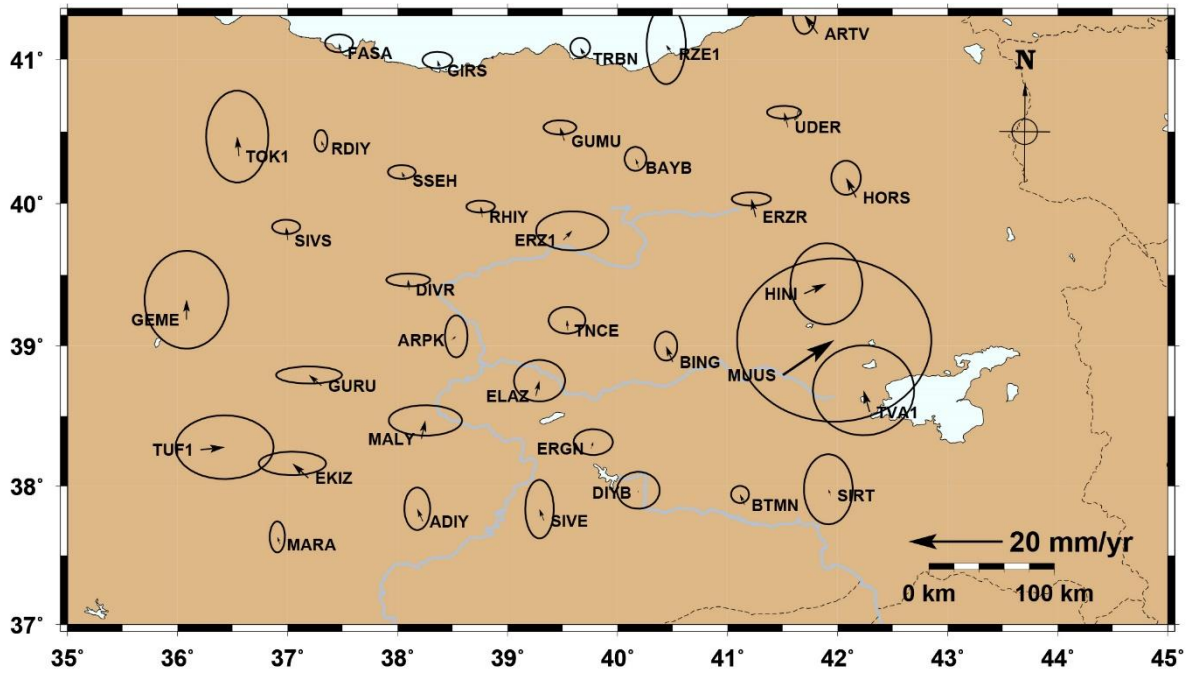


Figure 5.5. Velocity differences between Ozdemir (2016) and this study. The velocity error ellipses are at 95% confidence level.

Regarding the comparison (Figure 5.5 and Table 5.5), it has been found that the results from this study are almost consist with the ones from Ozdemir (2016) despite its length of data is longer. However, the significant differences of velocity uncertainties are still can be seen (Figure 5.5, 5.6), especially those suspected stations ruled out in the previous noise analysis, such as stations MUUS, HINI and GEME. In Figure 5.6, the source of the differences comes from rotation, sytematically. Obviously, it can be related with reference frame problem than the differences of time duration.

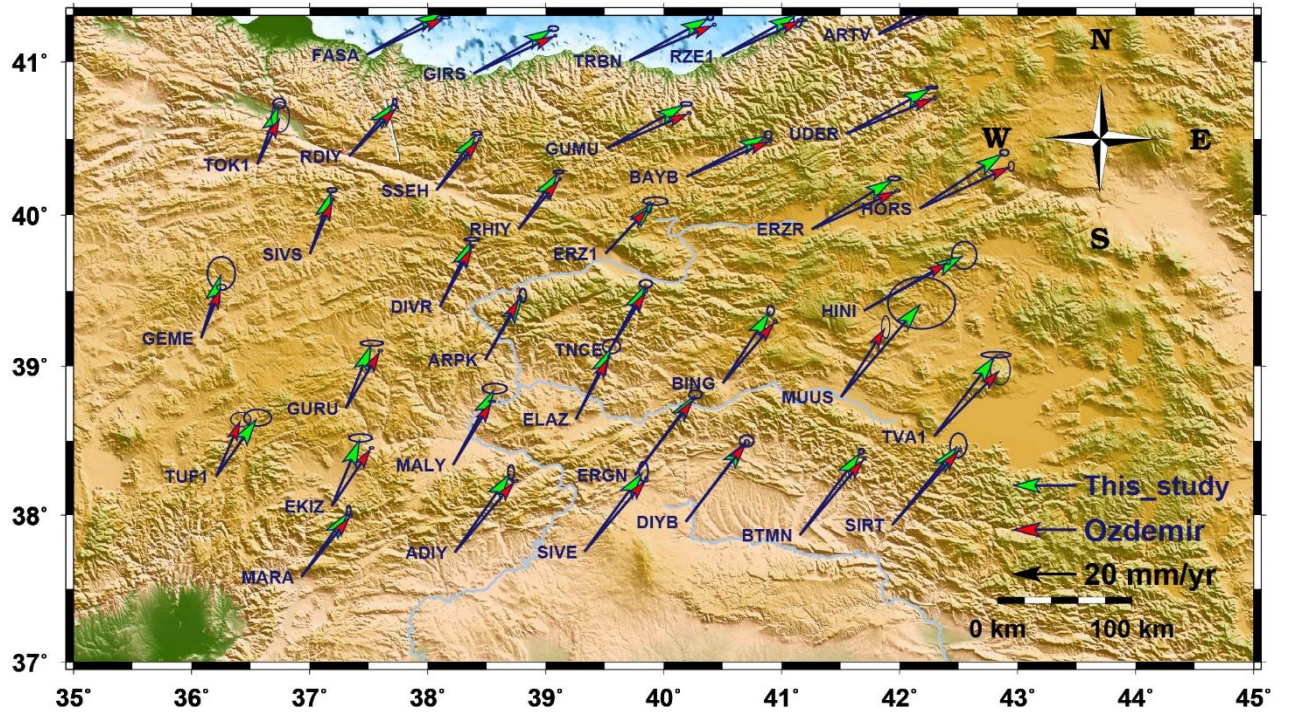


Figure 5.6. Comparison of our velocity solution with Ozdemir (2016)'s. The velocity error ellipses are at 95% confidence level.

In order to view the velocities in a frame that is natural for geophysical interpretation, this study also realized the velocity field with respect to the Eurasia fixed reference frame [Altamimi et al, 2012] in next comparison. And again, for the purpose of getting more realist velocity error, it invokes the value of random walk noise, which is given from the earlier FOGM Extrapolation process, into the velocity solution. Here Table 5.6 shows the result obtained.

Table 5.6. Velocity field in Eurasia fixed frame from the 37 stations.

SITE	Lon. (deg)	Lat. (deg)	Evel. (mm/yr)	Nvel. (mm/yr)	σ_E (mm/yr)	σ_N (mm/yr)	Rne
ADIY	38.22968	37.74586	-7.81	12.56	0.67	0.59	0.028
ARPK	38.48732	39.04059	-14.44	8.30	0.70	0.62	0.019
ARTV	41.81832	41.17510	3.59	5.77	0.69	0.63	0.016
BAYB	40.19144	40.25015	0.00	1.15	0.68	0.61	0.016
BING	40.50078	38.88545	-10.47	10.68	0.70	0.63	0.026
BTMN	41.15448	37.86360	-6.31	14.35	0.67	0.61	0.036
DIVR	38.10388	39.39432	-15.15	8.66	0.70	0.62	0.017
DIYB	40.18749	37.95442	-6.30	12.95	0.70	0.63	0.029
EKIZ	37.18794	38.05883	-14.90	8.67	0.68	0.60	0.022
ELAZ	39.25646	38.64467	-14.82	10.28	0.68	0.61	0.025
ERGN	39.75819	38.26961	-6.84	13.16	0.67	0.60	0.029
ERZ1	39.50612	39.74584	-10.14	4.31	0.70	0.63	0.019
ERZR	41.25547	39.90561	0.10	4.31	0.68	0.62	0.021
FASA	37.48475	41.04553	-1.66	0.90	0.70	0.62	0.006
GEME	36.08084	39.18513	-19.55	5.67	0.67	0.59	0.015
GIRS	38.38816	40.92263	-0.26	1.99	0.70	0.63	-0.003
GUMU	39.51617	40.43707	-0.29	1.78	0.68	0.61	0.017
GURU	37.30787	38.71735	-16.88	7.45	0.70	0.62	0.020
HINI	41.69579	39.36879	4.73	2.94	0.68	0.61	0.026
HORS	42.16733	40.04165	0.92	5.80	0.68	0.62	0.022
MALY	38.21689	38.33770	-13.13	10.75	0.69	0.61	0.024
MARA	36.93113	37.58076	-10.48	8.13	0.68	0.60	0.025
MUUS	41.50216	38.79324	-3.01	16.44	0.68	0.61	0.030
RDIY	37.33567	40.38524	-11.32	4.06	0.73	0.66	0.007
RHIY	38.77080	39.90611	-12.77	5.94	0.67	0.59	0.016
RZE1	40.49309	41.03690	-1.81	1.36	0.69	0.63	0.012
SAM1	36.33376	41.30849	-1.66	0.26	0.72	0.63	-0.000
SIRT	41.93557	37.93191	-5.48	13.06	0.71	0.65	0.031
SIVE	39.32927	37.75240	-6.90	12.60	0.69	0.62	0.029
SIVS	37.00249	39.74370	-18.13	7.25	0.67	0.60	0.013
SSEH	38.07489	40.16247	-12.52	5.40	0.68	0.60	0.011
TNCE	39.54563	39.10967	-13.96	8.77	0.69	0.62	0.018
TOK1	36.55747	40.33098	-17.95	5.82	0.74	0.66	0.008
TRBN	39.71149	41.00541	-0.17	1.72	0.68	0.62	0.010
TUF1	36.20845	38.26055	-12.81	6.04	0.71	0.63	0.017
TVA1	42.29078	38.52965	-6.85	13.77	0.75	0.68	0.028
UDER	41.54755	40.53128	1.29	3.00	0.68	0.62	0.010

As it can be seen, just from the velocity solutions in the Eurasia fixed reference frame, it cannot be told which station has a good quality of value. Here the results are compared

with another one of previous studies, i.e. Aktug et al. (2016), which also used the Eurasia fixed reference frame. In the light of the latest study Aktug et al. (2016) which processed 18 of the network stations same as this study, it produced intermittently 7-year long velocity field from 1998 to 2010, which ignored the time series and noise analysis. Table 5.7 presents the comparison between two studies.

Table 5.7. Comparing the velocity solution from the same station between previous study and this one.

SITE	Aktug et al., 2016					This study				
	Evel. (mm/yr)	Nvel. (mm/yr)	σ_E (mm/yr)	σ_N (mm/yr)	Rne	Evel. (mm/yr)	Nvel. (mm/yr)	σ_E (mm/yr)	σ_N (mm/yr)	Rne
ADIY	-5.7	13.0	0.3	0.3	0.035	-7.81	12.56	0.67	0.59	0.028
ARPK	-14.5	9.9	0.4	0.4	0.029	-14.44	8.30	0.70	0.62	0.019
BTMN	-5.4	15.4	0.3	0.4	0.022	-6.31	14.35	0.67	0.61	0.036
DIVR	-14.8	9.7	0.5	0.6	0.019	-15.15	8.66	0.70	0.62	0.017
DIYB	-6.6	17.2	0.1	0.1	-0.006	-6.30	12.95	0.70	0.63	0.029
EKIZ	-13.4	8.9	0.4	0.4	0.030	-14.90	8.67	0.68	0.60	0.022
ELAZ	-15.0	10.8	0.4	0.4	0.024	-14.82	10.28	0.68	0.61	0.025
ERGN	-6.6	14.9	0.4	0.4	0.013	-6.84	13.16	0.67	0.60	0.029
GURU	-13.6	8.7	0.4	0.4	0.024	-16.88	7.45	0.70	0.62	0.020
MALY	-12.1	10.8	0.3	0.4	0.028	-13.13	10.75	0.69	0.61	0.024
MARA	-9.9	9.2	0.7	0.7	0.014	-10.48	8.13	0.68	0.60	0.025
MUUS	-12.8	16.1	0.4	0.4	0.023	-3.01	16.44	0.68	0.61	0.030
NICO	-5.0	1.3	0.2	0.2	0.060	-7.53	3.6	0.58	0.51	-0.026
SIRT	-4.4	15.5	0.5	0.6	0.039	-5.48	13.06	0.71	0.65	0.031
SIVE	-6.1	14.1	0.4	0.4	0.024	-6.90	12.60	0.69	0.62	0.029
TNCE	-14.4	9.4	0.4	0.4	0.060	-13.96	8.77	0.69	0.62	0.018
TUF1	-13.0	6.9	0.4	0.4	0.025	-12.81	6.04	0.71	0.63	0.017
TVA1	-2.4	15.7	0.9	0.1	0.030	-6.85	13.77	0.75	0.68	0.028

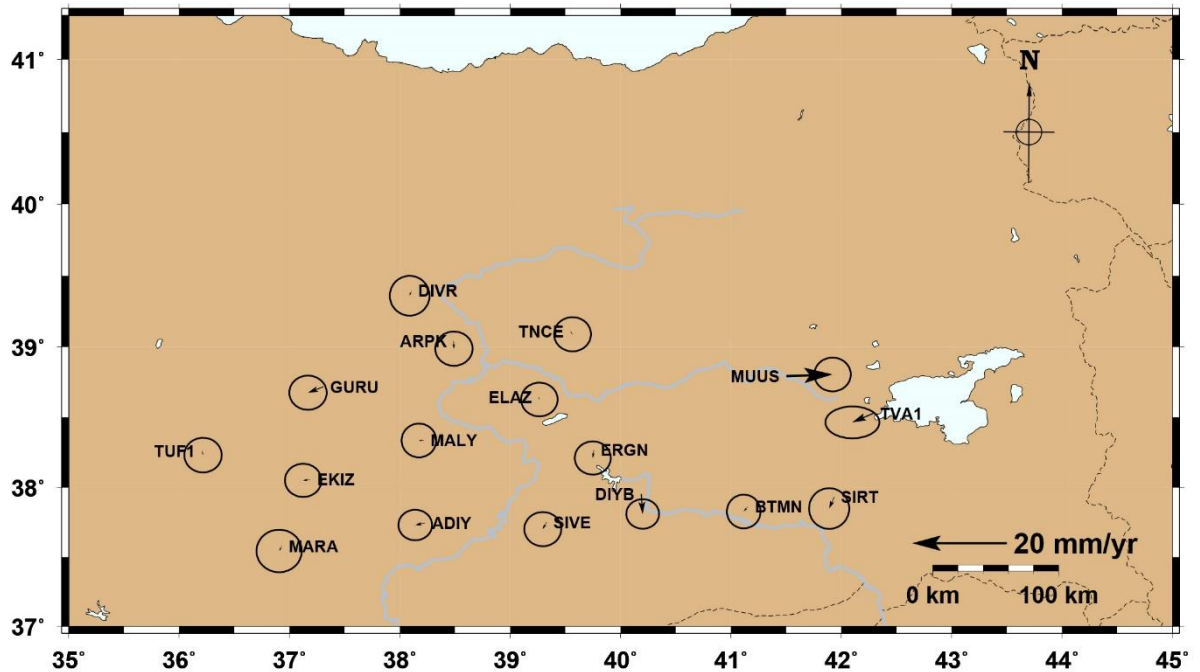


Figure 5.7. Velocity differences between Aktug et al. (2016) and this study. The velocity error ellipses are at 95% confidence level.

As it shows (Figure 5.6 and Table 5.7), for most of the stations, there are just slight differences of the velocities from these two studies, but the velocity uncertainties from this study are a bit larger than that from Aktug et al. (2016) since the former involved the noise model in the time series analysis and input the estimated value of random walk noise, which makes the results much more close to reality. Whereas the time span of data is too short, which is two years, for this study, the velocity field we obtained are still lack of accuracy. And yet, some information can be gained from this comparison if we look back to the criteria decided by the spectral index and linear trend rate uncertainties of each station's time series gotten previously from the MLE process. One of the highly doubted sites which are in the comparison, MUUS, caused the most significant difference of velocity between Aktug's and this study. It is 9.79 mm/yr of difference value on the east component. This may indirectly prove concerns of this study that the station with the worst quality is site MUUS (Figure 5.6). So, the other two stations, GEME and HINI, which are highlighted by the same criteria, should be reconsidered when someone manages to derive velocity solution from them since

the results are not quite reliable. Here it is plotted of those velocity fields from two studies on a map (Figure 5.8).

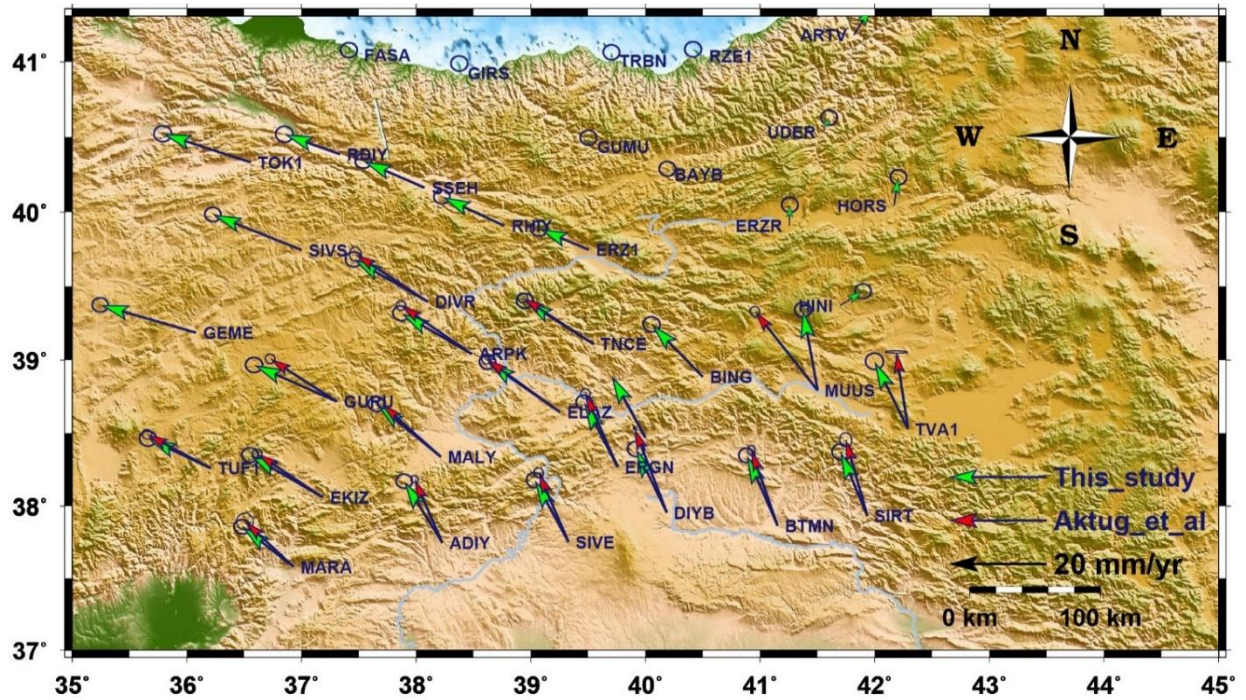


Figure 5.8. Comparison of our velocity field with Aktug et al (2016)'s. The velocity error ellipses are at 95% confidence level.

Moreover, Figure 5.8 shows the horizontal velocity field with respect to the fixed Eurasian plate which is almost consist with the previous study. It presents the general pattern motion of both Anatolian and Arabian plates. However, the distinct differences of velocity on station MUUS and TVA1 can be easily observed. It is not sure what reason causes the singularity for this comparison on the station TVA1. But according outcome of previous sections, it can been found that the spectral index and linear trend uncertainty of station TVA1's time series, from the MLE process by assuming white plus power law noise model, only on its east component are > 0.7 and > 2.5 mm/yr, respectively. There may be some antenna problem on this station causing such velocity uncertainties. However, up till now, it could be easily confirmed that the permanent station MUUS is definitely not reliable for velocity estimates with 2-year data (Figure 5.9).

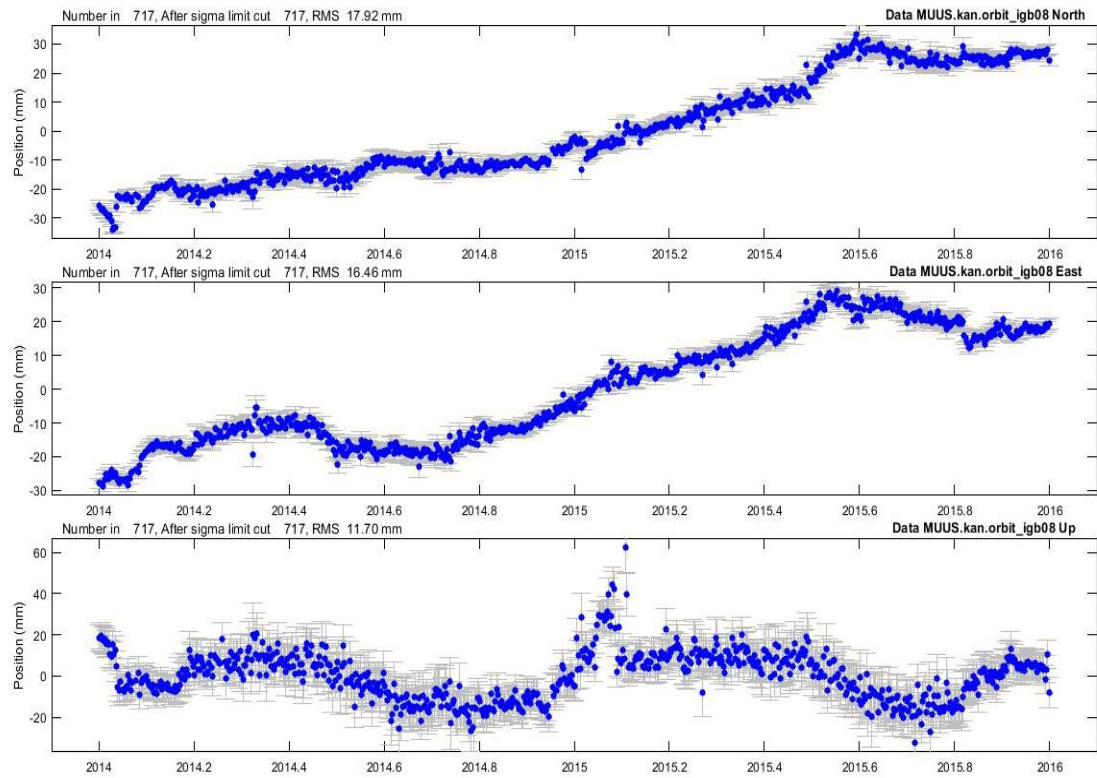


Figure 5.9. GPS position time series of station MUUS.

6. DISCUSSION AND CONCLUSION

In this study, I performed a noise analysis of 37 continuous GPS position time series of CORS-TR for the limited time span from 2014 to 2015. These stations are distributed in the eastern Turkey, mostly along the EAF and the east section of the NAF, which has the great significance for the geodetic study on the crustal deformation around this region. For the purpose of campaign type study in the future, we have the motivation of figuring out which permanent station is reliable and stable. In the GAMIT process, it has been found that the station BTMN keeps receiving signal with noisy phase on some specific days, especially in the summer of each year. But this seems not affect the velocity estimate of its displacement, which was done in later section of this study. However, the GAMIT results are still not enough to decide which station has the bad quality, since sometime even the results within normal range but time series shows outliers. So I generated the 700~730 daily position time series of each station through GLOBK then. To make sure the consistency of time series, I firstly removed the outliers from the stations with not good repeatability. After obtaining relatively clean time series, I started the noise analysis. Firstly, most common noise model was considered, i.e. the random walk noise model in time series. It is expected for the First Order Gauss-Markov (FOGM) process to estimate the value of the random walk noise ($5.30\text{e-}7 \text{ m}^2/\text{yr}$ and $7.46\text{e-}7 \text{ m}^2/\text{yr}$ on east and north components, respectively) as the next input to globk to generate more realistic sigma of velocity uncertainties. In this case, from the set of the selected 37 stations with 2 years of observation, about 35% of them (the stations EKIZ, ELAZ, ERZI, GEME, GURU, HINI, MALY, MUUS, RZE1, SIRT, SIVE, TUF1 and TVA1, referred to the Figure 5.4) reach the value of uncertainty above 1 mm/yr for the horizontal components. Secondly, through the Maximum Likelihood Estimation (MLE) analysis for the white plus power law noise model with spectral indices, it has been found a significant amount of stations (about 59.5%) in this study have more complicated noise sources in time series than the others, since Williams et al. (2004) assumed the existence of the white and power-law noise combination in the GPS time series, trying to apply the MLE

process which would represent the character of the stochastic part of the time series. For this combination of noises, the uncertainties of the determined velocities rarely increased 1-3 times in comparison with the ones of random walk noise assumed. And six of the selected 37 stations (i.e. DIYB, ELAZ, GEME, HINI, MUUS and SIRT) reach the value of uncertainty above 1 mm/yr with spectral indices over 0.6. Moreover, 3 of them (i.e. GEME, HINI and MUUS) even go beyond the value of 2.5 mm/yr with spectral indices larger than 0.7. So values of the spectral indices and the linear trend rate uncertainties result from the MLE process became the principle criteria for us to decide which station has good quality. In the last comparison with the previous studies of velocity solutions on the same continuous stations, although there is the limitation on the data of this study, almost all the results are consist with previous ones. Moreover, in the second comparison with velocity filed of Aktug et al (2016), it indirectly proved our assumption about that the station MUUS has the worst quality with the position time series. And it has been predicted that this huge value of spectral index and uncertainty it has are quite probably because of the non-tectonic deformation without being modeled at this site. The other two stations, GEME and HINI, are marked out by the same criteria and apparently not used in the Aktug et al (2016)'s study, it can be also predicted that they are highly likely the station with really bad quality for velocity estimates. So this study suggests the researchers that they should reconsider while managing to derive velocity solution from these three station since the results may not be quite reliable. Furthermore, for our upcoming campaign type GPS study along the Hazar-Palu segment of the EAF, these three stations can be ignored from the related network. In the future, with reliable and available data, a proper block model will be built along this study area. And, noise sources will be identified as many as possible for those problematic stations.

REFERENCES

- Allen, C. R., 1969. Active faulting in northern Turkey, Division of Geological Science, *Calif. Inst. Technol. Contrib.*, 1577, 32.
- Ambraseys, N. N. and J. A. Jackson, 1998. Faulting associated with historical and recent earthquakes in the eastern Mediterranean region, *Geophys. J. Int.*, 133, 390–406.
- Ambraseys, N. N., 1970. Some characteristic features of the Anatolian fault zone, *Tectonophysics*, 9, 143–165.
- Ambraseys, N. N., 1989. Temporary seismic quiescence: SE Turkey, *Geophys. J.*, 96, 311–331.
- Arpat, E. and F. Saroglu, 1972. The East Anatolian fault system: thoughts on its development, *M.T.A. Bull.*, 78:33–39.
- Bayrak, E., Yilmaz, S., Softa, M., Turker, T., Bayrak, Y., 2015. Earthquake hazard analysis for East Anatolian Fault Zone, Turkey. *Nat Hazard.* 76:1063–1077, doi: 10.1007/s11069-014-1541-5.
- Bos, M.S., Fernandes, R.M.S., Williams, S.D.P., Bastos, L., 2008. Fast error analysis of continuous GPS observations. *J. Geod.*, 82:157–166, doi: 10.1007/s00190-007-0165-x
- Bos, M.S., Fernandes, R.M.S., Williams, S.D.P., and Bastos, L., 2013. Fast Error Analysis of Continuous GNSS Observations with Missing Data. *J. Geod.*, Vol 87(4), 351-360, doi: 10.1007/s00190-012-0605-0.

- Cavalié, O. and Jónsson, S., 2014. Block-like plate movements in eastern Anatolia observed by InSAR, *Geophys. Res. Lett.*, 41, 26–31, doi:10.1002/2013GL058170.
- Cetin, H., H. Guneyli, and L. Mayer, 2003. Paleoseismology of the Palu-Lake Hazar segment of the East Anatolian Fault Zone, Turkey, *Tectonophysics*, 374, 163–197.
- Emre, Ö., Duman, T. Y., Özalp, S., Elmacı, H., Olgun, Ş. and Şaroğlu, F., 2013. Active Fault Map of Turkey with and Explanatory Text. General Directorate of Mineral Research and Exploration, Special Publication Series-30. Ankara-Turkey.
- Faccenna, C., and T. W. Becker, 2010. Shaping mobile belt from small scale convection, *Nature*, 465, 602–605
- Feigl, K.L., Agnew, D.C., Bock, Y., Dong, D., Donnellan, A., Hager, B.H., Herring, T.A., Jackson, D.D., Jordan, T.H., King, R.W., Larsen, S., Larson, K.M., Murray, M.H., Shen, Z. and Webb, F.H. (1993). Space geodetic measurement of crustal deformation in central and southern California, 1984–1992. *Journal of Geophysical Research* 98: doi: 10.1029/93JB02405. issn: 0148-0227.
- Friedman, J.H. and Stuetzle, W. 1981. "Projection Pursuit Regression", *Journal of the American Statistical Association* 76:817–823. doi:10.1080/01621459.1981.10477729.
- Gurtner, W., G. Mader, D. MacArthur, 1989. "A Common Exchange Format for GPS Data." *Proceedings of the Fifth International Geodetic Symposium on Satellite Systems*, pp. 917ff, Las Cruces.
- Hager BH, King RW, Murray MH. 1991. Measurement of crustal deformation using the Global Positioning System. *Annu. Rev. Earth Planet. Sci.* 19:351–82.

- Heidbach, O., 2005. Velocity Field of the Aegean-Anatolian Region From 3D Finite Element Models, pp. 169–185, Friedemann Wenzel, Springer, Berlin, Heidelberg.
- Hempton, M. R., 1987. Constraints on Arabian plate motion and extensional history of the Red Sea, *Tectonics*, 6:687–705.
- Hüsing, S.K., Dekkers, M.J., Franke, C. and Krijgsman, W., 2009a, The Tortonian reference section at Monte dei Corvi (Italy): evidence for early remanence acquisition in greigite-bearing sediments, *Geophys. J. Int.*, in revision.
- Hüsing, S.K., Kuiper, K.F., Link, W., Hilgen, F.J., Krijgsman, W., 2009b. Monte dei Corvi (Northern Apennines, Italy): a Mediterranean reference section for the Tortonian Stage. *Earth Planet. Sci. Lett.* 282, 140–157.
- Hüsing, S.K., Zachariasse, W.J., van Hinsbergen, D.J.J., Krijgsman, W., Inceöz, M., Harzhauser, M., Mandic, O., Kroh, A., 2009c. Oligocene-Miocene basin evolution in SE Anatolia, Turkey: constraints on the closure of the eastern Tethys gateway. In: Van Hinsbergen, D.J.J., Edwards, M.A., Govers, R. (Eds.), *Collision and Collapse at the Africa-Arabia-Eurasia Subduction Zone*, Vol. 311. Special Publication: Geological Society London, pp. 107–132.
- Jackson, J. & McKenzie, D., 1984. Active tectonics of the Alpine-Himalayan belt between western Turkey and Pakistan. *Geophys. J. Roy. Astron. Soc.* , 77, 185-264.
- Klos, A., Bogusz, J., Figurski, M. and Kosek, W., 2014. Uncertainties of geodetic velocities from permanent GPS observations: the Sudeten case study. *Acta Geodynamica et Geomaterialia*, Vol. 11, No. 3 (175), 201–209. doi: 10.13168/AGG.2014.0005.

- Klos, A., Bogusz, J., Gruszczynska, M. and Gruszczynski, M., 2015. Investigation of Noise in the EPN Weekly Time Series. *Acta Geodynamica et Geomaterialia*, Vol. 12, No. 2 (178), 117– 126. doi: 10.13168/AGG.2015.0010.
- Kong, Y.-L.; Meng, Y.; Li, W.; Yue, A.-Z.; Yuan, Y. Satellite Image Time Series Decomposition Based on EEMD. *Remote Sens.* 2015, 7, 15583-15604.
- Le Pichon, X., and C. Kremer (2010), The Miocene-to-present kinematic evolution of the Eastern Mediterranean and Middle East and its implications for dynamics, *Annu. Rev. Earth Planet. Sci.*, 38, 323–351, doi:10.1146/annurev-earth-040809-152419.
- Lyberis, N., T. Yurur, J. Chorowicz, E. Kasapoglu, and N. Gundogdu, *The East Anatolian Fault: an oblique collisional belt*, *Tectonophysics*, 204, 1–15, 1992.
- Mandelbrot, B. B. and Van Ness, J. W. 1968. Fractional Brownian motions, fractional noises and applications. *SIAM Rev.* 10 422–437.
- Mann, S. P., 1995, *Statistics For Business and Economics*, Wiley, USA.
- Mao, A., C. G. A. Harrison, and T. H. Dixon, 1999: Noise in GPS coordinate time series. *J. Geophys. Res.*, 104, 2797-2816, doi: 10.1029/1998JB900033.
- McClusky, S., S. Balassanian, A. Barka, C. Demir, S. Ergintav, I. Georgiev, O. Gurkan, M. Hamburger, K. Hurst, H. Kahle, K. Kastens, G. Kekelidze, R. King, V. Kotzev, O. Lenk, S. Mahmoud, A. Mishin, M. Nadariya, A. Ouzounis, D. Paradissis, Y. Peter, M. Prilepin, R. Reilinger, I. Sanli, H. Seeger, A. Tealeb, M. N. Toksoz, and G. Veis, 2000. Global Positioning System constraints on plate kinematics and dynamics in the eastern Mediterranean and Caucasus, *J. Geophys. Res.*, 105(B3), 5695–5719.

- McKenzie, D. P., 1972. Active tectonics of the Mediterranean Region, *Geophys. J. R. Astron. Soc.*, 30:109–185
- McKenzie, D. P., 1976. The East Anatolian fault: a major structure in eastern Turkey. *Earth Planet Sci Lett* 29:189–193.
- Mckenzie, D.P., 1978. Some remarks on the development of sedimentary basins. *Earth Planet Sci Letters* 40: 25-32.
- Mekik, C., Yildirim O. and Bakici S., 2011a. An Overview of RTK Network of Turkish Republic (TUSAGA-Aktif). International Global Navigation Satellite Systems Society-IGNSS Symposium 2011. Sydney, Australia, November 15-17.
- Nalbant, S. S., J. McCloskey, S. Steacy, and A. A. Barka, 2002. Stress acumulation and increased seismic risk in eastern Turkey, *Earth Planet. Sci. Lett.*, 195, 291–298.
- Nocquet, J.-M., 2012. Present-day kinematics of the Mediterranean: A comprehensive overview of GPS results. *Tectonophysics*, 579, 220–242. doi: 10.1016/j.tecto.2012.03.037.
- Ozeren, M. S. and W. E. Holt, 2010. The dynamics of the eastern Mediterranean and eastern Turkey, *Geophysical Journal International*, 183, 1165–84.
- Taymaz, T., H. Eyidogan, and J. Jackson, 1991. Source parameters of large earthquakes in the East Anatolian Fault Zone (Turkey), *Geophys. J. Int.*, 106/3, 537–550.
- Toksoz, M. N., Shakal, A. F., and Michael, A. J., 1979, Space-time migration of earthquakes along the North Anatolian fault zone and seismic gaps: *Pure and Applied Geophysics*, v. 117, p. 1258–1270.

- Wang, W., Zhao, B., Wang, Q. and Yang, S., 2012. Noise analysis of continuous GPS coordinate time series for CMONOC. *Advances in Space Research*, 49, 943– 956. doi: 10.1016/j.asr. 2011.11.032
- Wilbur B. Davenport and Willian L. 1987. *An Introduction to the Theory of Random Signals and Noise*. Root, IEEE Press, New York, ISBN 0-87942-235-1.
- Williams, S.D.P., 2003. The effect of coloured noise on the uncertainties of rates estimated from geodetic time sereis. *J. Geod.* 76 (9-10): 483 – 494.
- Williams, S.D.P., Bock, Y., Fang, P., Jamason, P., Nikolaidis, R.M., Prawirodirdjo, L., Miller, M., Johnson, D.J., 2004. Error analysis of continuous GPS position time series. *J. Geophys. Res.* 109 (B03412), doi:10.1029/2003JB002741.
- Xu, H., 2016. *Development of Beidou navigation system set to flourish*, http://en.ce.cn/Insight/201605/03/t20160503_11149733.shtml, May 2016.
- Zhang, J., Y. Bock, H. Johnson, P. Fang, S. Williams, J. Genrich, S. Wdowinski, and J. Behr, 1997: Southern California permanent GPS geodetic array: Error analysis of daily position estimates and site velocities. *J. Geophys. Res.*, 102, 18035-18055, doi: 10.1029/97JB01380.

APPENDIX A: SESSION TABLE

Session Table

Processing Agency = MIT

.....

Satellite Constraint = Y ; Y/N (next two lines are free-format but 'all' must be present)

—	all	a	e	i	n	w	M	rad1	rad2	rad3	rad4	rad5	rad6
rad7	rad8	rad9											
—		0.01	0.01	0.01	0.01	0.01	0.01	0.01	0.01	0.01	0.01	0.01	0.01
0.01	0.01	0.01											

.....

—<< Controls must begin in column 1 >>

Choice of Experiment = BASELINE ; BASELINE/RELAX./ORBIT

Type of Analysis = 1-ITER ; 1-ITER (autcln prefit and conditional redo) / 0-ITER (no postfit autcln) / PREFIT

AUTCLN redo = Y ; Y/N; 3rd soln only if needed, assume 'Y' if 'Type of analysis = 1-ITER'

Choice of Observable = LC_AUTCLN ; LC_AUTCLN (default), LC_HELP (codeless L2), L1_ONLY (L1 soln from dual freq),
 — L2_ONLY (L2 soln from dual freq), L1,L2_INDEPENDENT (L1 + L2 from dual freq)
 — L1&L2 (same as L1, L2_INDEPENDENT but with ion constraint);
 — L1_RECEIVER (must add 'L1only' in

autcln.cmd) Station Error = ELEVATION 10 5 ; 1-way L1, a**2 +
 (b**2)/(sin(elev)**2) in mm. default = 10. 0.

AUTCLN reweight = Y ; Y/N; reweight data from autcln rms; replaces 'Use N-file' in releases < 10.32

AUTCLN Command File = autcln.cmd ; Filename; default none (use default options)

Decimation Factor = 4 ; FOR SOLVE, default = 1

Quick-pre decimation factor = 10 ; 1st iter or autcln pre, default same as Decimation Factor

```

Quick-pre observable = LC_ONLY      ; for 1st soln, default same as Choice of observable

Ionospheric Constraints = 0.0 mm + 8.00 ppm
Ambiguity resolution WL = 0.15 0.15 1000. 99. 15000. ; for LC_HELP, ignored for LC_AUTCLN
Ambiguity resolution NL = 0.15 0.15 1000. 99. 15000. ; allow long baselines with LC_AUTCLN

Zenith Delay Estimation = Y          ; Yes/No (default No)
Interval zen = 2                    ; 2 hrs = 13 knots/day (default is 1 ZD per day)
Zenith Constraints = 0.50            ; zenith-delay a priori constraint in meters (default 0.5)
Zenith Variation = 0.02 100.         ; zenith-delay variation, tau in meters/sqrt(hr), hrs (default .02 100.)
Elevation Cutoff = 0                 ; default 0 to use value in autcln.cmd
Atmospheric gradients = Y           ; Yes/Np (default No)
Number gradients = 2                 ; number of gradient parameters per day (NS or ES); default 1
Gradient Constraints = 0.01          ; gradient at 10 deg elevation in meters; default 0.03 m

Update T/L files = L_ONLY            ; T_AND_L (default), T_ONLY, L_ONLY, NONE
Update tolerance = .3                ; minimum adjustment for updating L-file coordinates, default .3 m
Met obs source = UFL GPT 50          ; hierarchical list with humidity value at the end; e.g. RNX UFL GPT 50 ;
default GTP 50
—                                     if [humid value] < 0, use RNX, UFL(VMF1), or GPT2 if available
Output met = N                       ; write the a priori met values to a z-file (Y/N)
Use met.list = N                     ; not yet supported
Use met.grid = N                     ; not yet supported
DMap = VMF1                          ; GMF (default)/VMF1/NMFH; GMF now invokes GPT2 if gpt.grid is available (default)
WMap = VMF1                          ; GMF (default)/VMF1/NMFW; GMF now invokes GPT2 if gpt.grid is available (default)
Use map.list = N                     ; VMF1 list file with mapping functions, ZHD, ZWD, P, Pw, T, Ht
Use map.grid = Y                     ; VMF1 grid file with mapping functions and ZHD
Yaw Model = Y                        ; Y/N default = Y
Radiation Model for ARC = BERNE      ; SPHRC/BERNE/BERN1,BERN2/UCLR1/UCLR2/SRDYB/SVBDY/NONE default = BERNE
Earth radiation model = TUME1        ; NCLE1/NCLE2/TUME1/TUME2/NONE default = NONE; MIT repro2 = NCLE1
Antenna thrust model = ANTBK         ; ANTBK/NONE default = NONE; MIT repro2 = ANTBK
Inertial frame = J2000               ; J2000/B1950 default = J2000

```

```

Reference System for ARC = EGM08 ; WGS84/EGM96/EGM08/EGR08  default = EGM008; MIT repro2 = EGR08 (relativity)
.
Tides applied = 31          ; Binary coded: 1 earth  2 freq-dep  4 pole  8 ocean  16 remove mean for pole
tide
—                          ; 32 atmosphere;  default = 31
Use otl.list = N            ; Ocean tidal loading list file from OSO
Use otl.grid = Y            ; Ocean tidal loading grid file, GAMIT-format converted from OSO
Etide model = IERS03        ; IERS96/IERS03
Earth Rotation = 11         ; Diurnal/Semidirunal terms: Binary coded: 1=pole 2=UT1 4=Ray model; 8=IERS2010
16=include libration
terms; default=11
Apply atm loading = N       ; Y/N for atmospheric loading
Use atml.list = N           ; Atmospheric (non-tidal) loading list file from LU
Use atml.grid = N           ; Atmospheric (non-tidal) loading grid file from LU, converted to GAMIT format
Use atl.list = N            ; Atmospheric tides, list file, not yet available
Use atl.grid = N            ; Atmospheric tides, grid file

Antenna Model = AZEL        ; NONE/ELEV/AZEL  default = ELEV   Use AZEL for IGS absolute ANTEX files
SV antenna model = ELEV     ; NONE/ELEV      default = NONE    Use ELEV for IGS ANTEX files
SV antenna off = N          ; Y/N to estimate satellite antenna offsets (default N)

Delete AUTCLN input C-files = Y  ; Y/N ; default Y to force rerun of MODEL
Scratch directory = /tmp      -<< List of additional controls not

commonly - blank first column to indicate a comment >>

.....
—Simulation con              : s-file name
—Inertial frame = B1950      ; B1950/J2000 (default = J2000)
.....

```

```

—Initial ARC                ; Y/N default = Yes
—Final ARC                  ; Y/N default = No
—Radiation Model for ARC    ; SPHRC/BERNE/SRDYB/SVBDY default = SPHRC
—Reference System for ARC    ; WGS72/WGS84/MERIT/IGS92/EGM96/EGM08 (incremental_updates) (default = EGM08)
—Reference System for ARC = EGM08 ; WGS72/WGS84/MERIT/IGS92/EGM96/EGM08/EGR08 default = EGM008; MIT repro2 =
EGR08 (relativity)

—Tabular interval for ARC    ; 900. seconds (new default), 1350. seconds (old default)
—Stepsize for ARC           ; 75. seconds (new default), 168.75 seconds (old default)
—Arc debug flag             ; Turn on various print and test options (see arc.f) (default = 0 )
.

—Earth Rotation              ; Diurnal/Semidirunal terms: Binary coded: 1=pole 2=UT1 4=Ray model;
8=IERS2010 ; default=11
—Estimate EOP                ; Binary coded: 1 wob    2 ut1    4 wob rate    8 ut1 rate
—Wobble Constraint = 3. 0.3   ; Default 3. (arcsec) 0.3 (arcsec/day)
—UT1 Constraint = 0.00002 0.02 ; Default .00002 (sec) 0.02 (sec/day)
...

—Number Zen = 4              ; number of zenith-delay parameters (default 1)
—Zenith Constraints = 0.50    ; zenith-delay a priori constraint in meters (default 0.5)
—Zenith Model = PWL          ; PWL (piecewise linear)/CON (step)
—Zenith Variation = 0.02 100. ; zenith-delay variation, tau in meters/sqrt(hr), hrs (default .02 100.)
—Gradient Constraints = 0.03  ; gradient at 10 deg elevation in meters
—Gradient Variation = .01 100 ; gradient variation
—Tropospheric Constraints = NO ; YES/NO    (spatial constraint)

—Ion model = GMAP            ; NONE/GMAP (default NONE) use 2nd/3rd order ionspheric corrections
—Mag field = IGRF12          ; IGRF12/IGRF11/IGRF10/DIPOLE (default IGRF12)

—Yaw Model                   ; YES/NO default = YES
—I-file = N                  ; Use I-file (Y/N)   (default Y)
.....

```

—AUTCLN Postfit = Y ; Assume 'Y' if 'Type of analysis = 1-ITER' (autcln.cmd.postfit file also)
 —Delete AUTCLN input C-files = Y ; YES/NO/Intermediate (default no)
 —AUTCLN Command File ; Filename; default none (use default options)
 —Delete eclipse data = POST ; ALL/NO/POST (Default = NO)
 —SCANDD control ; BOTH (default) /NONE/FIRST/FULL/IFBAD see manual sec. 5.2
 —Iteration ; CFILES / XFILES (default)
 —Edit AUTCLN Command File ; YES/NO; default = NO (For clocks, no longer needed)

—Ambiguity resolution WL ; default = 0.15 0.15 1000. 10. 500.
 —Ambiguity resolution NL ; default = 0.15 0.15 1000. 10. 500.
 —Type of Biases ; IMPLICIT (default for quick), EXPLICIT (default for full)
 —H-file solutions ; ALL; LOOSE-ONLY
 —Skip loose ; Y / N (default) sometimes necessary for
 short baselines —Station Error = BASELINE 10. 0. ; 1-way L1, $a^{**2} + (b^{**2})(L^{**2})$ in mm, ppm, default = 10. 0.
 —Station Error = UNIFORM 10. ; 1-way L1 in mm, default = 10.
 —Station Error = ELEVATION 4.3 7.0 ; 1-way L1 , $a^{**2} + b^{**2}/\sin(\text{elev})^{**2}$ in mm, default =
 4.3 7.0 —Satellite Error = UNIFORM 0. ; 1-way L1 in mm (added quadratically to
 station error) default = 0.
 —Select Epochs ; Enter start and stop epoch number (applies only to SOLVE)
 —Decimation Factor ; FOR SOLVE, default = 1
 —Elevation Cutoff = 15. ; For SOLVE, overrides the MODEL or AUTCLN values if they are lower
 —Correlation print ; Threshold for printing correlations (default 0.9999)

—Export Orbits ; YES/NO default = NO
 —Orbit id ; 4-char code read only if Export Orbits = YES
 —Orbit Format ; SP1/SP3 (NGS Standard Products)
 —Orbit organization ; 3-char code read only if Export Orbits = YES
 —Reference System for Orbit = ITR93; ITR92/ITR91/ITR90/WGS84/MERIT (for SP3 header)
 —Reference System for ARC = EGM08; WGS84/EGM96/EGM08/EGR08 default = EGM008; MIT repro2 = EGR08 (relativity)

```

—Lunar eclipses = Y          ; Set = N to turn off lunar eclipses in ARC to match model of GAMIT < 10.2
(default Y)

—                               (no longer supported: see arc_debug below)
—Delete all input C-files    ; YES/NO default = NO
—Delete MODEL input C-files ; YES/NO default = NO
—Delete AUTCLN input C-files ; YES/NO default = NO
—Update T/L files           ; T_AND_L (default), T_ONLY, L_ONLY, NONE
—                               (Applies only to update for final solution after initial)
—Update tolerance           ; minimum adjustment for updating L-file coordinates, default .3 m
—SOLVE-only = YES           ; YES/NO default = NO
—X-compress = YES           ; Uncompress/compress X-files default = NO
—SCANDD control              ; FULL (default), FIRST, BOTH, IFBAD, NONE
—Run CTOX = YES              ; Make clean X-files from C-files default = NO
—Bias apriori = 100.         ; Optional constraint on biases for LC_AUTCLN (default 0 -> no constraint)
—SOLVE print = Y            ; Turn on SOLVE output to screen (default N)

—Bias apriori = 1000.        ; Optional constraint on biases for LC_AUTCLN (default 1000, 0 -> constraint)
—Bias rcond = 10000.         ; Condition number ratio for fixing dependent biases (default 10000.)

```

APPENDIX B: PROCESS.DEFAULTS

```
# process.defaults
#
# Do not remove any of these entries. To by-pass a function, set the
value to null: ""
## LOCAL DIRECTORIES
# Directory for translation of raw data
set rawpth = "$procdir/raw"
# Directory path for raw archives (search all levels); e.g. /data18/simon
set rawfnd = ""
# Input files for RINEX translators set mpth = "$procdir/mkrinex"
# RINEX files directory set rpth = "$procdir/rinex"
# Directory path for RINEX archives (search all levels); e.g.
/data18/simon set rnxfnd =
"/truba/home/yerbilimleri/sergintav/process_daf_krip/2015_rinx"
# Broadcast orbit directory set bpth = "$procdir/brdc"
# IGS files directory set ipth = "$procdir/igs"
# G-files directory
set gpth = "$procdir/gfiles"
# GAMIT and GLOBK tables directory set tpth = "$procdir/tables"
# Output gifs directory set gifpth = "$procdir/gifs"
# Globk solution directory set glbpth = "$procdir/gsoln" # Globk binary
h-file directory set glfpth = "$procdir/glbfd"
# Directory path for other h-files (LA, LB, LC options; search all
levels)
# e.g. "/raid1/tah/SIO_GLL"; ( /raid6/ftp/pub/MIT_GLL/H07
/raid2/simon/gps_analysis/cgps_hfiles )
set hfnd = "" # Template files
set templatepth = "$procdir/templates" # Place to store temporary
control files
set cpth = "$procdir/control"
# Archive root directory (cannot be null) set archivepth =
"$procdir/archive"
## FTP INFO FOR REMOTE FILES
# Raw data archive
# set rawarchive = 'chandler.mit.edu'
# set rawdir = 'pub/continuous/mitnet'
# set rawlogin = "anonymous simon@chandler.mit.edu"
# Addresses for CDDSI, SOPAC, IGSCB, UNAVCO, BKG, IGN, USNO are given in
template/ftp_info
##GAMIT
# Set sampling interval, number of epochs, and start time for processing
set sint = '30' set nepc = '2880' set stime = '0 0'
# Variables for updating tables set stinf_unique = "-u" set stinf_nosort
= "-nosort" set stinf_slthgt = "2.00"
# Set "Y" to use RINEX header coordinates not in lfile or apr file set
use_rxc = "Y"
# Broadcast orbits set brdc = 'brdc'
# Minimum x-file size to be processed (Def. 300 blocks; most OS use 1 Kb
blocks)
set minxf = '600'
```



```

# Set search window for RINEX files which might contain data for day -
default check the
previous day set rx_doy_plus = 1 set rx_doy_minus = 1
# Default globk .apr file set aprf = itrfr08_comb.apr
# Set compress (copts), delete (dopts) and archive (aopts) options.
(Don't forget to set the
archivepth.)
# Possible d-, c-, and a- opts: D, H, ao, ac, as, b, c, d, e, g, h, i, j,
k, l, m, o, p, q,
t, x, ps, all" set dopts = "" set copts = ( x k ao d ) set aopts = ( c
) # Set the rinex ftp archives (defined in ftp_info) you would like to
look for data in.
# (Default archives searched are: sopac, cddis and unavco). set
rinex_ftpsites = (sopac cddis unavco)
## RESOURCES
# Minimum raw disk space in Mbytes
set minraw = '1000'
# Minimum rinex disk space in Mbytes
set minrinex = '1000'
# Minimum archive disk space in Mbytes
set minarchive = '1000'
# Minimum working disk space in Mbytes set minwork = '5000'
## SYSTEM-DEPENDENT SETTINGS
# UNIX df command must be set to return the correct form
# Most machines (set udf = 'df -mk'
# but note that if you have free > 1 Tb, you will need to change this to
Mb
# set udf = 'df -m'
# HP
# set udf = 'bdf'
# UNIX mail command
# Most machines set umail = 'mail -s'
# HP
# set umail = 'mailx -s'
# Mail address for sending the processing report (if '' will default to
`whoami` in sh_gamit) set mailto = ''
# Host name for email and anonymous ftp password use (if '' will default
to `hostname` in
sh_gamit) set machine = '' # Ghostscript path set gspath = '/usr/bin'
# ImageMagick path for gif conversion
# set impath = '/usr/bin/X11' set impath = '/usr/bin'

```

APPENDIX C: SLURM

Overview

The Simple Linux Utility for Resource Management (Slurm) is an open source, fault-tolerant, and highly scalable cluster management and job scheduling system for large and small Linux clusters. Slurm requires no kernel modifications for its operation and is relatively self-contained. As a cluster workload manager, Slurm has three key functions. First, it allocates exclusive and/or non-exclusive access to resources (compute nodes) to users for some duration of time so they can perform work. Second, it provides a framework for starting, executing, and monitoring work (normally a parallel job) on the set of allocated nodes. Finally, it arbitrates contention for resources by managing a queue of pending work. Optional plugins can be used for accounting, advanced reservation, gang scheduling (time sharing for parallel jobs), backfill scheduling, topology optimized resource selection, resource limits by user or bank account, and sophisticated multifactor job prioritization algorithms.

Architecture

Slurm has a centralized manager, **slurmd**, to monitor resources and work. There may also be a backup manager to assume those responsibilities in the event of failure. Each compute server (node) has a **slurmd** daemon, which can be compared to a remote shell: it waits for work, executes that work, returns status, and waits for more work. The **slurmd** daemons provide fault-tolerant hierarchical communications. There is an optional **slurmdbd** (Slurm DataBase Daemon) which can be used to record accounting information for multiple Slurm-managed clusters in a single database. User tools include **srun** to initiate jobs, **scancel** to terminate queued or running jobs, **sinfo** to report system status, **squeue** to report the status of jobs, and **sacct** to get information about jobs and job steps that are running or have completed. The **smap** and **sview** commands graphically reports system and job status including network topology. There is an administrative tool **scontrol** available to monitor and/or modify configuration and state information on the cluster. The administrative tool used to manage the database is **sacctmgr**.

It can be used to identify the clusters, valid users, valid bank accounts, etc. APIs are available for all functions.

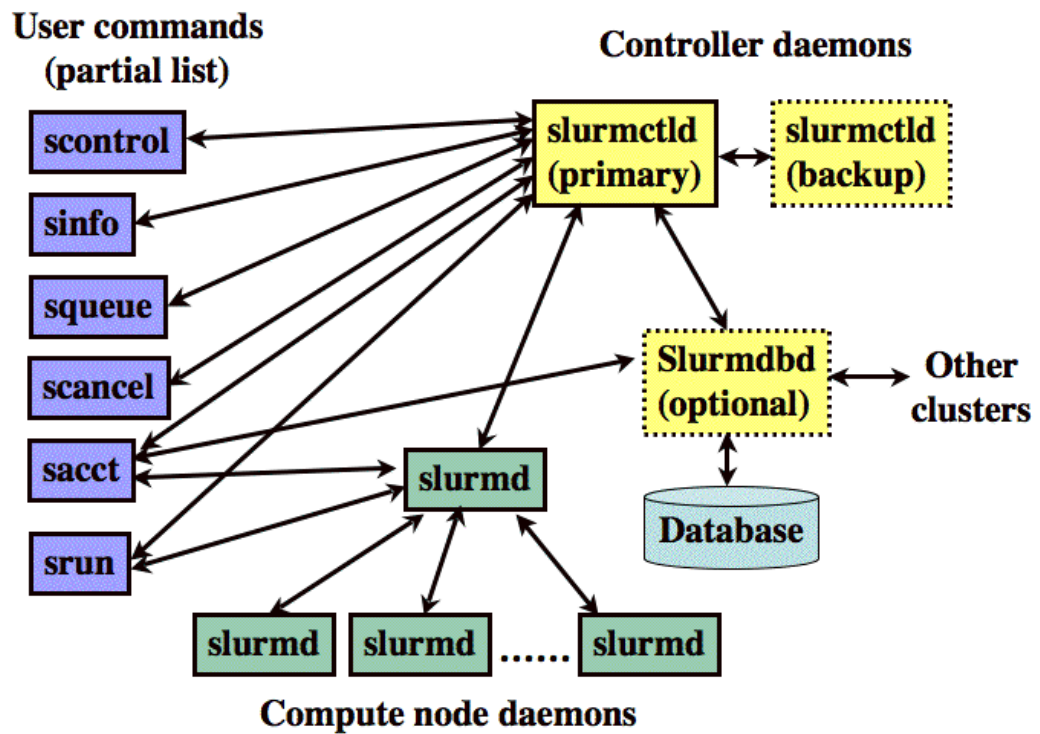


Figure C.1. Slurm components

Here is an example of the script we used in this study:

```
#!/bin/sh
#SBATCH -p mercan
#SBATCH -A sergintav
#SBATCH -J 2015_226-228
#SBATCH -N 1
#SBATCH -n 1
##SBATCH --nodelist=levrek15
##job array is 226-228
#SBATCH --array=226-228
#SBATCH --time=10:00:00
#SBATCH --mail-type=ALL
##SBATCH --mail-user=wumiti@gmail.com
#SBATCH --output=slurm-%A_%a.out
##SBATCH --error=slurm-%A_%a.err

export yb=/truba/home/yerbilimleri
export gamit=$yb/DEPO_PROG/gtgk
export
PATH=$yb/$gamit/com:$yb/$gamit/gamit/bin:$yb/$gamit/kf/bin:/
usr/bin:/usr/bin/ftp:$PATH

cd $yb/sergintav/process_daf_krip/2015/
sh_gamit -d 2015 $SLURM_ARRAY_TASK_ID -pres ELEV -c -expt
thes
```

APPENDIX D: HECTOR CONTROL FILE

estimatetrend.ctl:

DataFile	TEST_pre.mom
DataDirectory	./
OutputFile	TEST_out.mom
interpolate	no
seasonalsignal	yes
halfseasonalsignal	no
periodicsignals	
estimateoffsets	yes
NoiseModels	PowerlawApprox White
#NoiseModels	ARMA
LikelihoodMethod	AmmarGrag
PhysicalUnit	mm
ScaleFactor	1.0
TimeNoiseStart	1000.0
AR_p	1
MA_q	0

APPENDIX E: GPS POSTION TIME SERIES OF ALL STATIONS

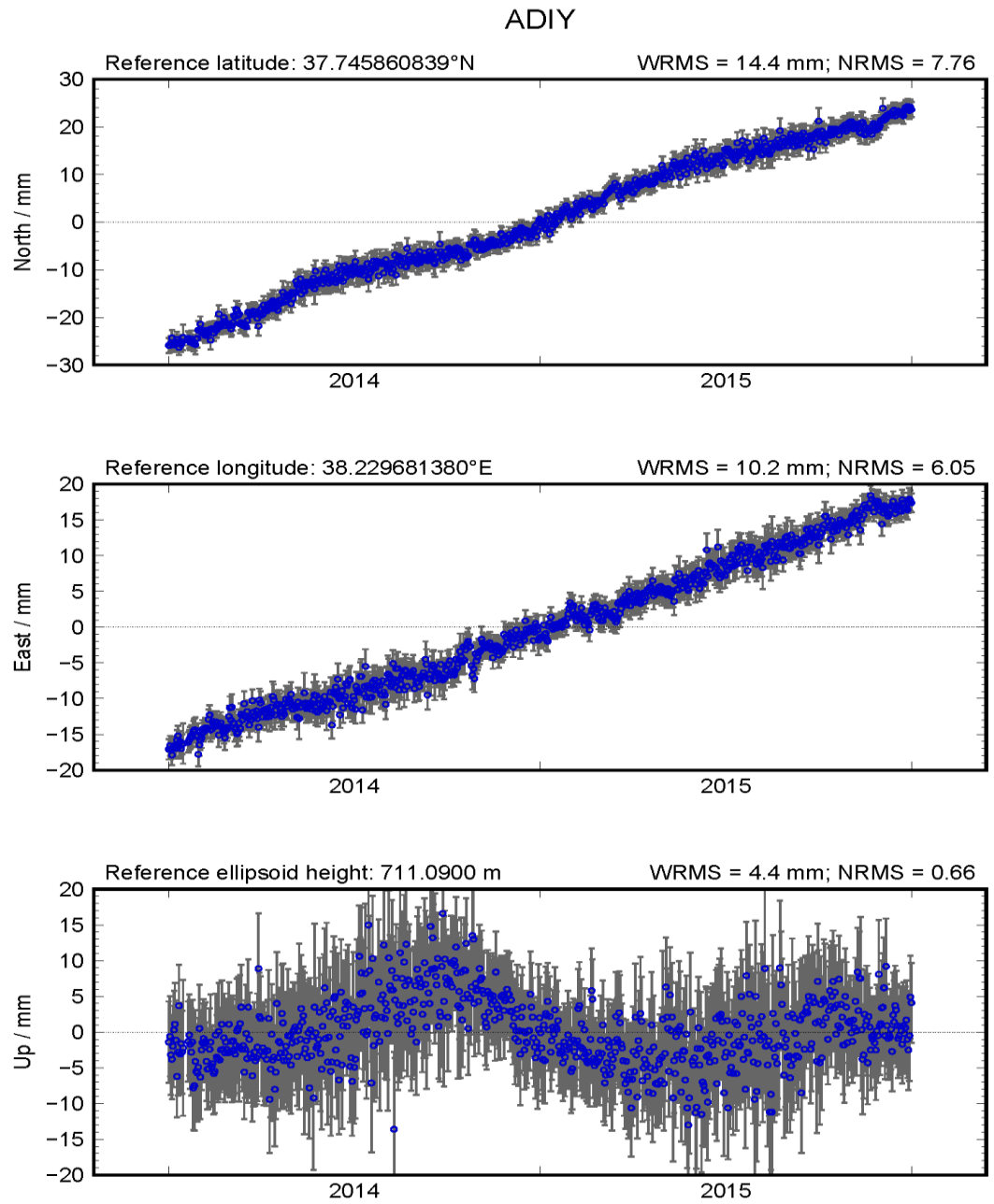


Figure E. 1. GPS time series of station ADIY.

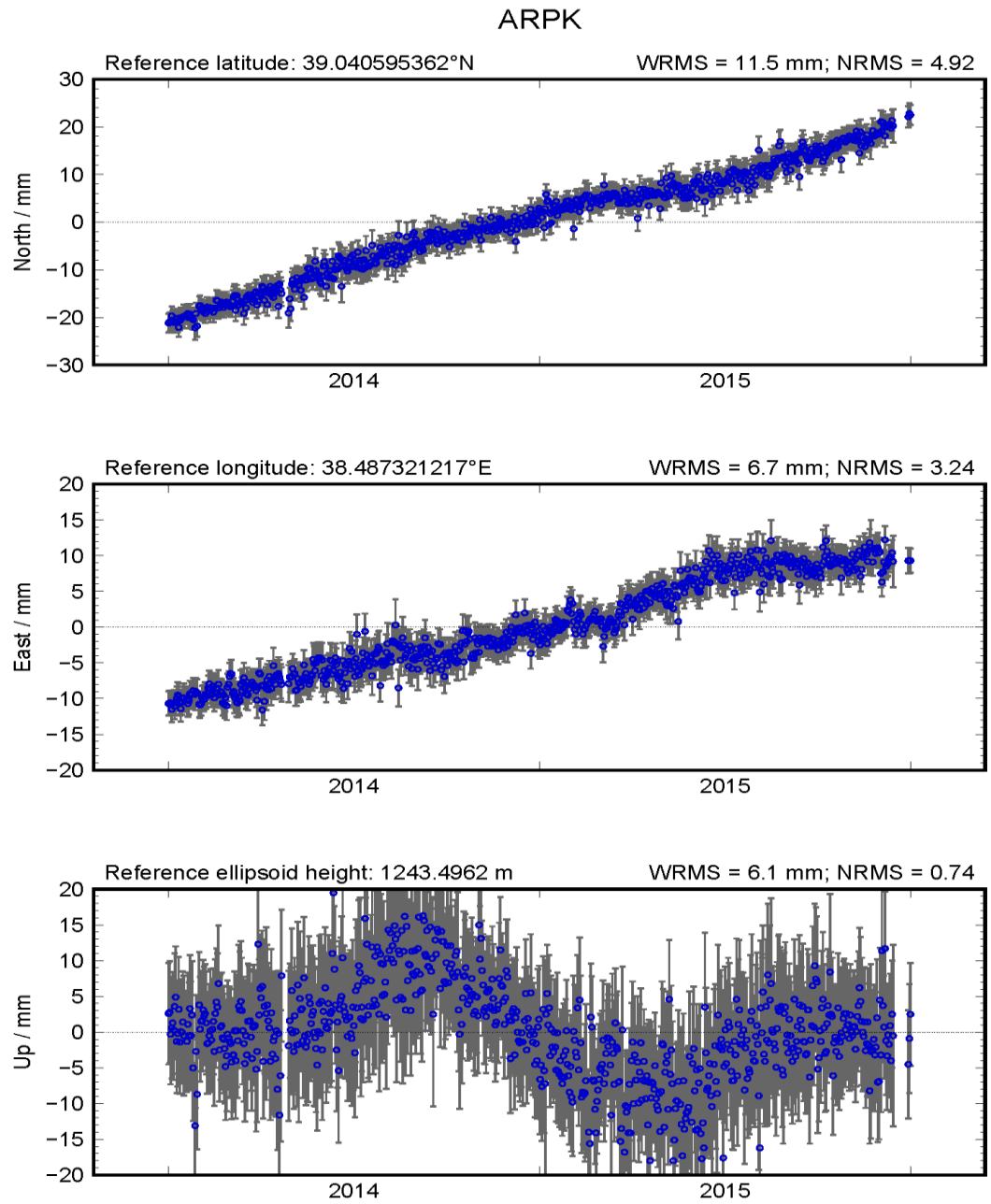


Figure E. 2. GPS time series of station ARPK.

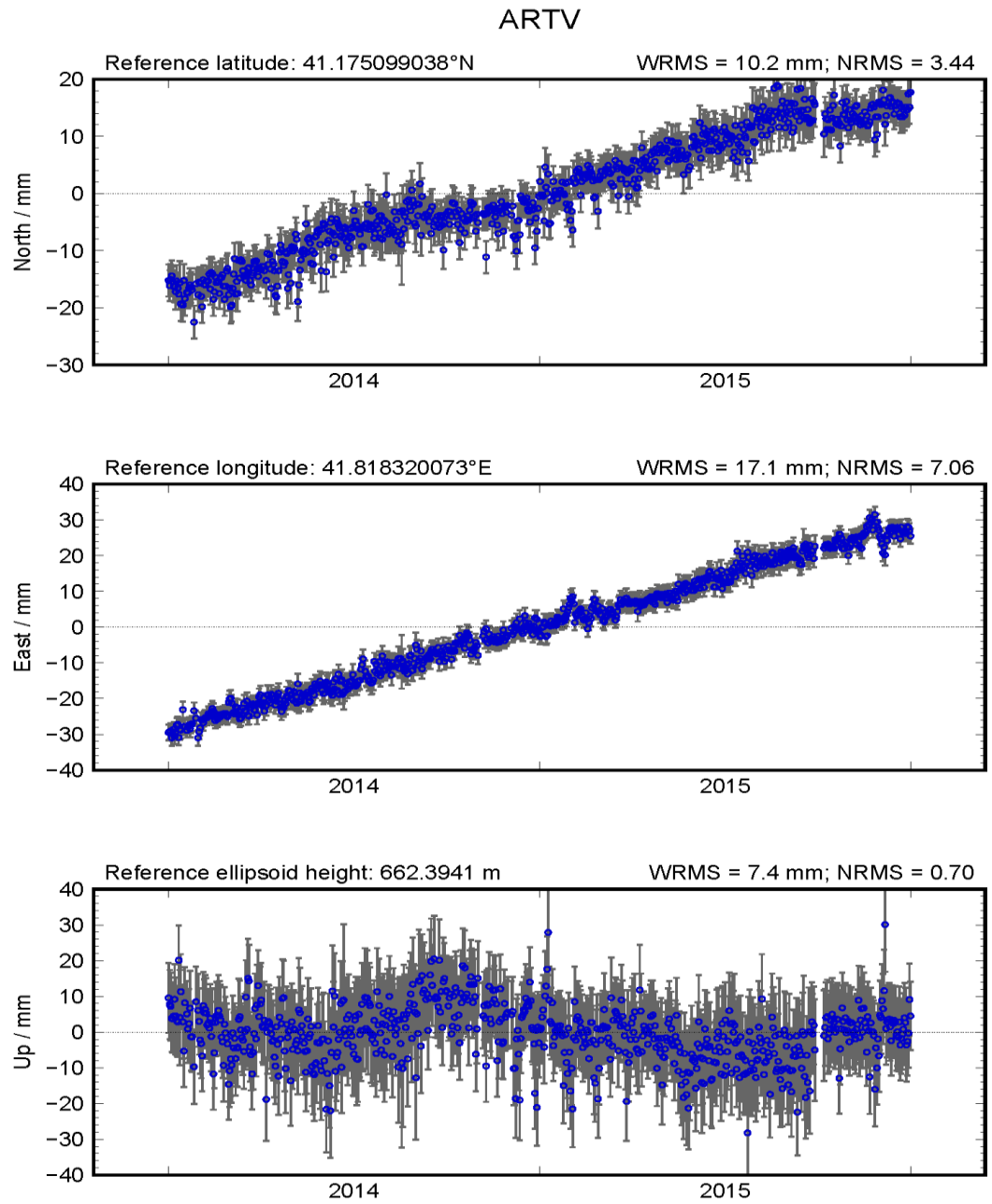


Figure E. 3. GPS time series of station ARTV.

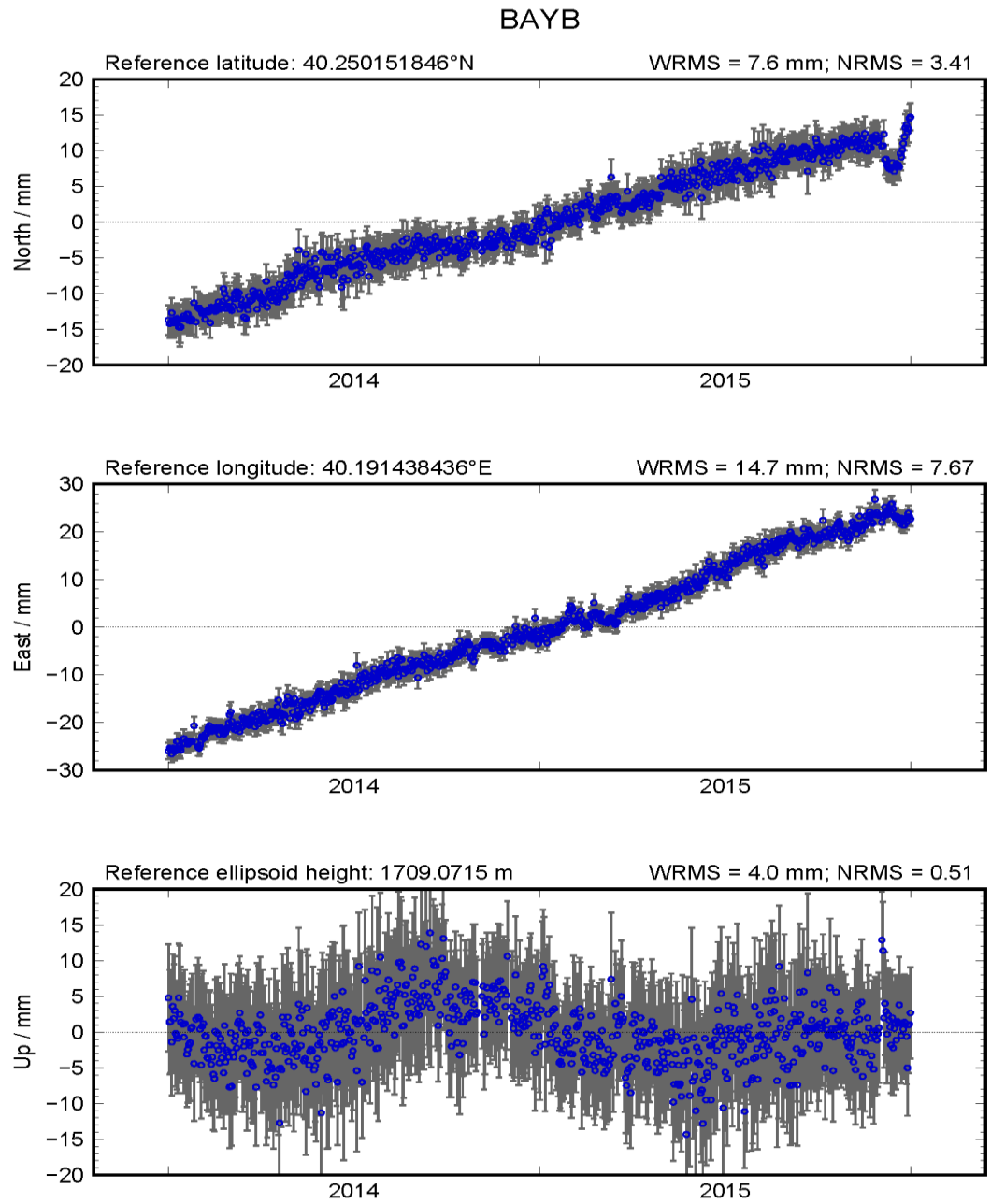


Figure E. 4. GPS time series of station BAYB.

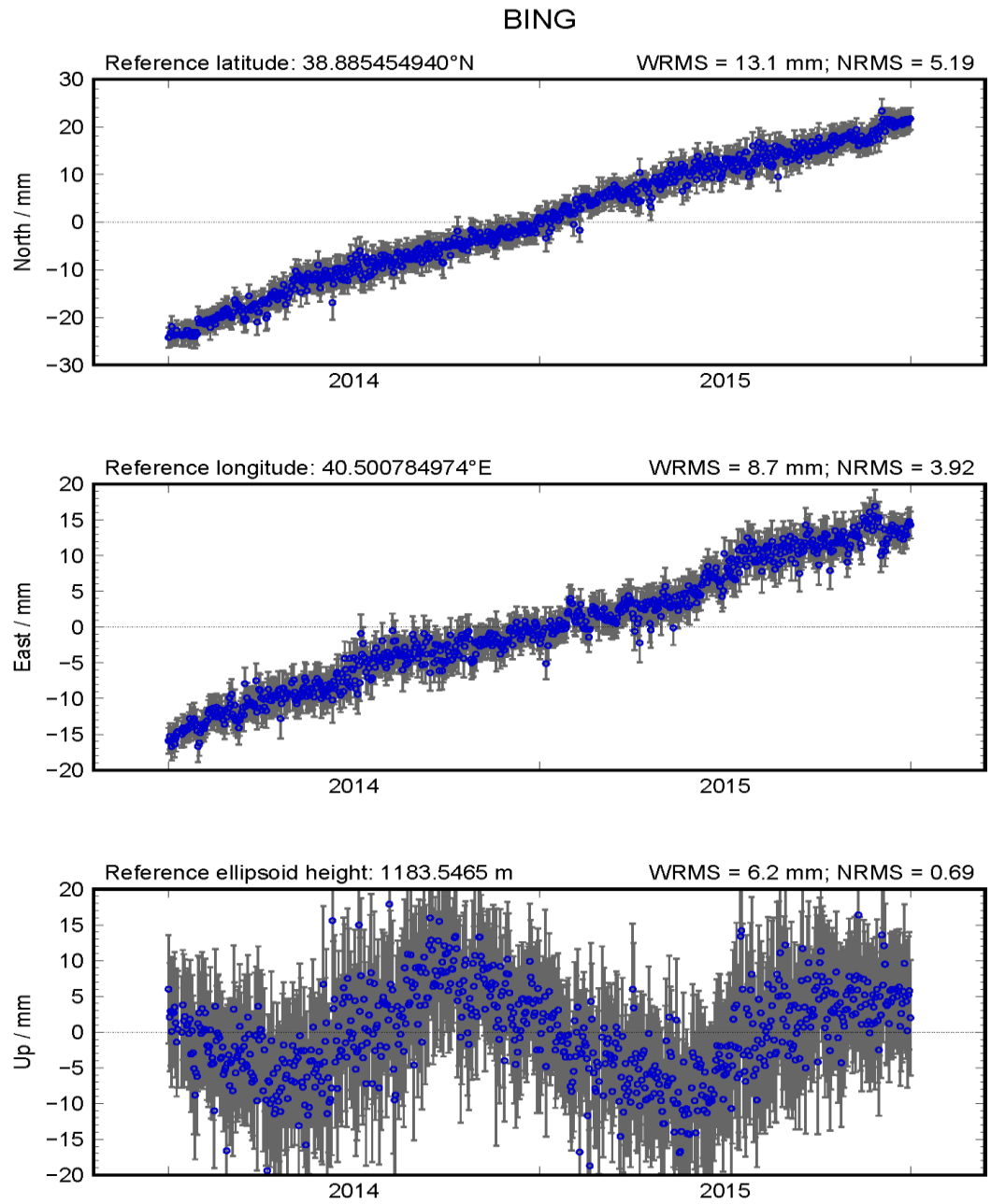


Figure E. 5. GPS time series of station BING.

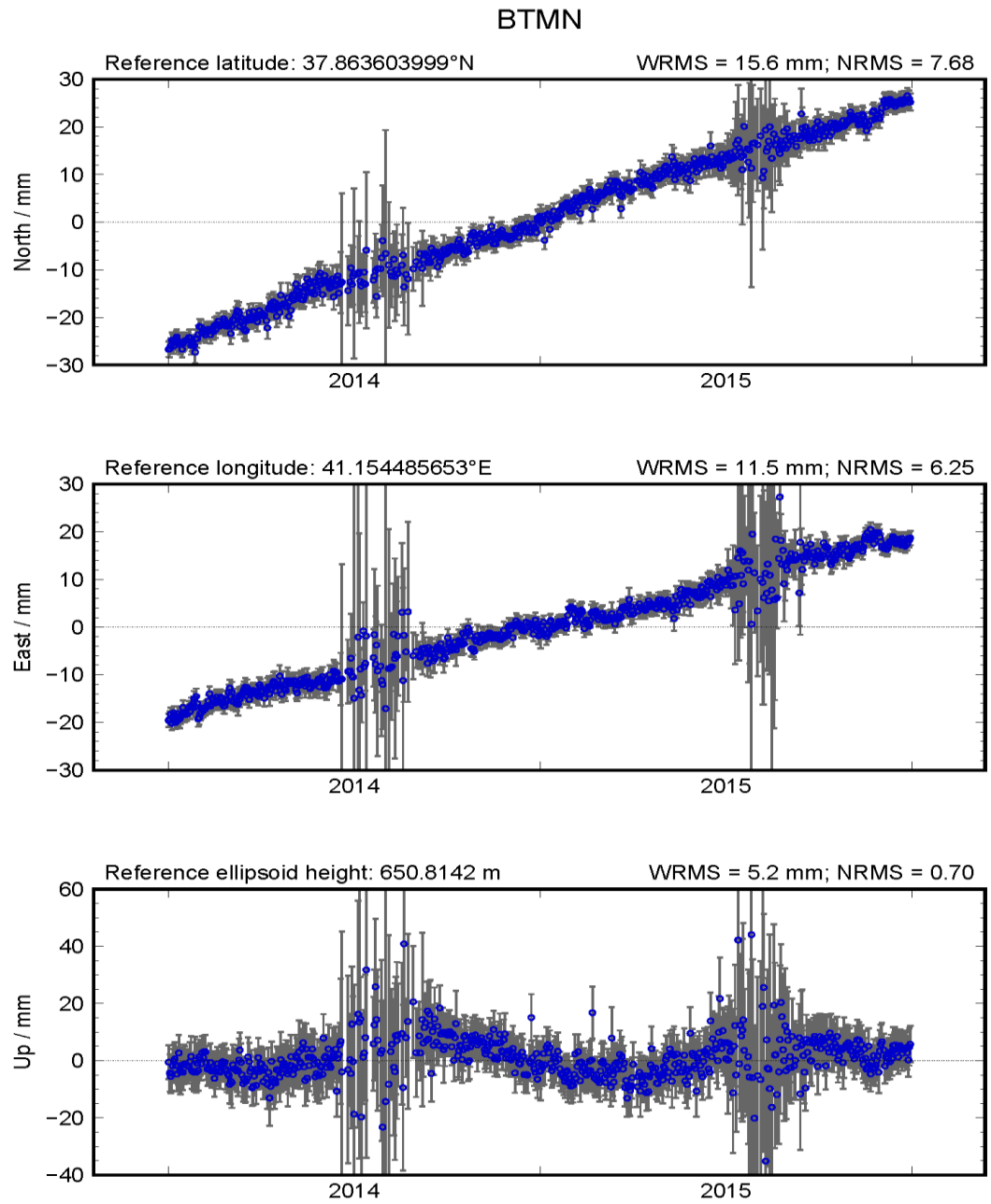


Figure E. 6. GPS time series of station BTMN.

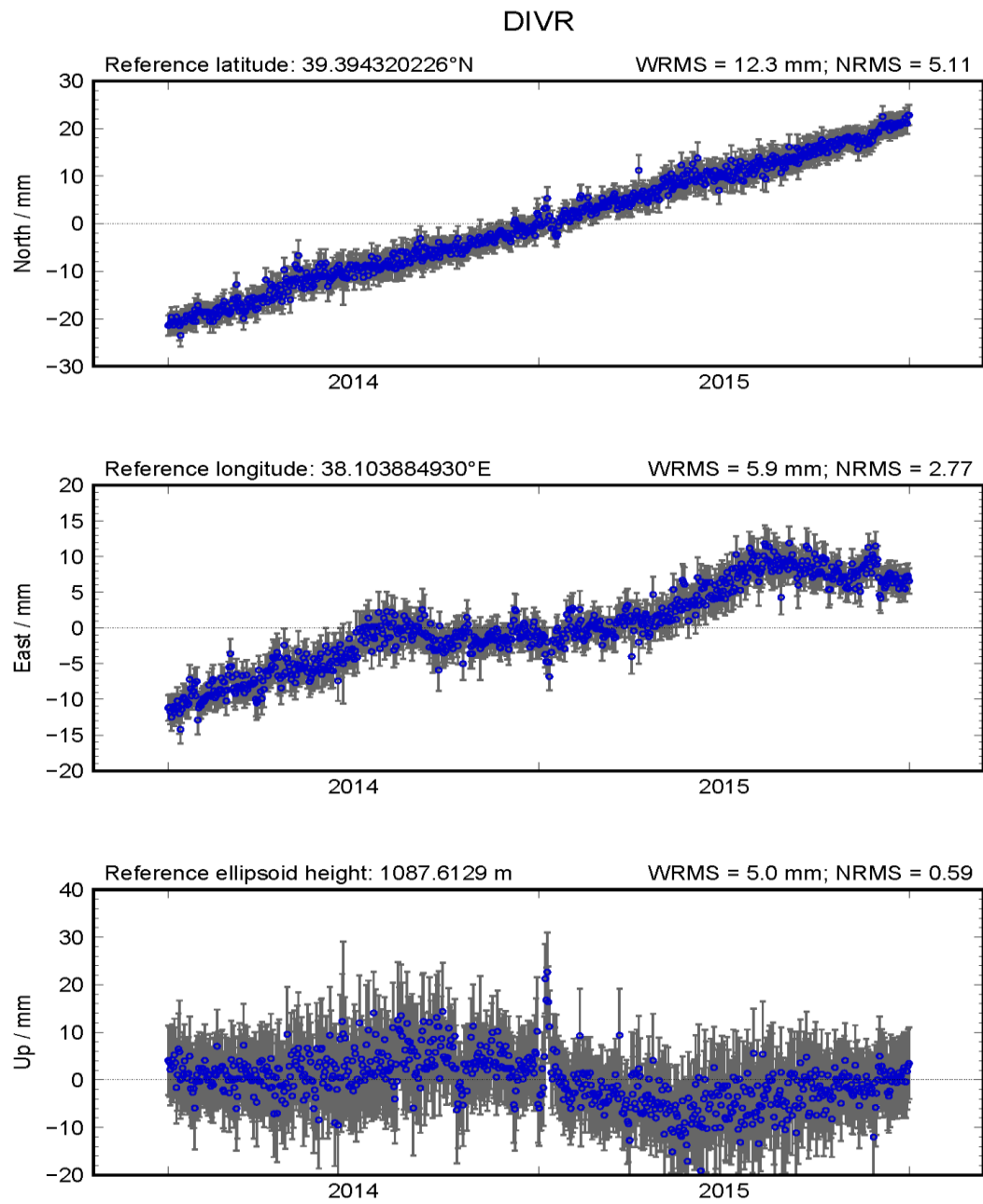


Figure E. 7. GPS time series of station DIVR.

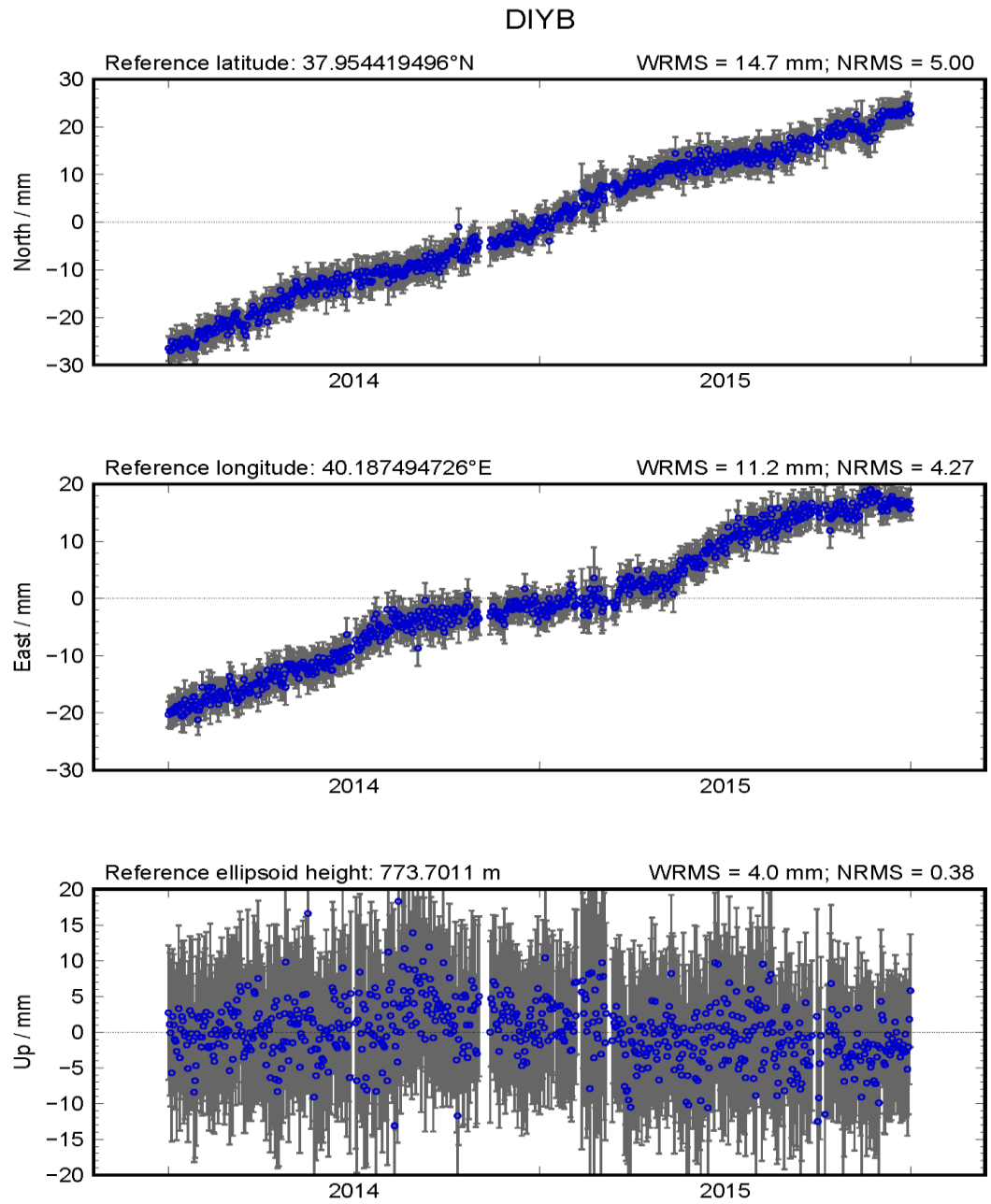


Figure E. 8. GPS time series of station DIYB.

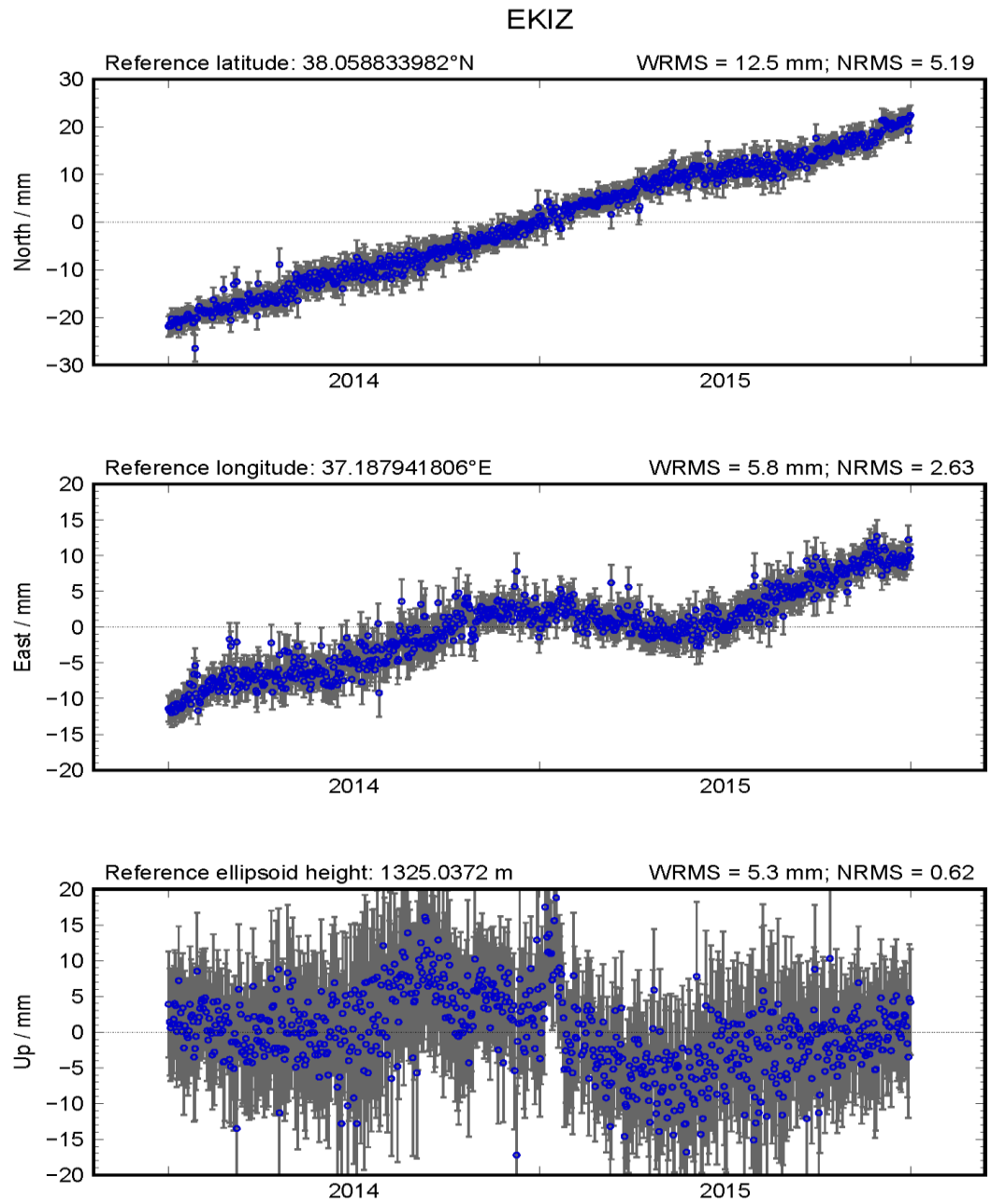


Figure E. 9. GPS time series of station EKIZ.

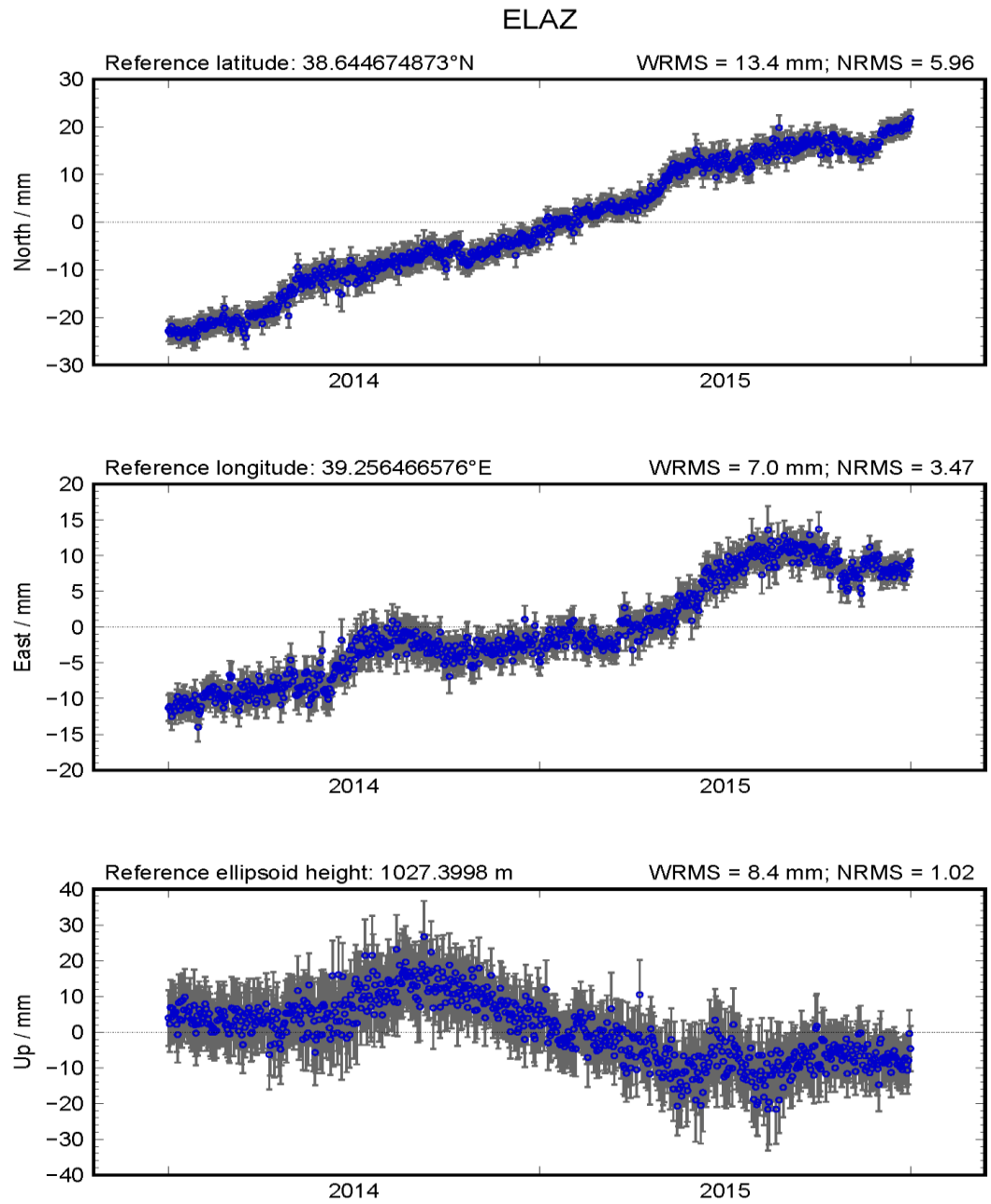


Figure E. 10. GPS time series of station ELAZ.

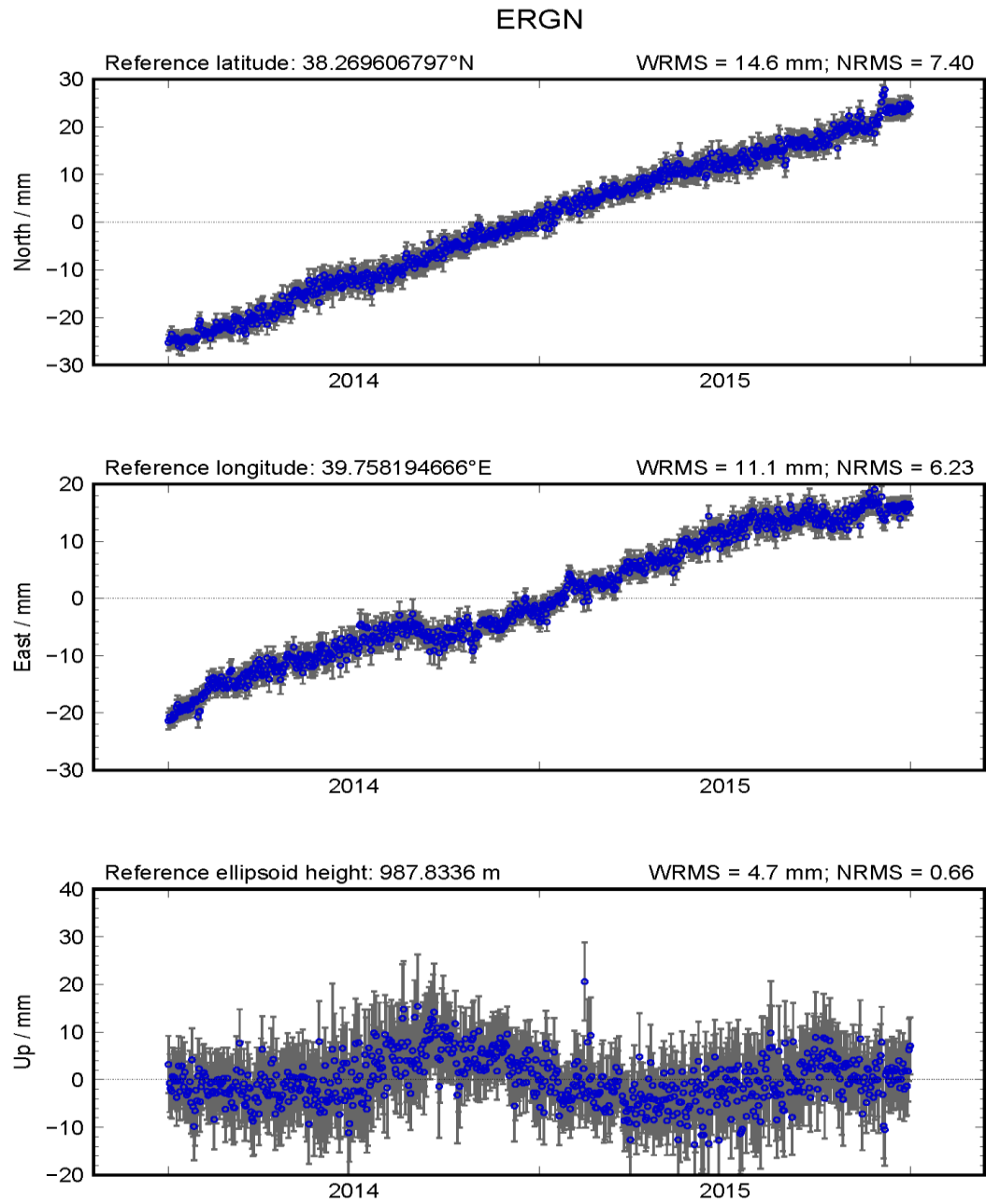


Figure E. 11. GPS time series of station ERGN.

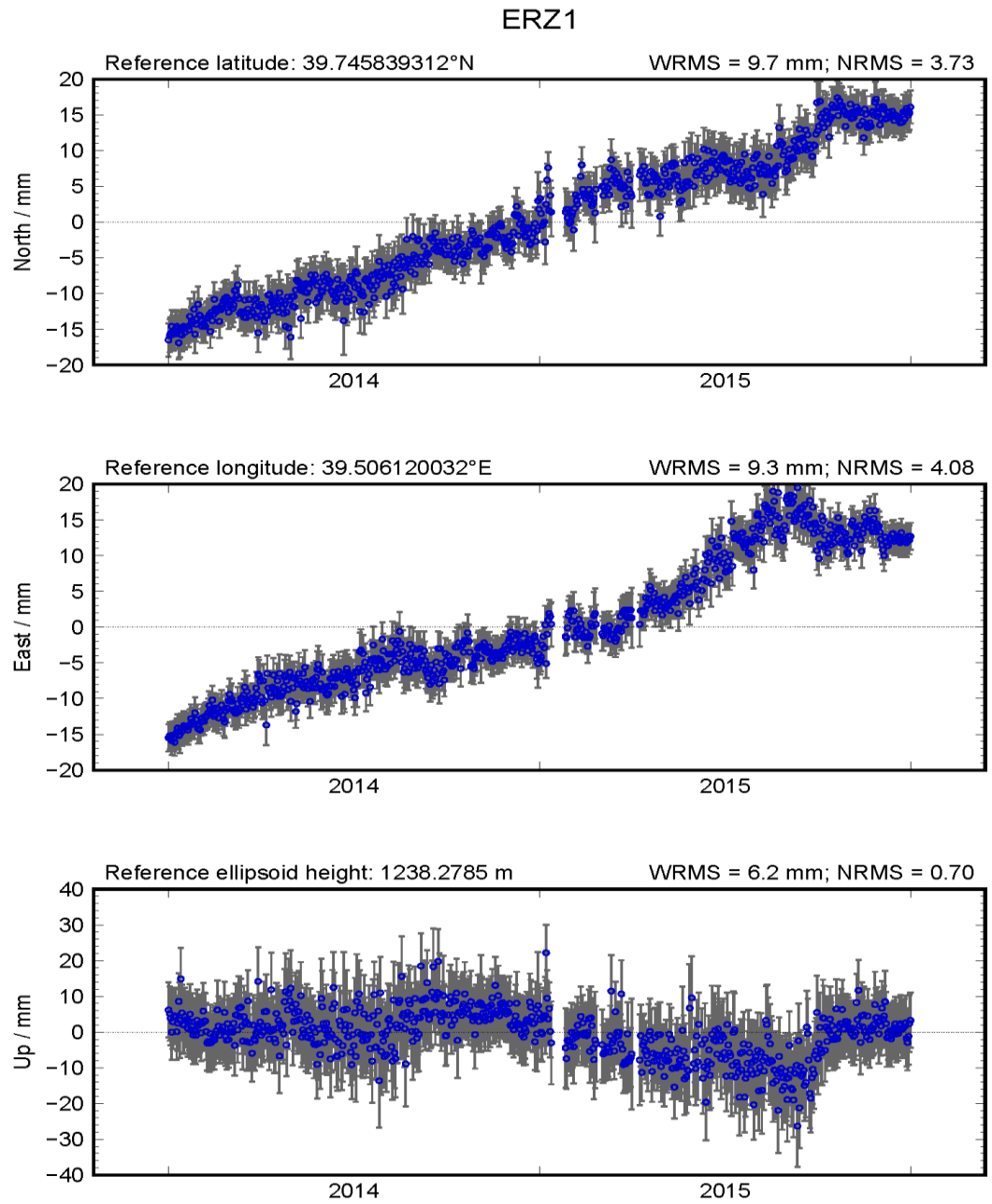


Figure E. 12. GPS time series of station ERZ1.

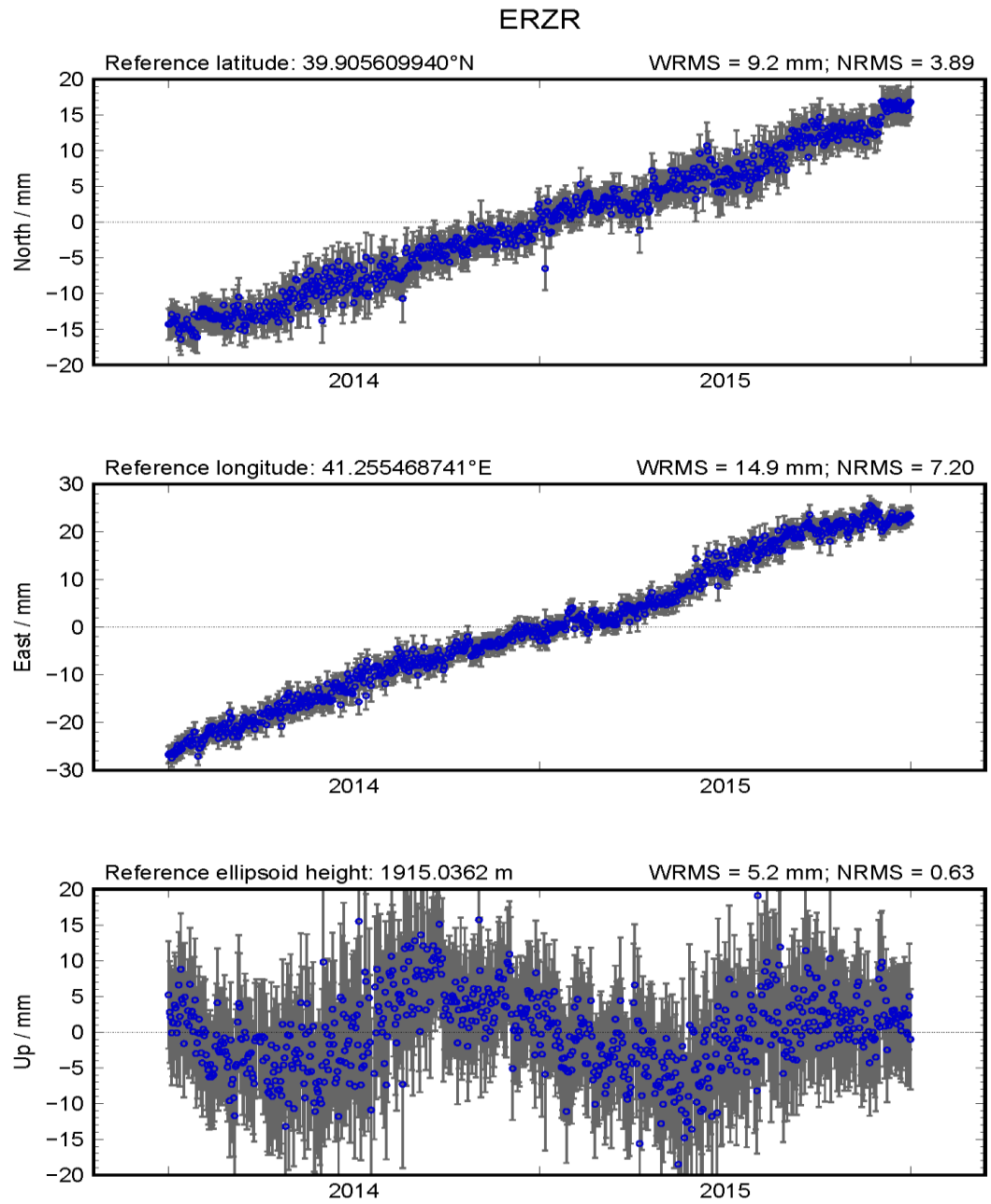


Figure E. 13. GPS time series of station ERZR.

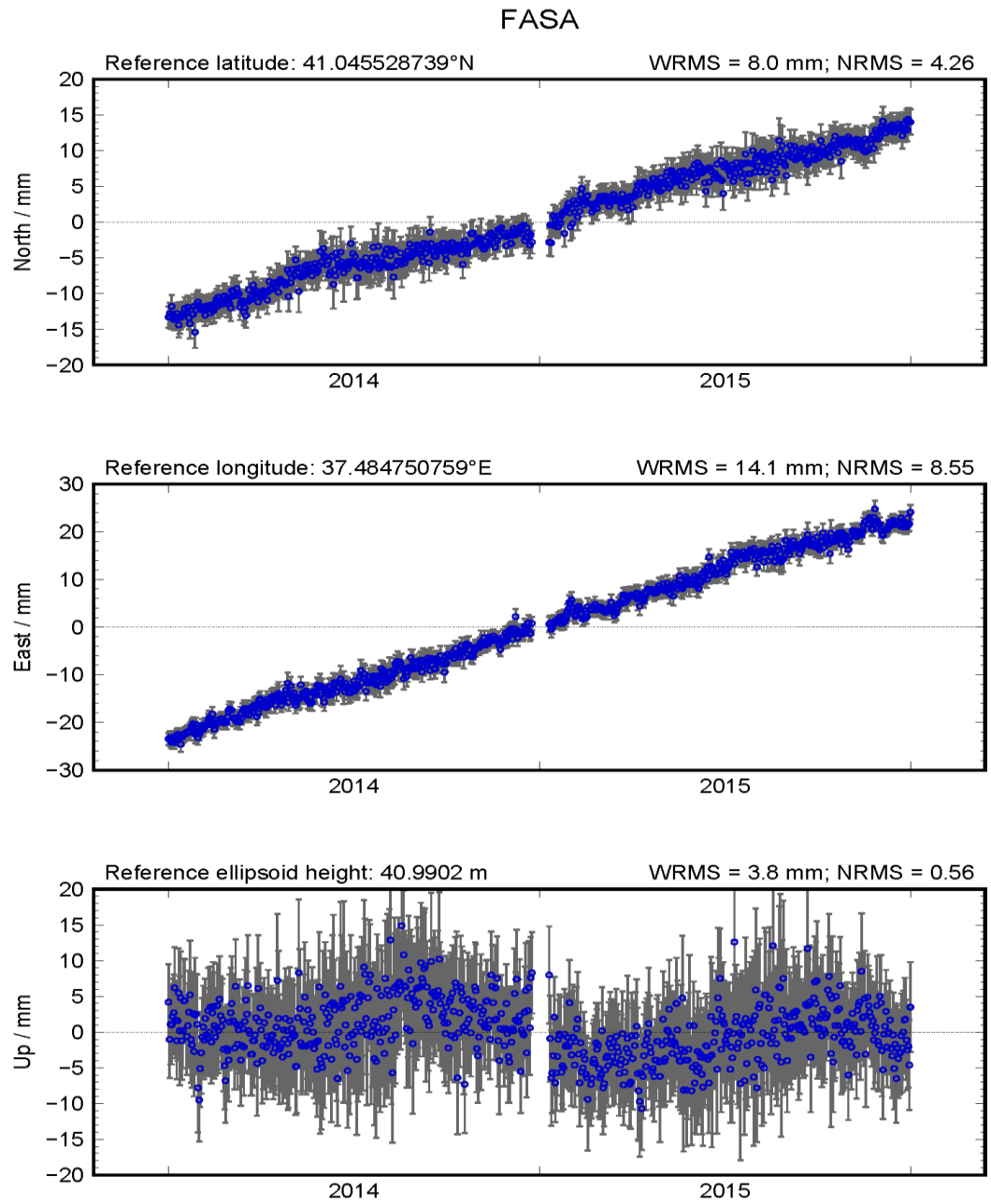


Figure E. 14. GPS time series of station FASA.

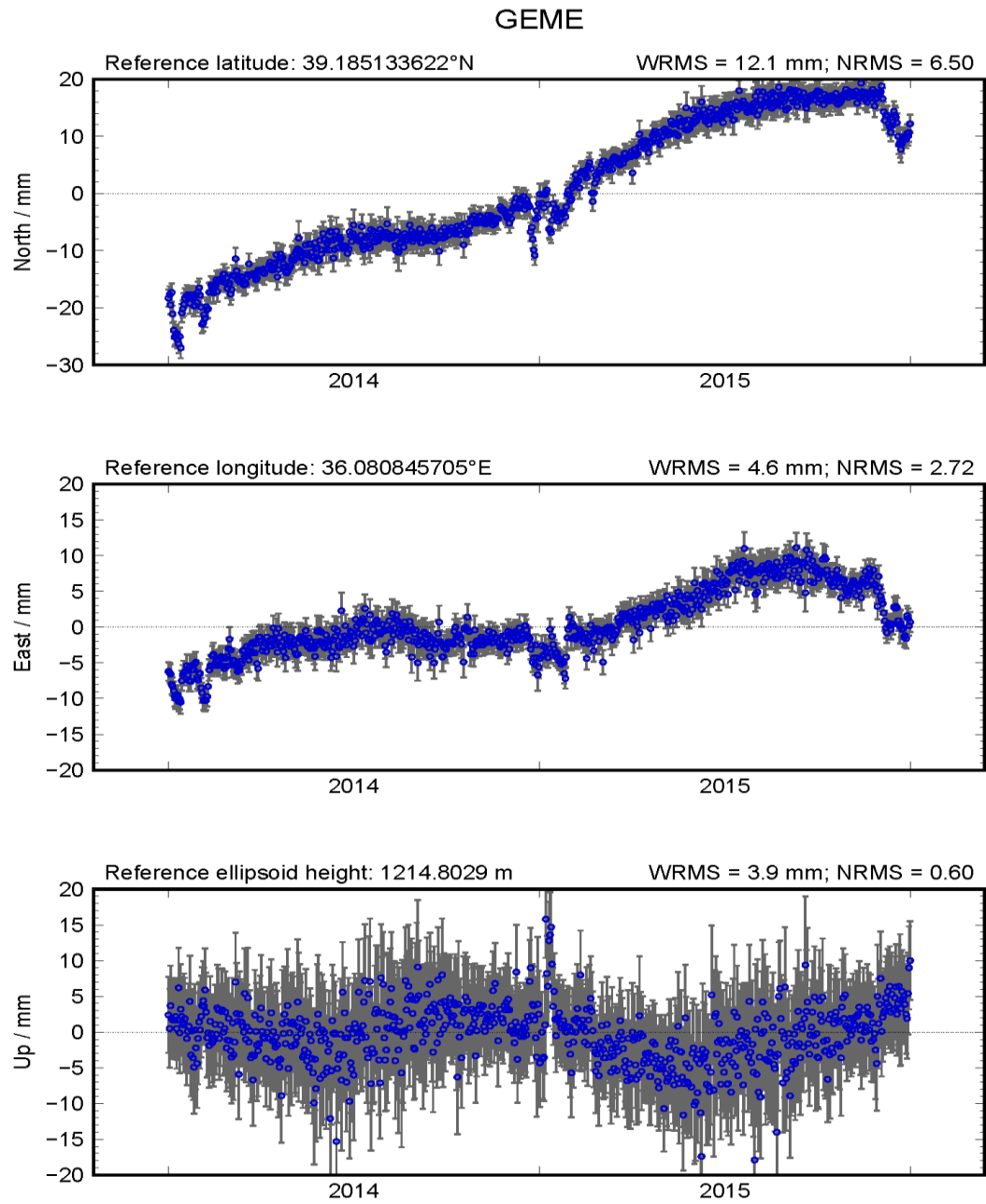


Figure E. 15. GPS time series of station GEME.

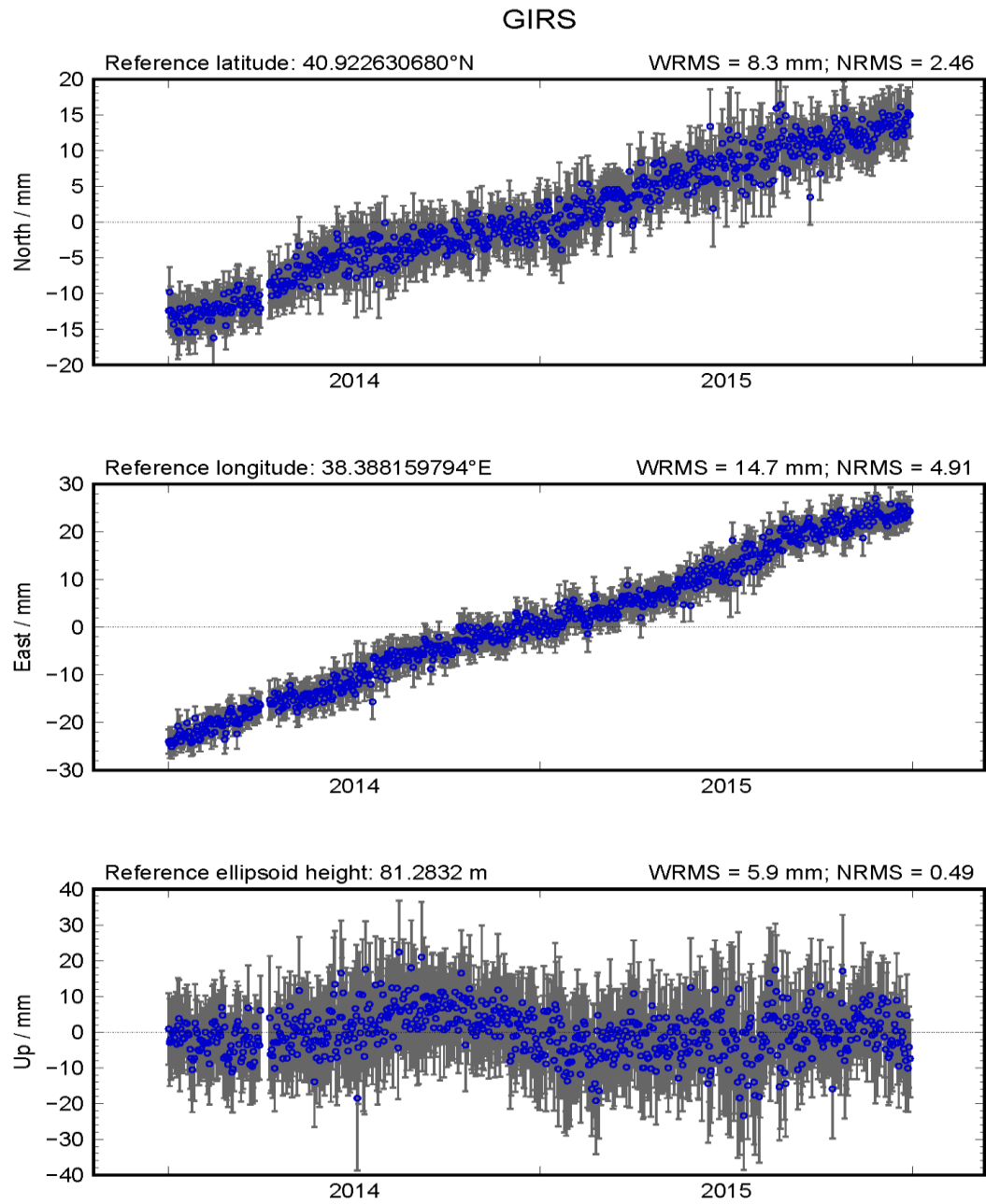


Figure E. 16. GPS time series of station GIRS.

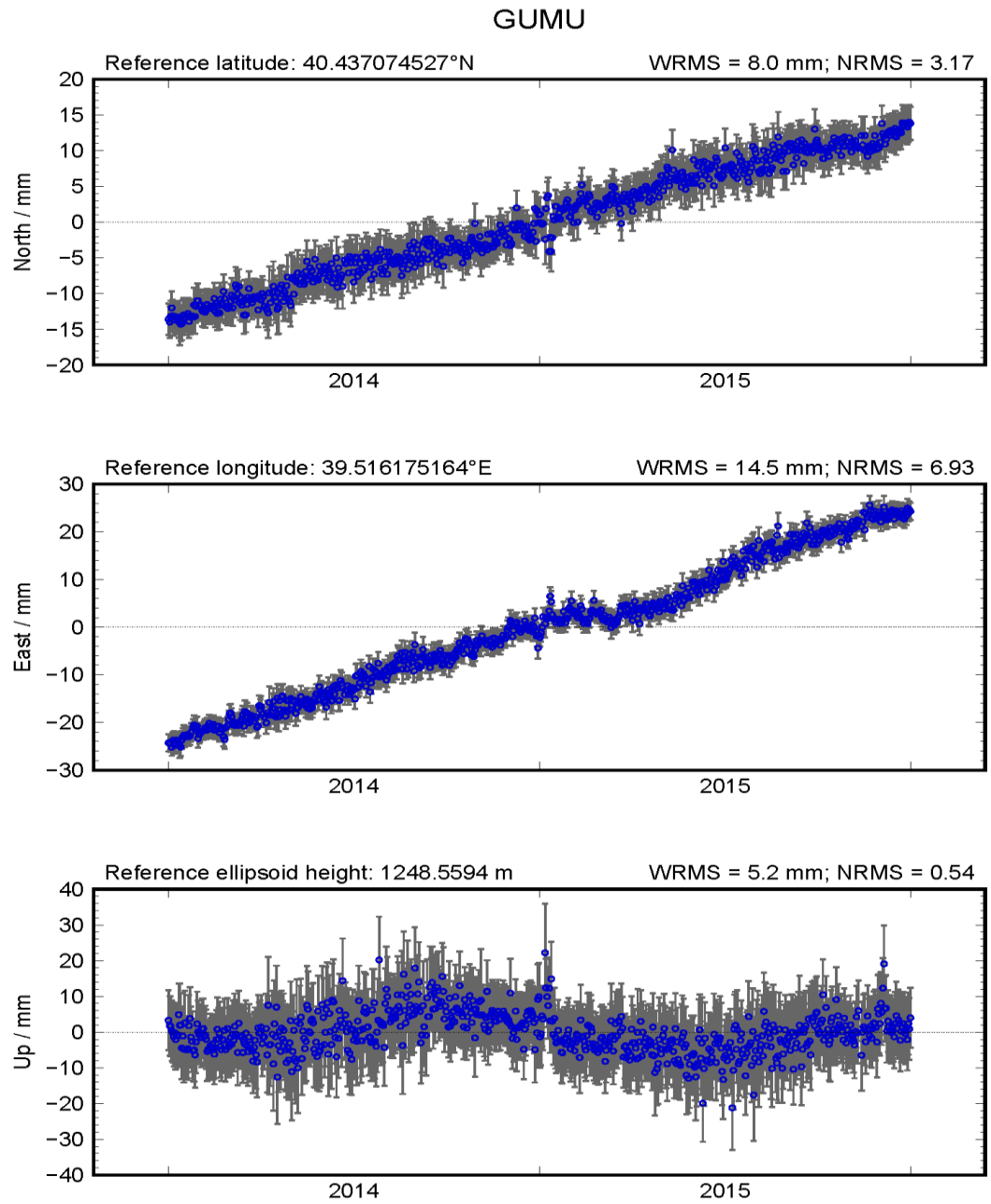


Figure E. 17. GPS time series of station GUMU.

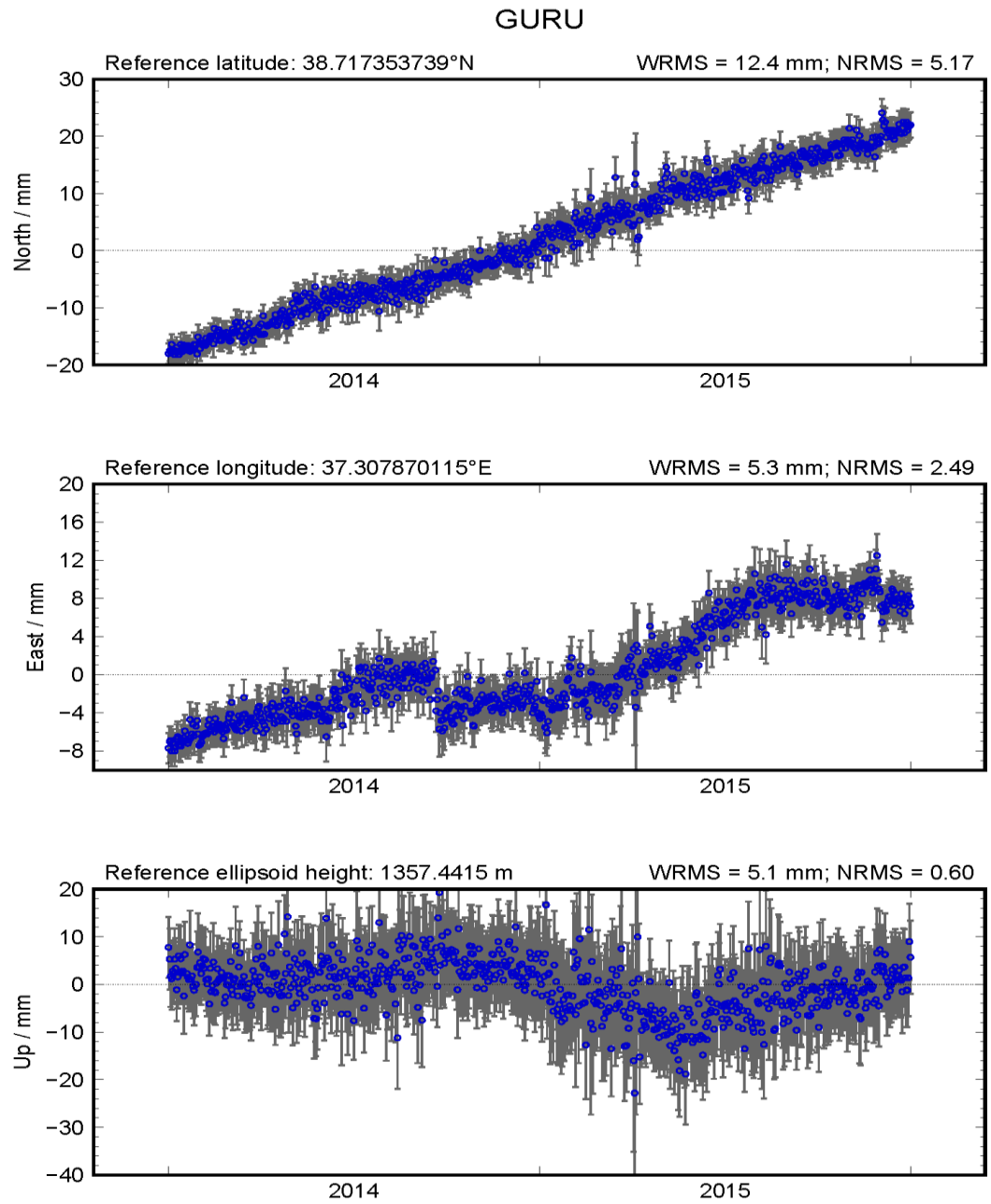


Figure E. 18. GPS time series of station GURU.

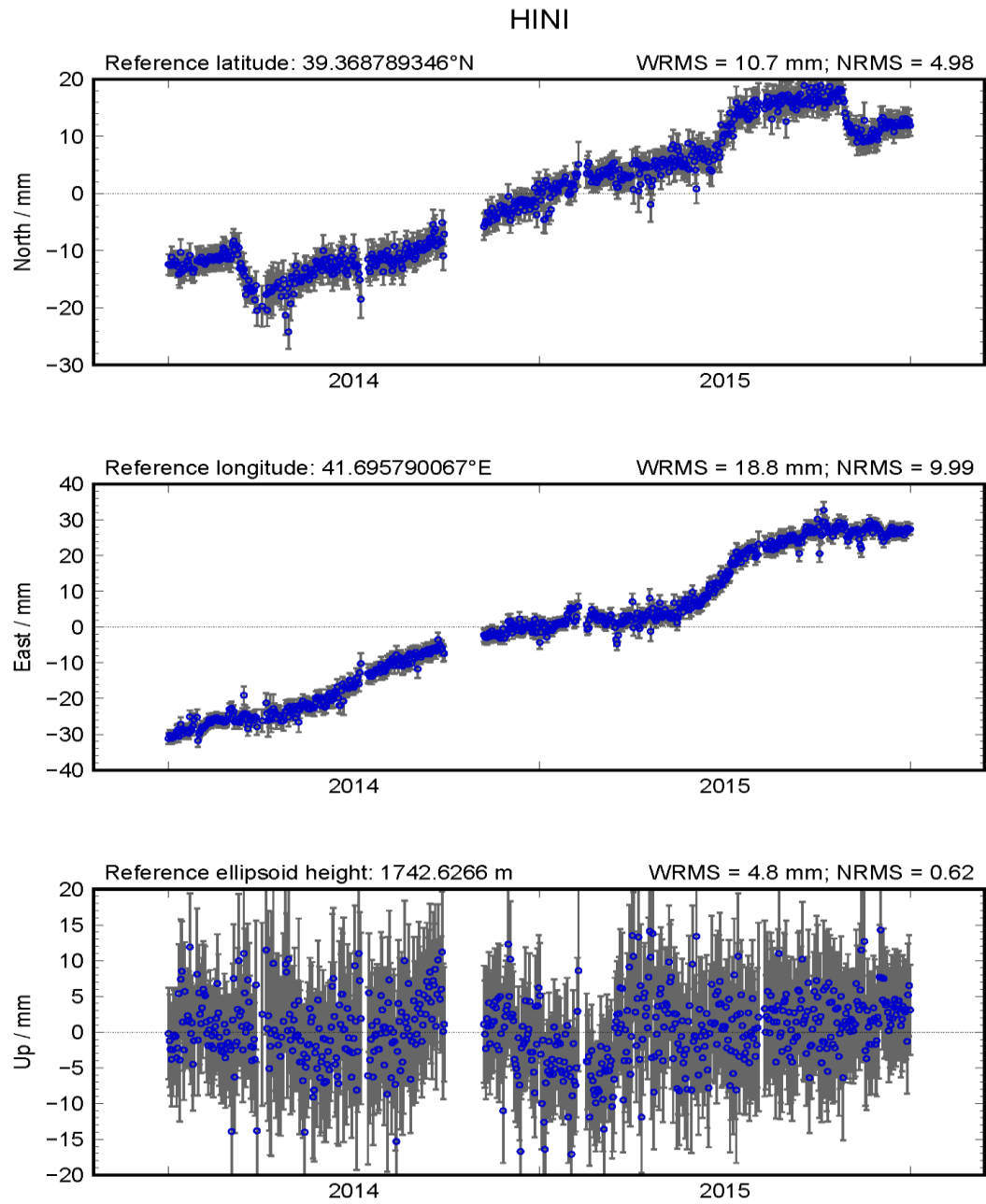


Figure E. 19. GPS time series of station HINI.

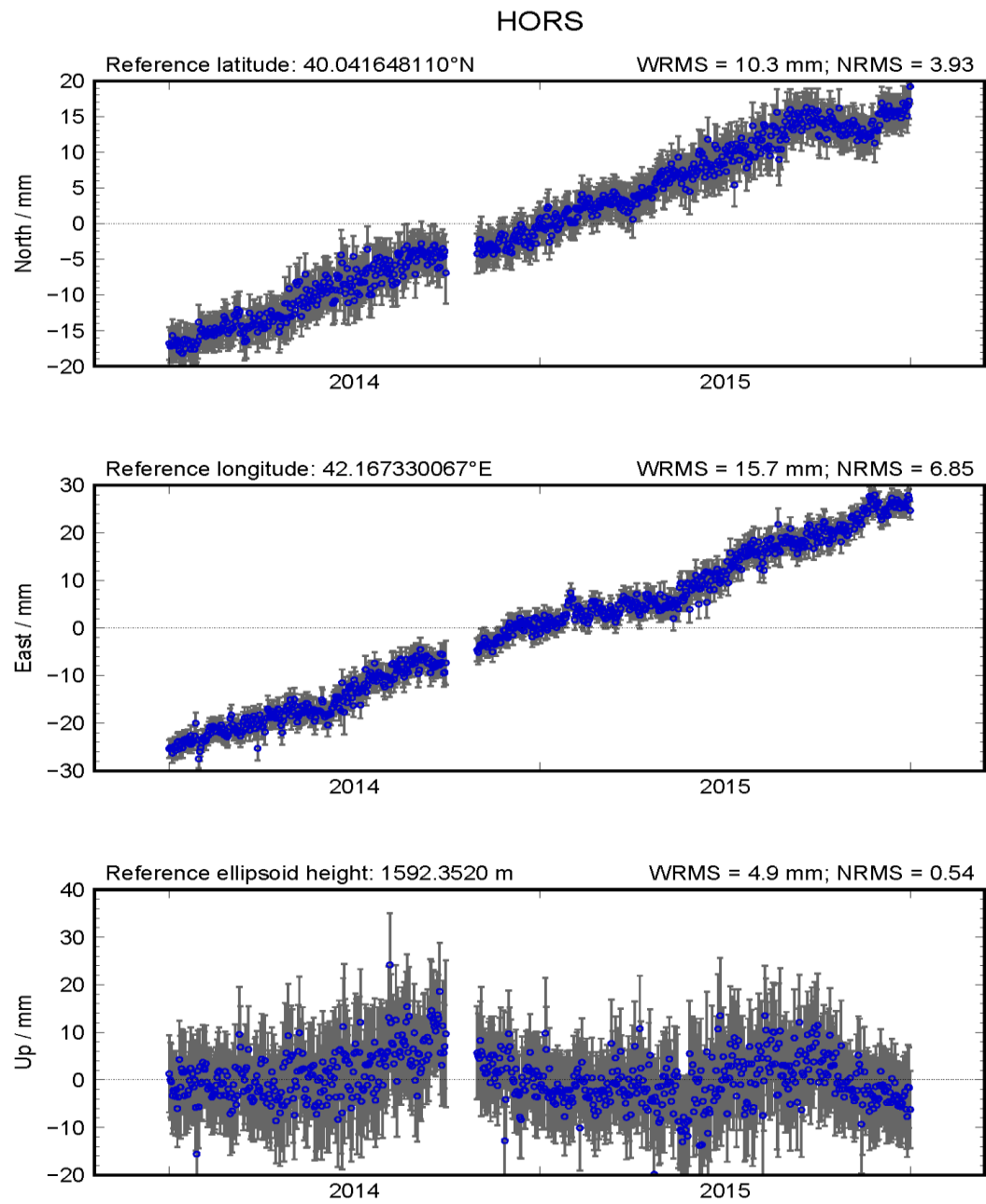


Figure E. 20. GPS time series of station HORS.

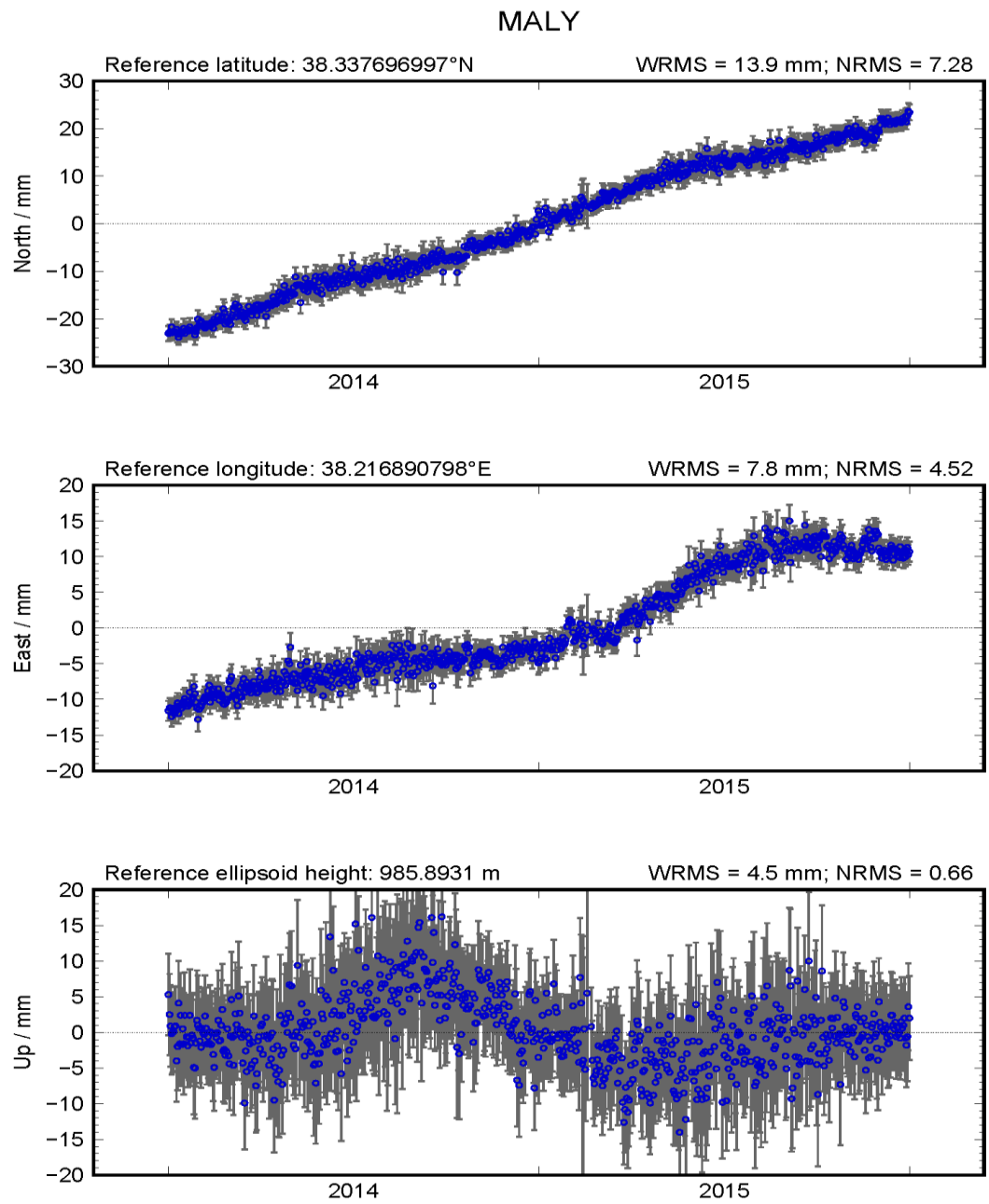


Figure E. 21. GPS time series of station MALY.

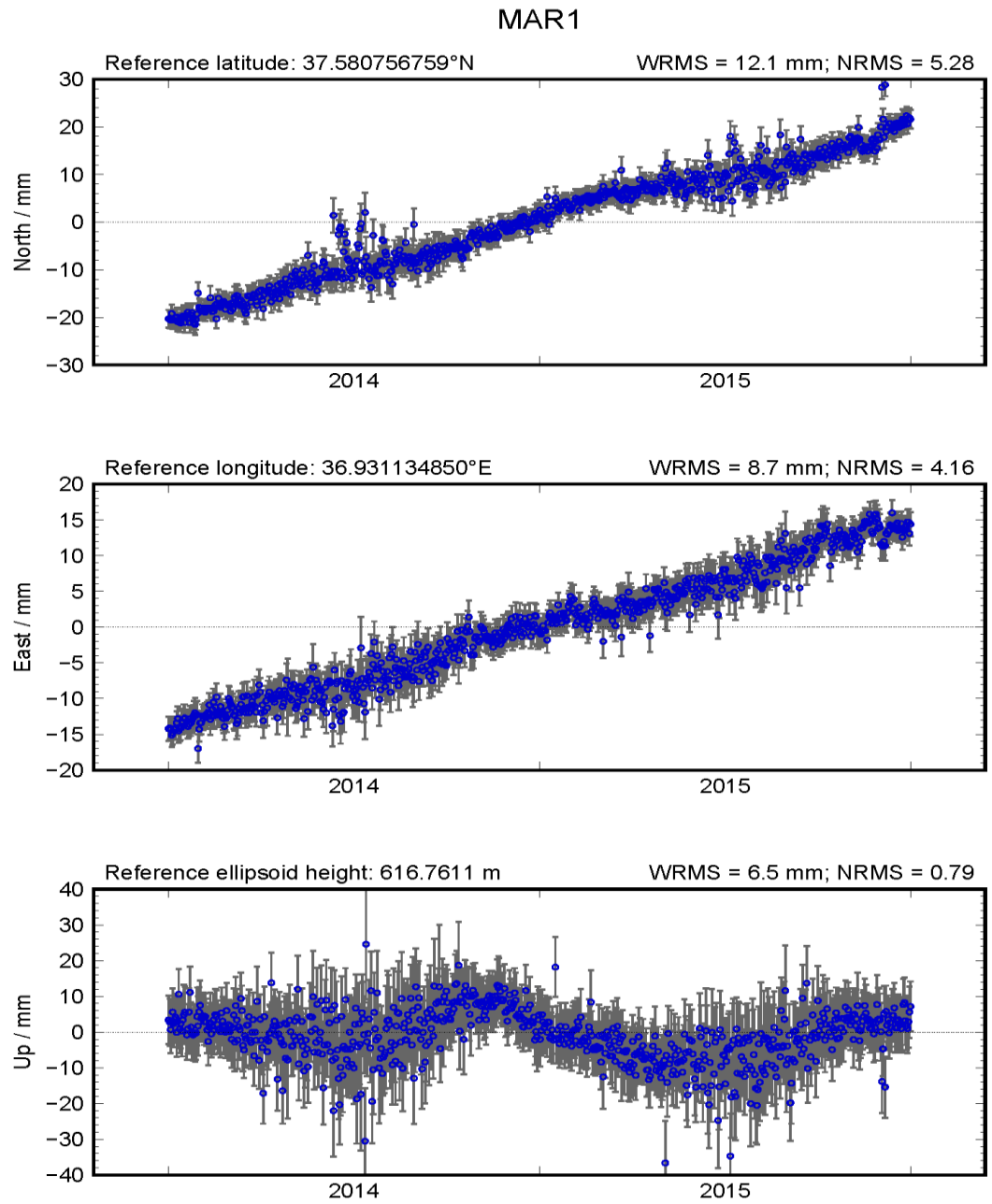


Figure E. 22. GPS time series of station MARA.

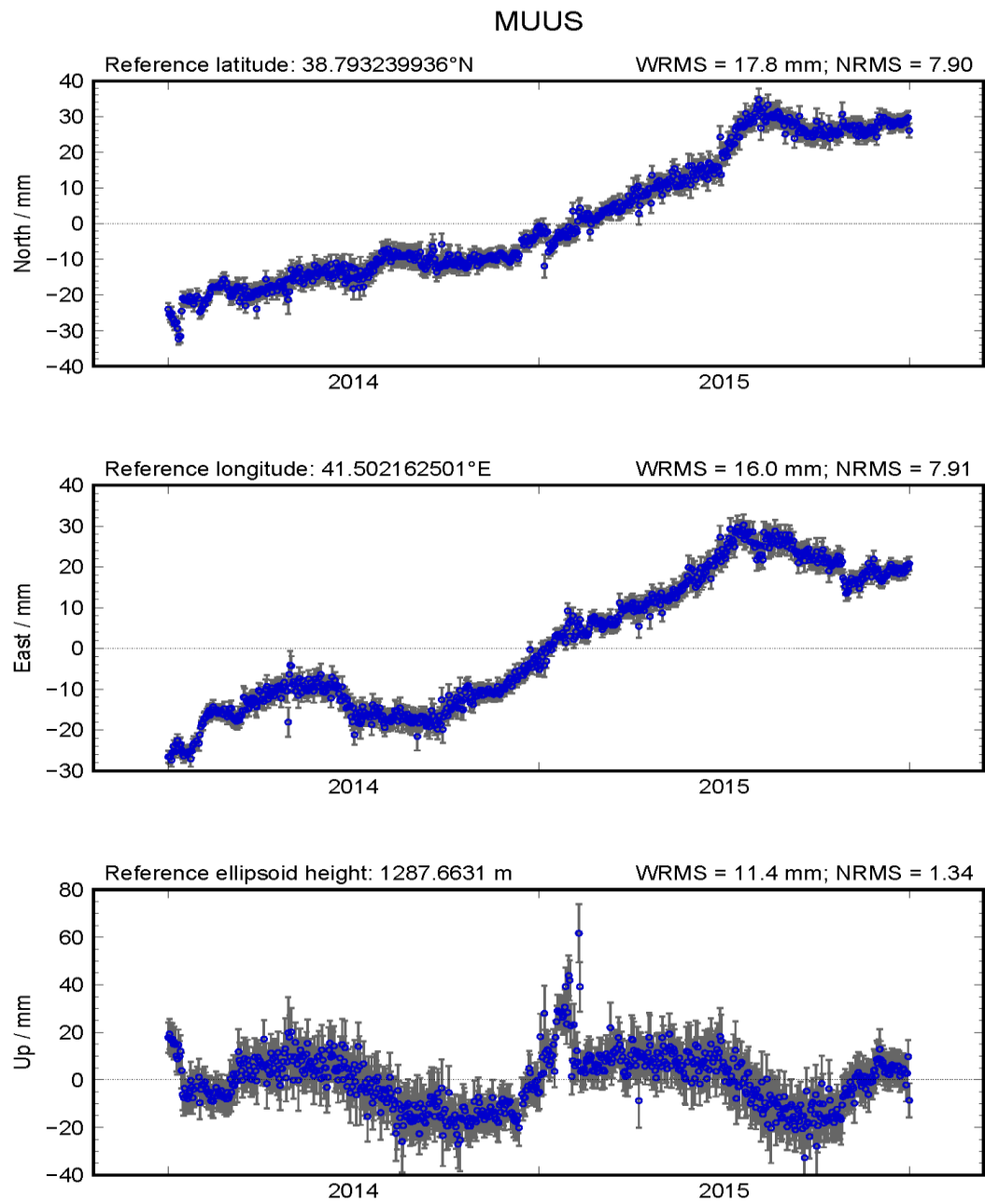


Figure E. 23. GPS time series of station MUUS.

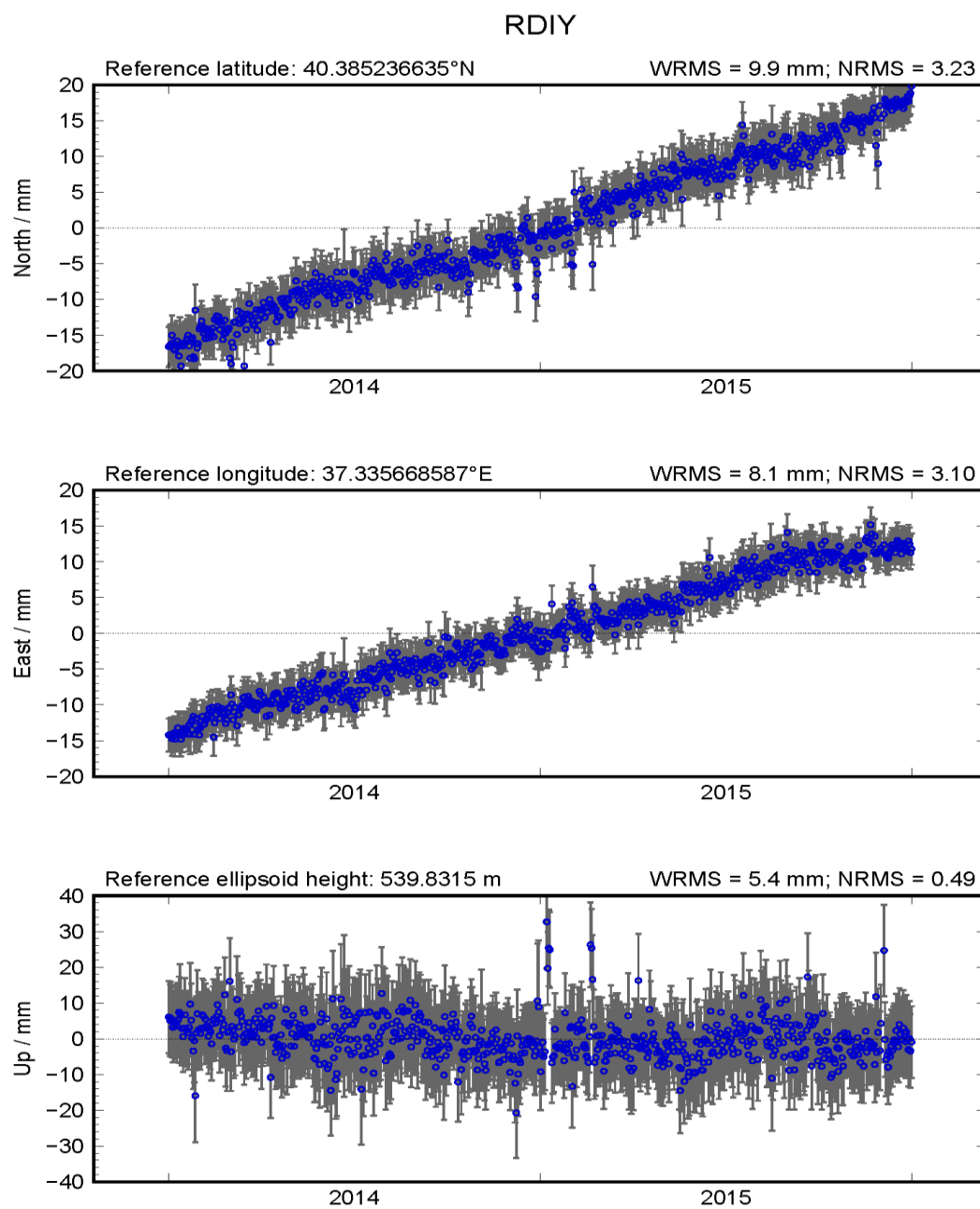


Figure E. 24. GPS time series of station RDIY.

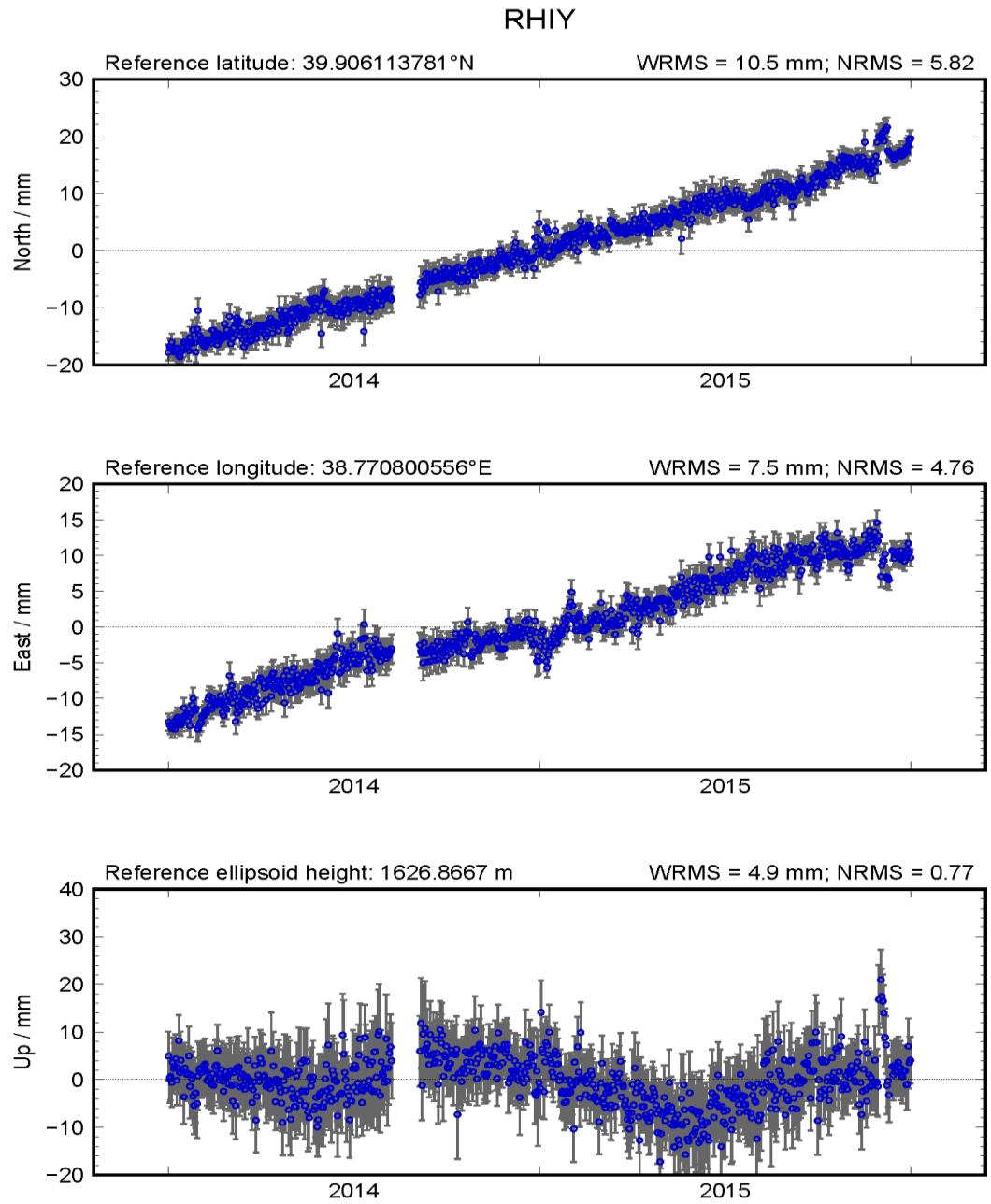


Figure E. 25. GPS time series of station RHIY.

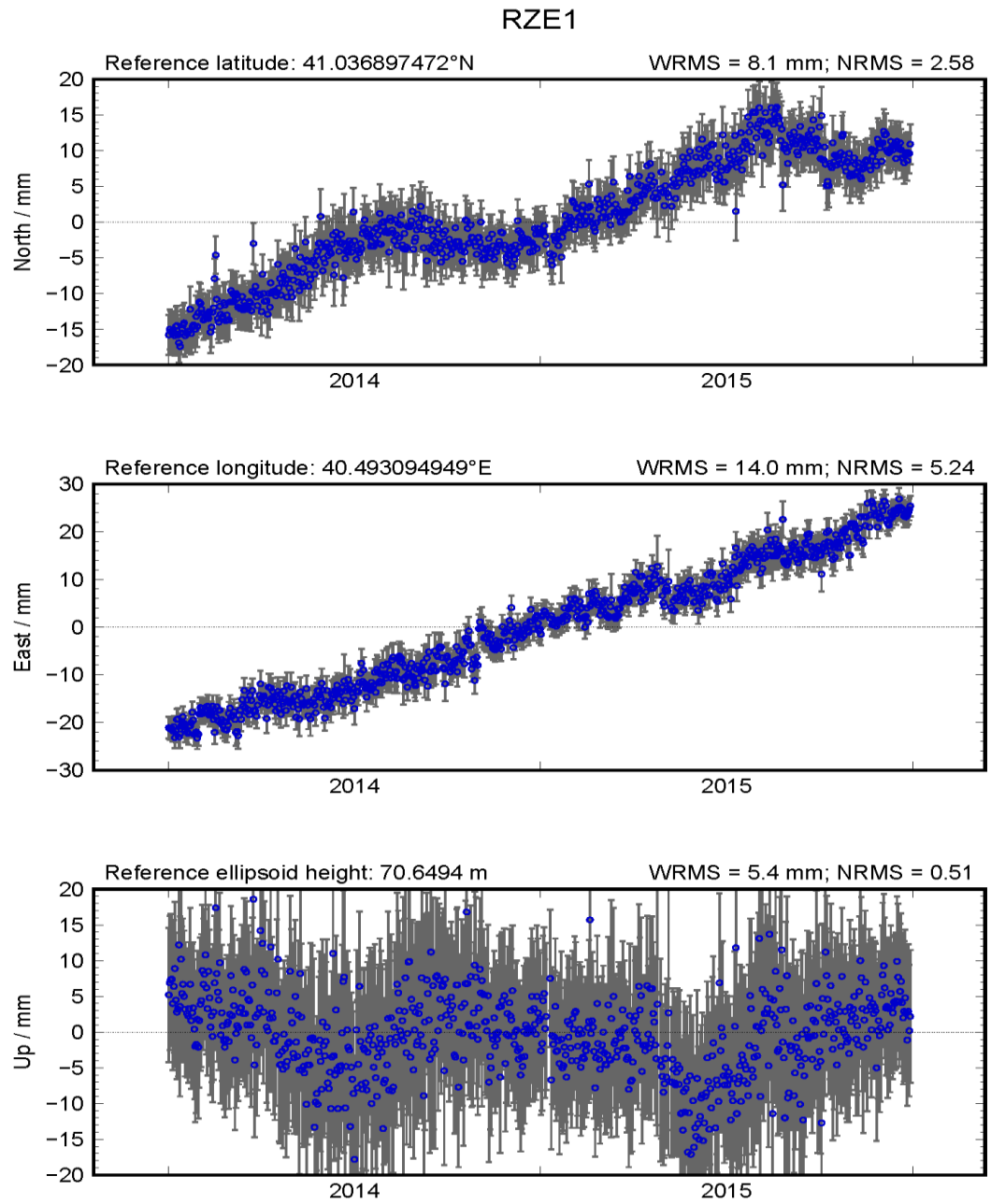


Figure E. 26. GPS time series of station RZE1.

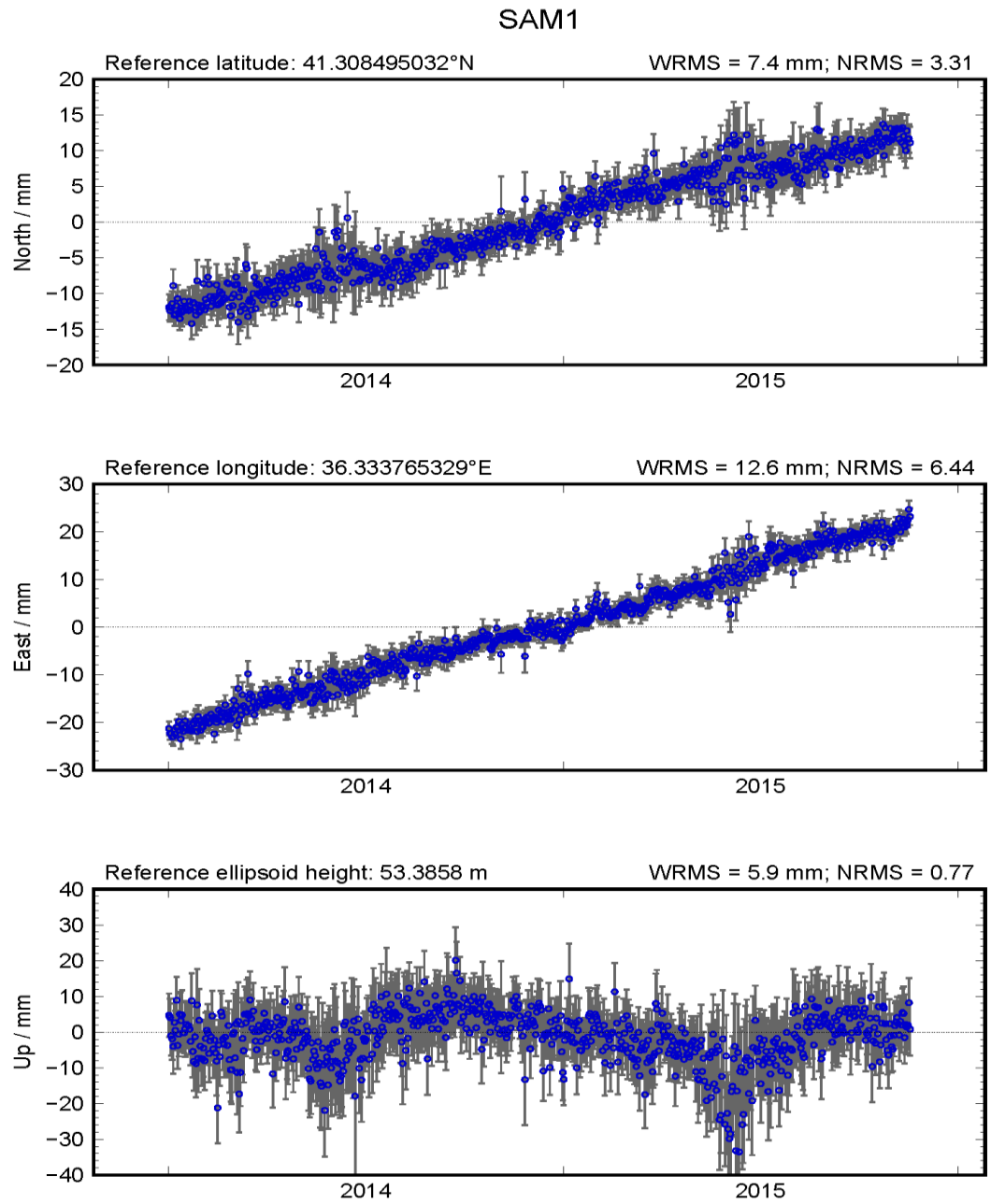


Figure E. 27. GPS time series of station SAM1.

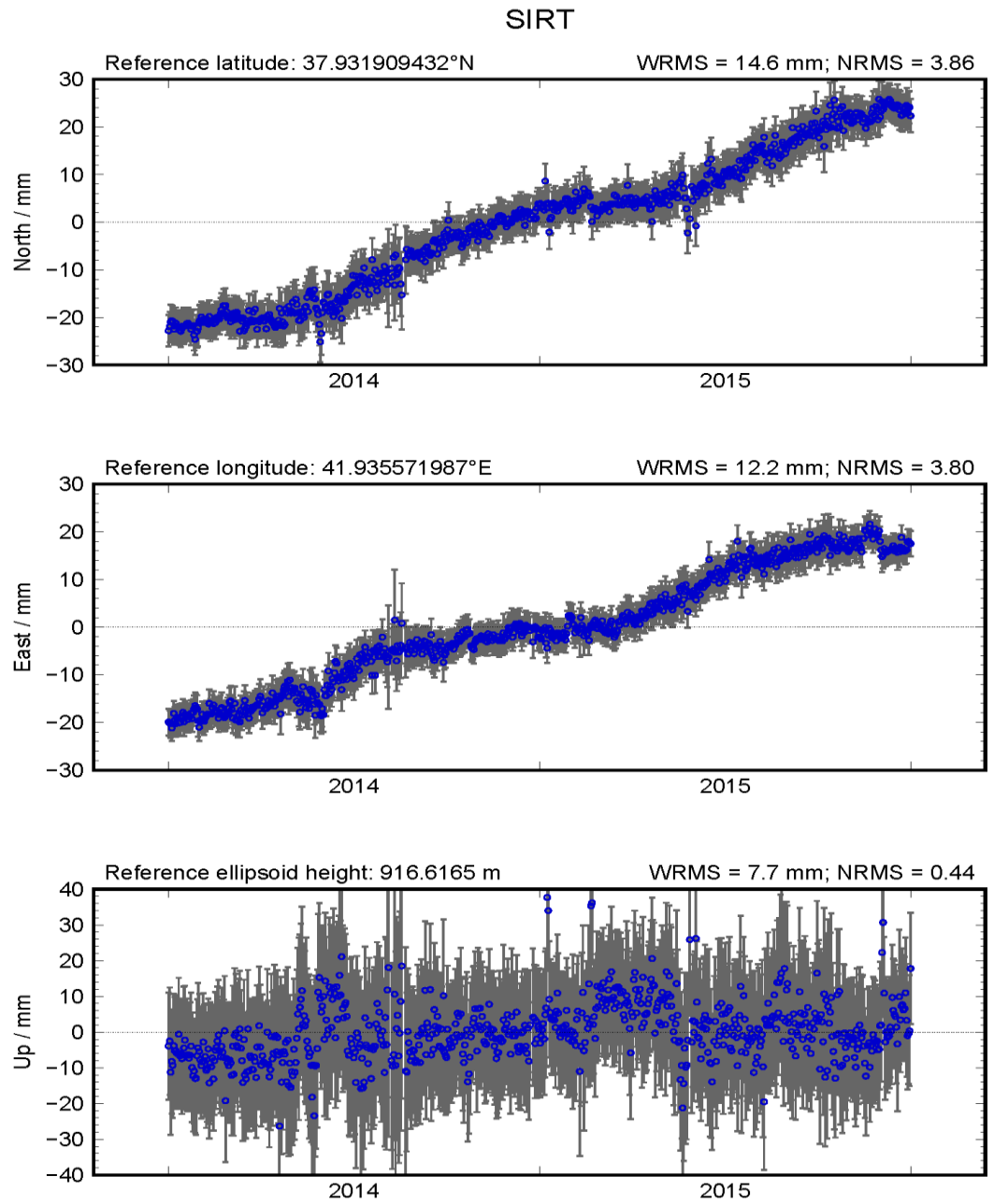


Figure E. 28. GPS time series of station SIRT.

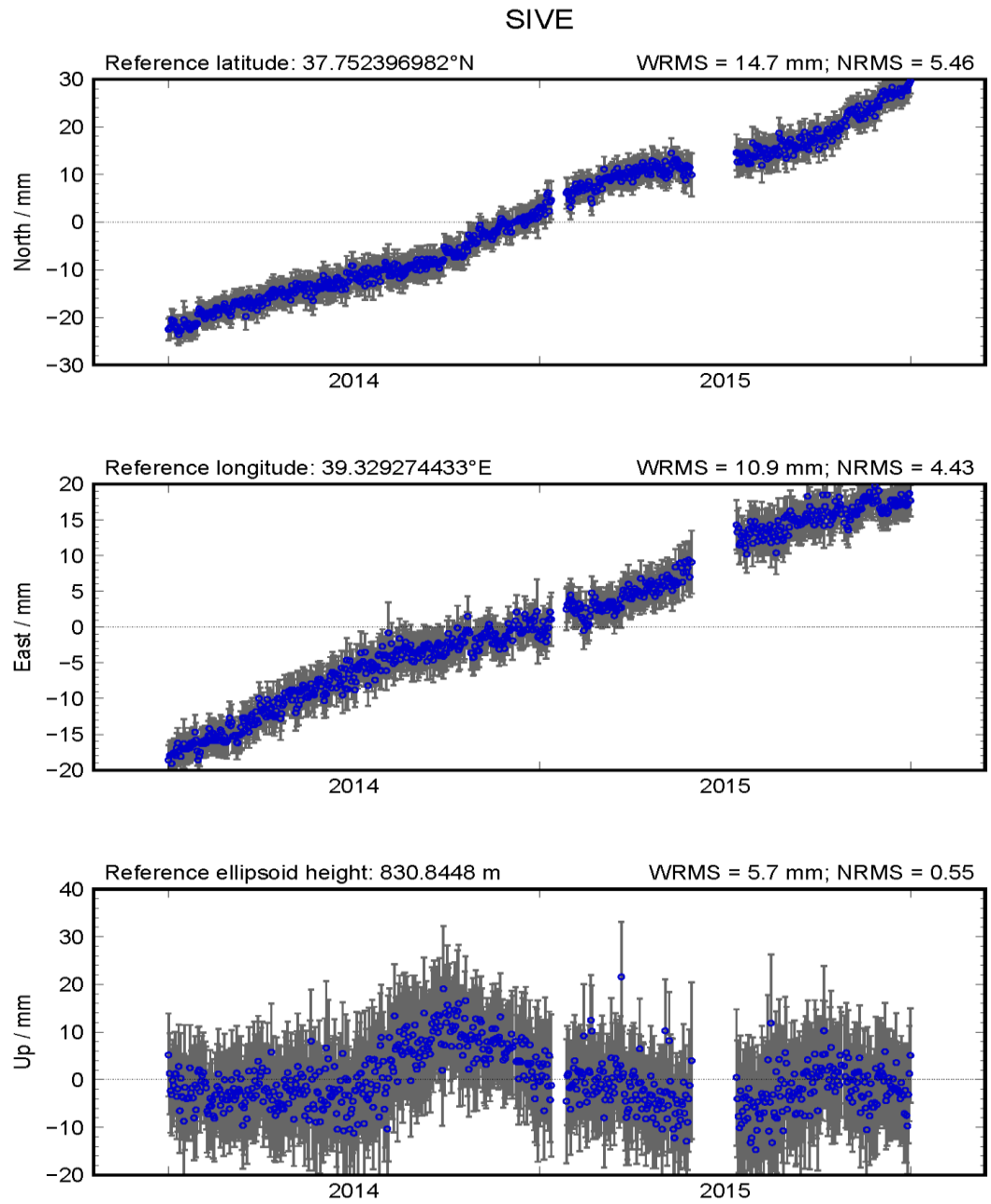


Figure E. 29. GPS time series of station SIVE.

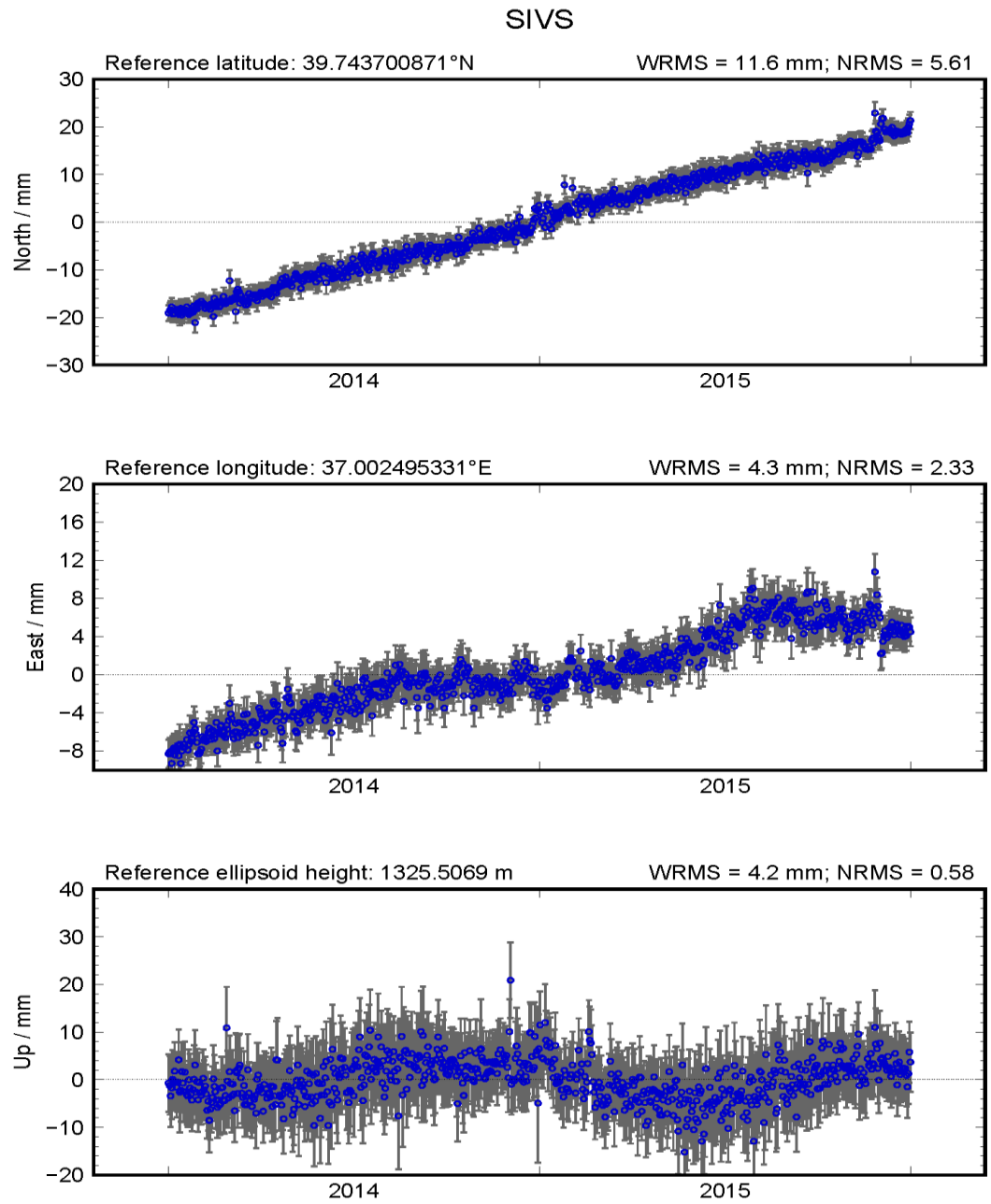


Figure E. 30. GPS time series of station SIVS.

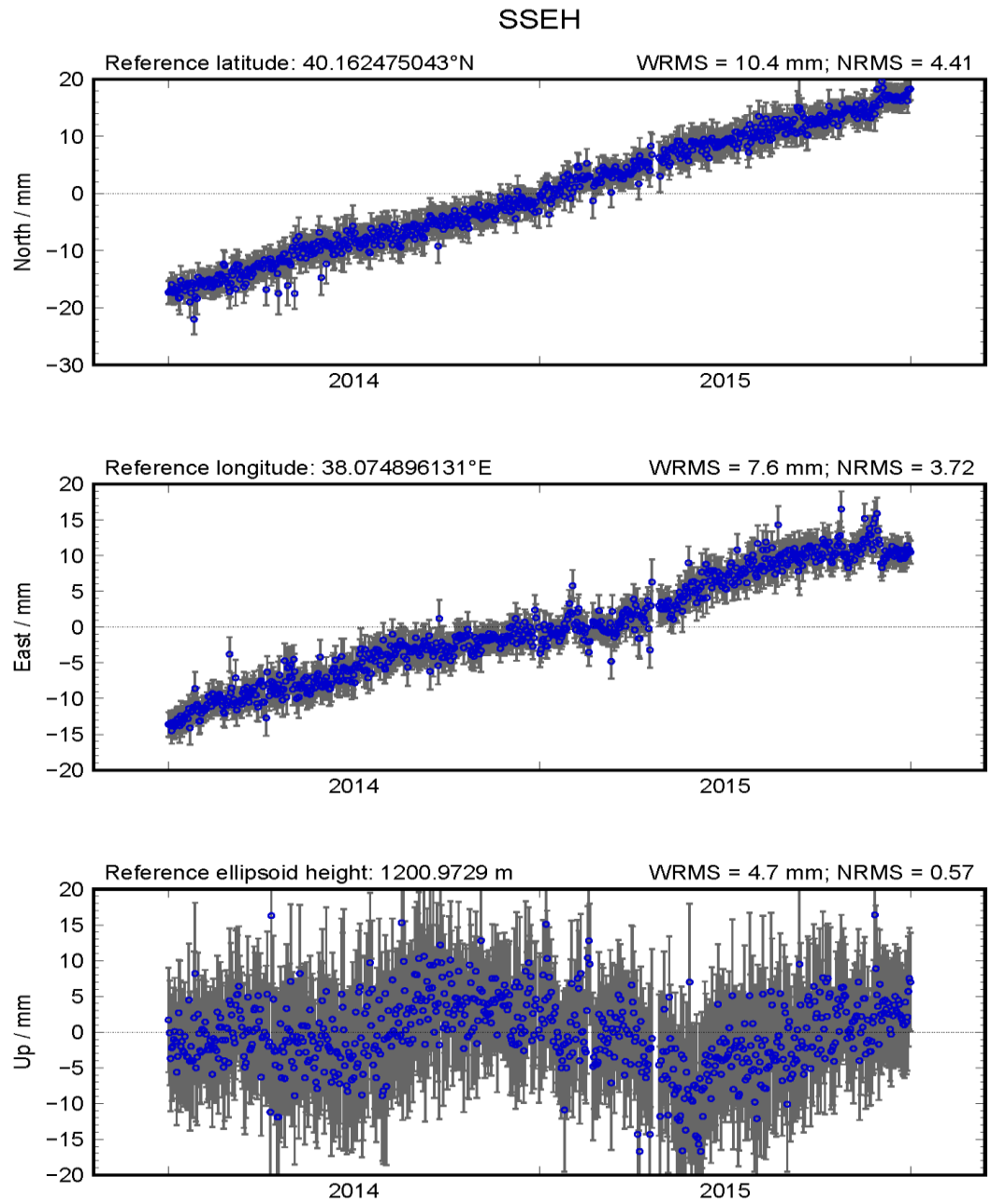


Figure E. 31. GPS time series of station SSEH.

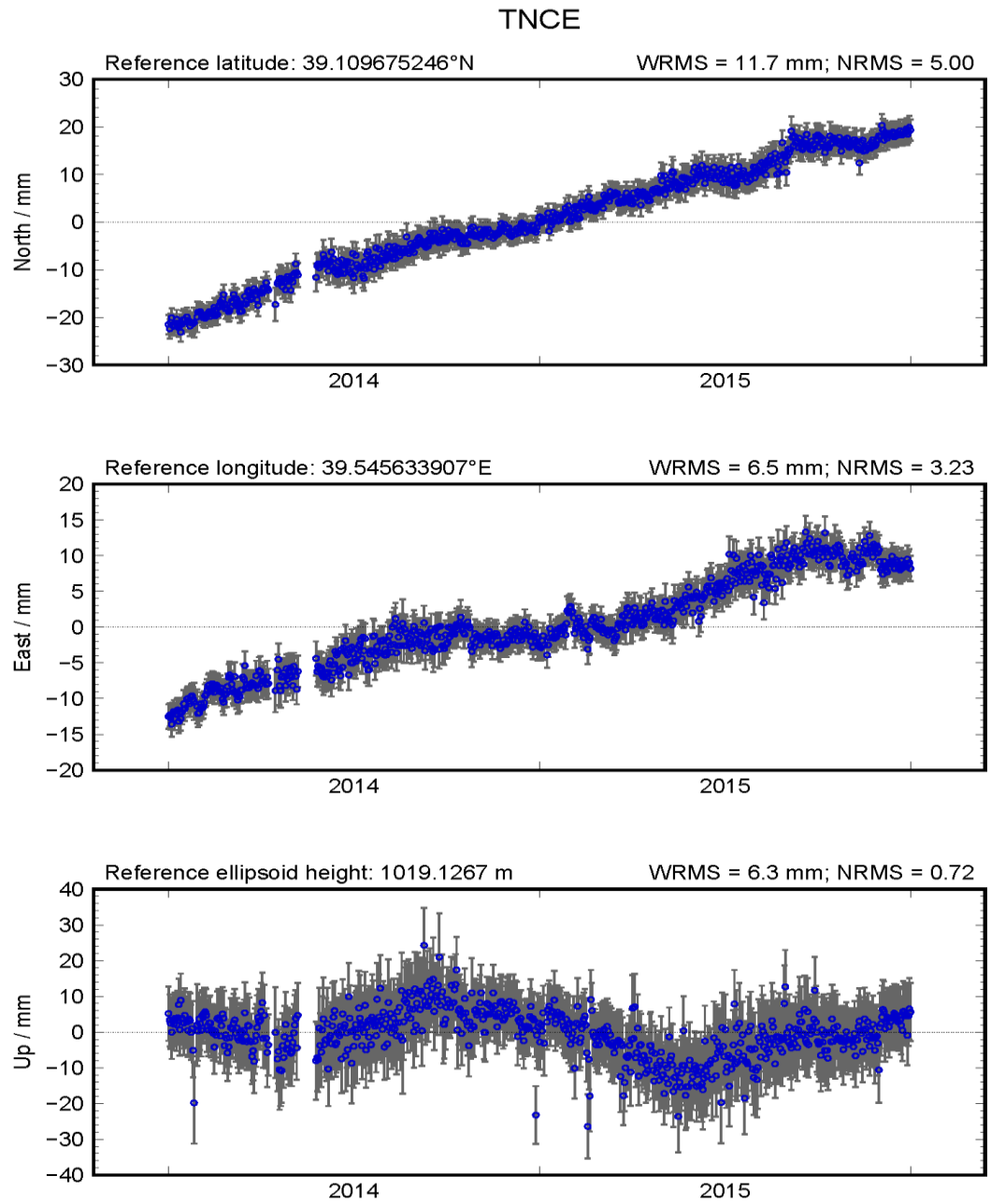


Figure E. 32. GPS time series of station TNCE.

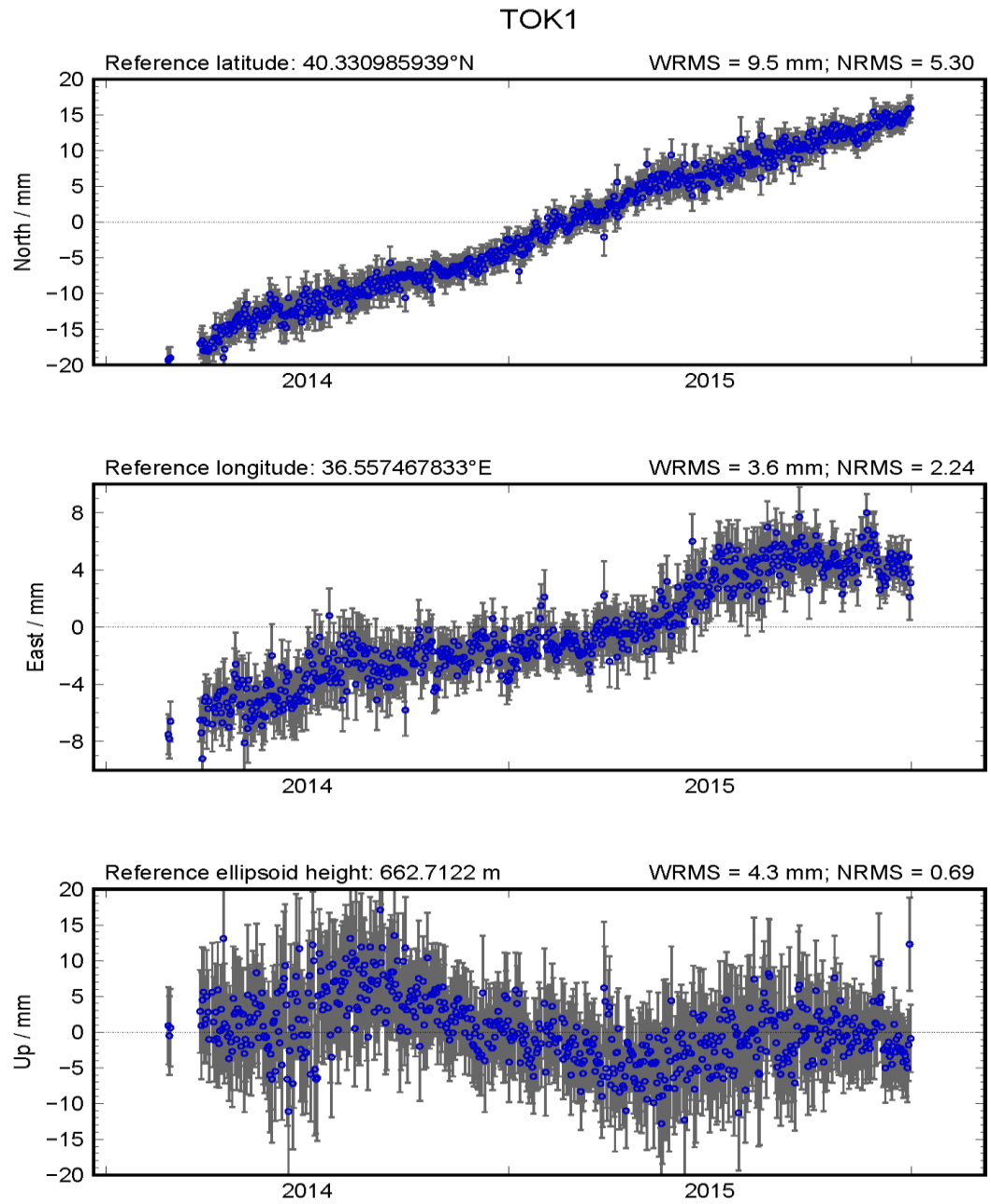


Figure E. 33. GPS time series of station TOK1.

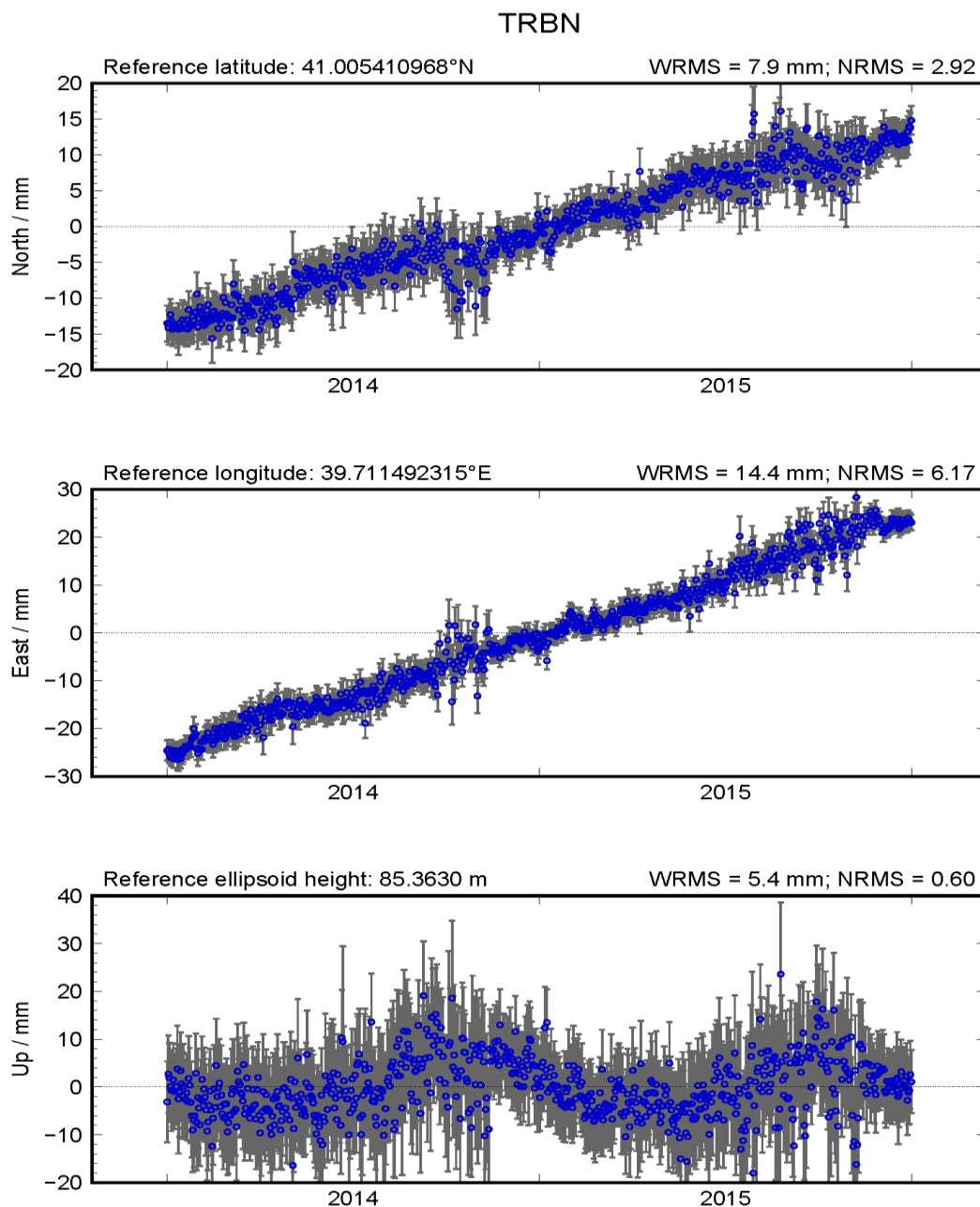


Figure E. 34. GPS time series of station TRBN.

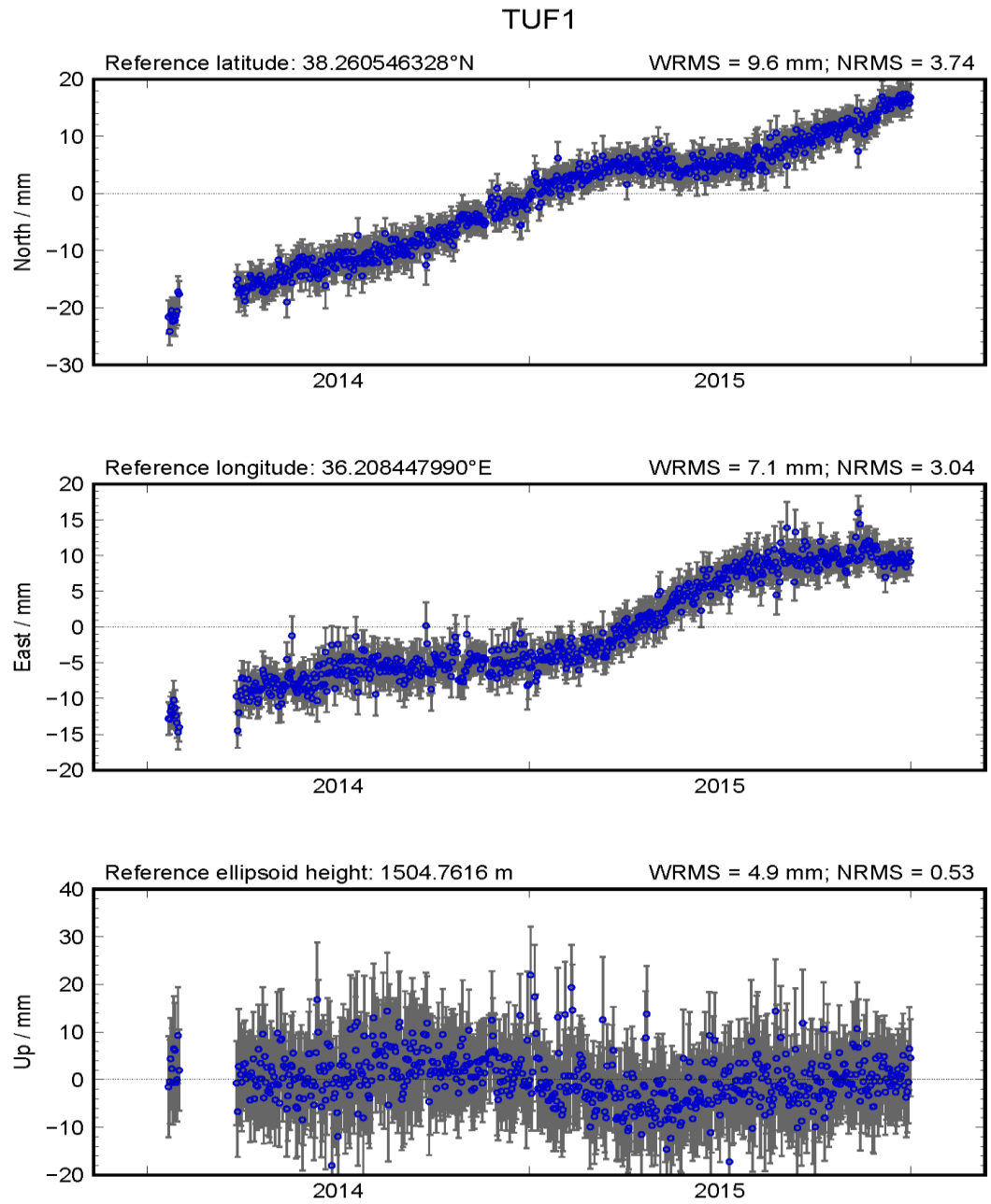


Figure E. 35. GPS time series of station TUF1.

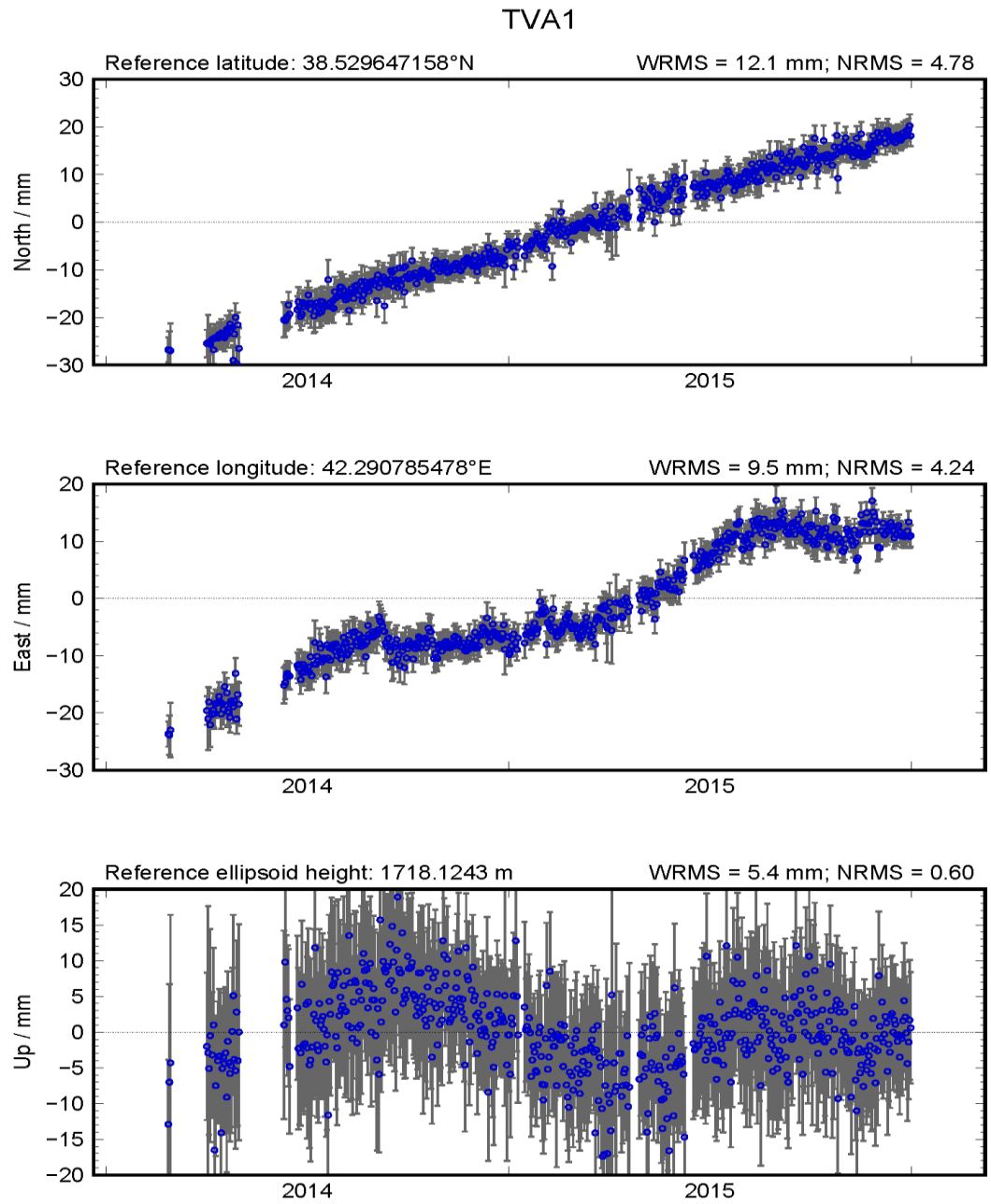


Figure E. 36. GPS time series of station TVA1.

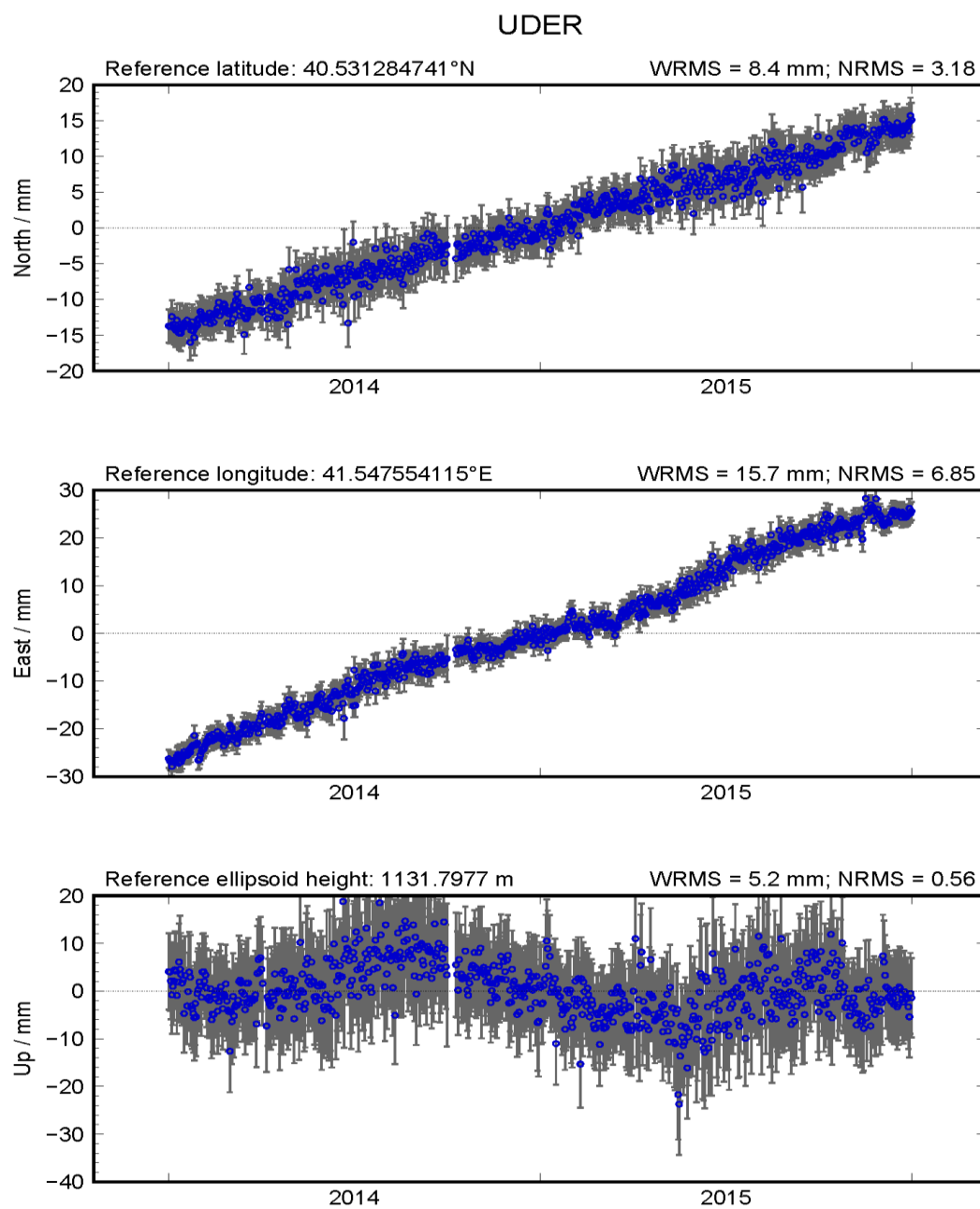


Figure E. 37. GPS time series of station UDER.